THE ANALYSIS AND SYNTHESIS OF A NOVEL ULTRA-WIDEBAND MICROWAVE DIFFERENTIAL PHASE SHIFTER

Frederik Viljoen Minnaar

Thesis Submitted
For the Degree of Doctor of Philosophy in Engineering
in the
Faculty of Engineering
UNIVERSITY OF PRETORIA

March 2000

ABSTRACT: THE ANALYSIS AND SYNTHESIS OF A NOVEL ULTRA-WIDEBAND MICROWAVE DIFFERENTIAL PHASE SHIFTER.

(i) **NAME** : Frederik Viljoen Minnaar
(ii) **LEADER** : Prof. J. Joubert
(iii) **DEPARTMENT** : Electrical, Electronic and Computer Engineering.
(iv) **DEGREE** : PhD Eng. Electronic

Realising the shortfalls of conventional microwave differential phase shifters, an in-depth and broad study was launched into this area, focussing on the synthesis of ultra-wideband devices covering up to more than a decade of bandwidth. This study excluded ferrite, MMIC, waveguide and some other technologies which are relatively band-limited.

By noting the unique and very valuable frequency-independent quadrature property of symmetric TEM couplers, a novel class of phase shifter is proposed. Realising that the phase shift characteristics can be related to the coupling characteristics of the coupler, bandwidth and ripple performance is significantly enhanced. Comparison to the classical wideband Tresselt phase shifter is presented and the practical bandwidth-limiting obstacles are shown to be eliminated. The phase shifter is then analysed thoroughly to determine its sensitivity with respect to errors due to manufacturing tolerances. Error and performance parameters are defined and sensitivities calculated. These results clearly demonstrate the practicality of the idea and also pinpoint the areas of the phase shifter that are most sensitive to manufacturing tolerances.

The elements comprising the phase shifter are then separately analysed and practically explored. A unique splitter is developed to ensure phase and amplitude tracking at the coupler inputs. The periodic broadside coupled stripline (BCS) structure is also fully analysed and the structure's resonance nature predicted. The through-hole plated vias in the BCS structure are first analysed by both a full-wave and a finite element analysis to compare the results. An empirical element fit is conducted to provide future designers with very accurate via models. The splitter performance is then mathematically predicted and compared to an experimental example.

A tolerance analysis is also conducted on each element comprising the phase shifter, and compared to the phase shifter sensitivity analysis demands. Restrictions to the theory are discussed and the manufacturing requirements highlighted. A general synthesis procedure is derived to aid future

designs. Computer code was also developed to fully design the tapered coupler from material and electrical specifications.

The study concludes with a design example for a complete differential phase shifter, comparing analysis results with practical measured results and some general conclusions.

Keywords : microwave, differential, phase, shifter, bandwidth, quadrature, periodic, tracking, coupling, ripple.

OPSOMMING: DIE ANALISE EN SINTESE VAN 'N NUWE ULTRA-WYEBAND MIKROGOLF DIFFERENSIELE FASE VERSKUIWER.

(i) **NAAM** : Frederik Viljoen Minnaar

(ii) **LEIER** : Prof. J. Joubert

(iii) **DEPARTEMENT** : Electriese, Elektroniese en Rekenaar Ingenieurswese.

(iv) **GRAAD** : PhD Ing. Elektronies

Met begrip van die tekortkominge van konvensionele mikrogolf differensiële fase verskuiwers, is 'n diep en wye studie in hierdie veld aangepak. Daar is gefokus op ultra-wyeband komponente wat meer as 'n dekade bandwydte dek. Hierdie studie sluit ferriet, MMIC, golfleier en sommige ander tegnologieë, wat relatief band beperk is, uit.

Deur die unieke en baie waardevolle frekwensie onafhanklike kwadratuur eienskap van simmetriese TEM koppelaars toe te pas, word 'n nuwe klas fase verskuiwer voorgestel. Deur te besef dat die fase verskuiwing karakteristieke herlei kan word na die koppelaar se koppeling karakteristieke, word die bandwydte en riffel prestasie aansienlik verbeter. Hierdie word vergelyk met die klasieke Tresselt fase verskuiwer en aangetoon dat die praktiese band beperkende hindernisse ge-elimineer kan word. Die fase verskuiwer word dan deeglik ge-analiseer om sensitiwiteit ten opsigte van vakmanskap toleransie te bepaal. Fout- en prestasie parameters word gedefinieer en sensitiwiteite bereken. Die resultate demonstreer die praktiese implementeerbaarheid van die konsep en dui ook die areas aan waar die fase verskuiwer die meeste sensitief is vir toleransie.

Die verskeie elemente van die fase verskuiwer word apart ge-analiseer en prakties ondersoek. 'n Unieke drywingsverdeler was ontwikkel om fase en amplitude volging by die koppelaar insetpoorte te verseker. Die periodiese oorgekoppelde strooklyn (BCS) struktuur is deeglik ge-analiseer en die struktuur se resonansie karakter voorspel. Die deurgat geplateerde vias in die BCS struktuur is eers ge-analiseer deur beide 'n volgolf- en eindige element analise en die resuktate is vergelyk. 'n Empiriese element passing is gedoen om toekomstige ontwerpers met akkurate via modelle te voorsien. Die drywingsverdeler karakteristieke is dan wiskundig voorspel en vergelyk met 'n praktiese voorbeeld.

'n Toleransie analise is ook gedoen op elke element van die fase verskuiwer, en vergelyk met die fase verskuiwer se sensitiwiteit analise vereistes. Beperkinge tot die teorie is bespreek en die vakmanskap

vereistes uitgelig. 'n Algemene sintese prosedure is afgelei om toekomstige ontwerpe te steun. Rekenaar kode was ook ontwikkel om die tapsvormige koppelaar vanaf materiaal en elektriese spesifikasies te ontwerp.

Die studie sluit af met 'n ontwerp voorbeeld van 'n volledige differensiële fase verskuiwer, analise resultate word met gemete waardes vergelyk, asook algemene gevolgtrekkings.

Sleutelwoorde : mikrogolf, differensieël, fase, verskuiwer, bandwydte, kwadratuur, periodiese, volging, koppeling, riffel.

TABLE OF CONTENTS

CHAPTER 1. INTRODUCTION

1.1. Historical Background

Differential phase shifters have application in various microwave systems, for example in hybrid circuits and wide band phased-array antennas. Differential phase shifters are four-port networks providing constant differential phase shift across their two output ports. During the last 35 years phase shifters comprising coupled lines proved to exhibit the greatest bandwidth [1].

Wideband phase shifting networks suitable for application at low frequencies were widely investigated during the period 1946-1953 [2,3,4,5,6,7]. In 1956 Jones and Bolljahn [8] published an equation for the phase shift through a single C-section of coupled lines. Cohn [9] first suggested the use of the coupled-line all-pass network in broadband phase-shift networks in 1955, which led to the work of Schiffman in 1958 [10].

The basic Schiffman phase shifter, shown in Figure 1, consists of two separate TEM transmission lines, one of which is a length of uncoupled line called the reference line. The other line is a single C-section, consisting of a pair of parallel coupled transmission lines directly connected to each other at one end. The coupled section is one quarter wavelength long at the centre frequency. Schiffman classified types A, B, C, D, E and F networks covering combined C-sections in six basic configurations. He concluded that a 5 : 1 bandwidth may be covered using these networks.

Cascaded all-pass networks, also known as microwave C-sections, have been analysed by Steenart [11] in 1963 and Zysman and Matsumoto [12] in 1965. Crystal [13] solved the analysis problem and exact synthesis of cascaded C-sections in 1966, using matrix methods and Richard's Theorem [14], but restricted the various coupled sections to having equal lengths. Shortly afterward Schiffman derived analysis equations for multi-section phase shifters (see Figure 2) with any amount of coupled sections, also including unequal lengths [15], as shown in Figure 2. Late in 1966 Shelton and Mosko [16] described an approximate iterative synthesis technique for multiple-section Schiffman phase shifters and tabulated the results.

In 1968 Tresselt published a design procedure for a continuously-tapered coupled-section phase shifter [17]. He realised the important fact that the spread in coupling values between adjacent sections is large enough to produce significant reactive discontinuities in practical TEM line geometries, adversely affecting VSWR and phase accuracy of stepped devices at high frequency.

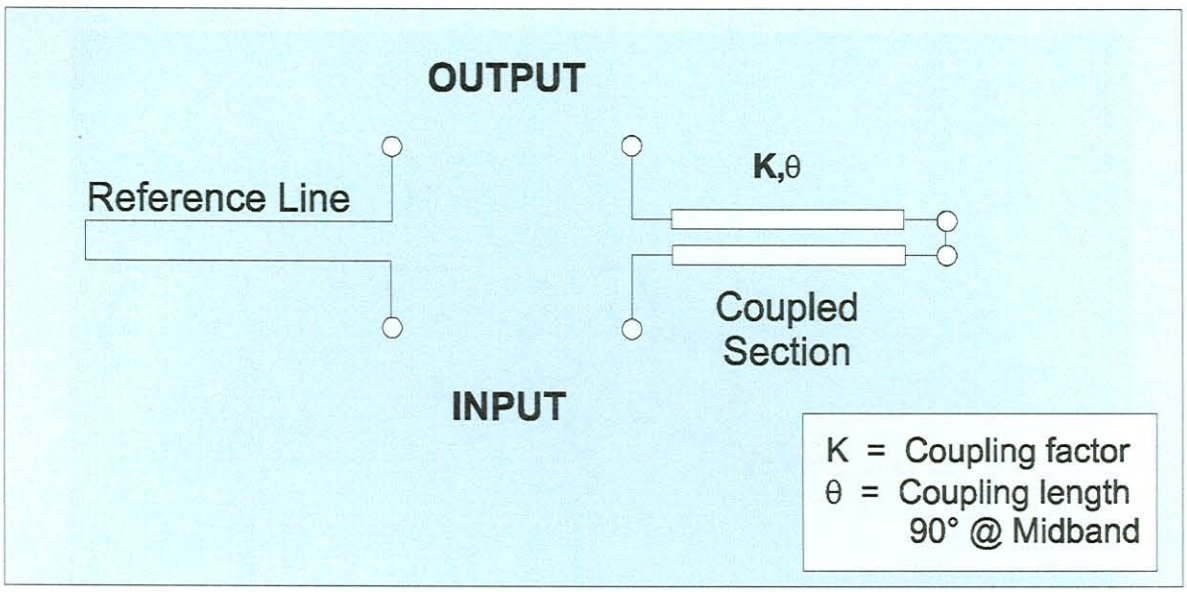

Figure 1 : The basic Schiffman phase shifter

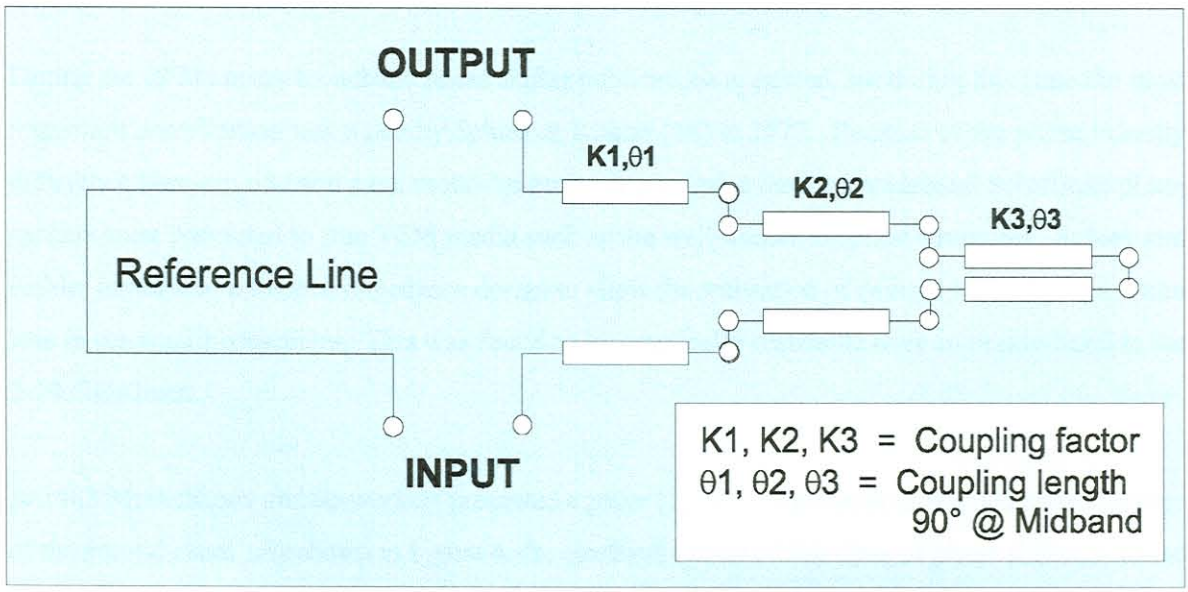

Figure 2 : Multi-section Schiffman phase shifter

His continuously tapered synthesis procedure considerably reduced the impact of these effects. Such a tapered-line phase shifter is shown in Figure 3. He then designed and constructed such a device over a 10 : 1 band. The results however showed that the parasitic effects due to the intra-connecting strap limited the upper frequency band and could only be partially compensated for, limiting the device application to about 9 GHz.

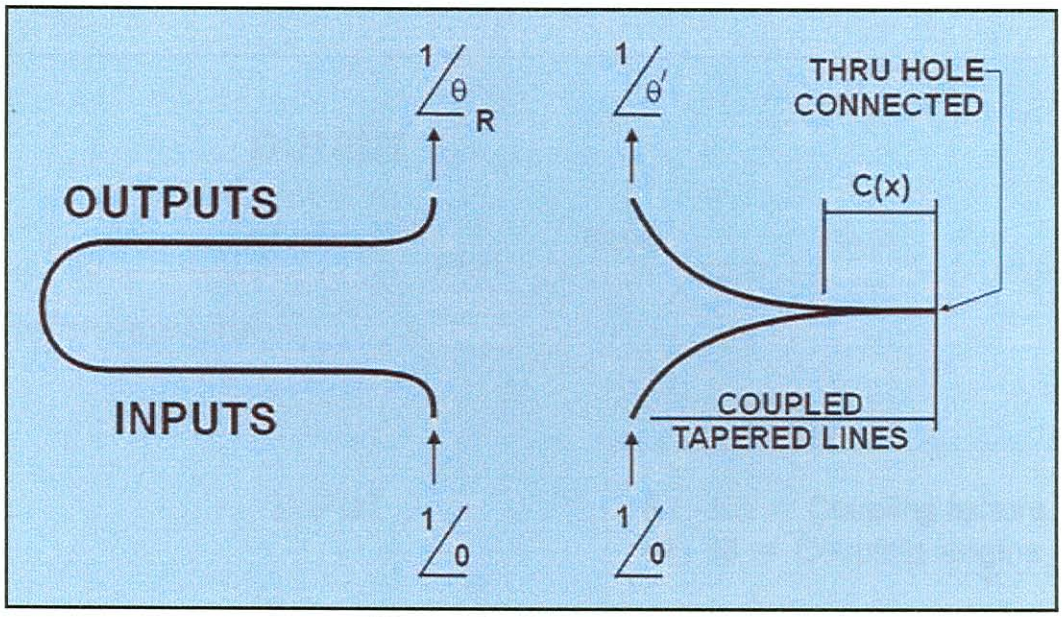

Figure 3 : Tapered line phase shifter

During the 1970's many broadband phase shifter publications appeared, but during this time the most important contribution was made by Schiek & Köhler [18] in 1977. Because of the phase velocity difference between odd and even modes in microstrip coupled devices, wideband Schiffman phase shifters were restricted to true TEM media such as the well-known stripline structures. Schiek and Köhler introduced a stepped impedance design to allow the realisation of devices with very low return loss in microstrip structures. This was found to be practically realisable over an octave band in the 2-10 GHz band.

In 1983 Meshchanov and co-workers presented a paper [1] on the synthesis of stepped phase shifters of the second class. As shown in Figure 4, the electrical circuit of this class of phase shifter is based on the cascaded connection of alternating sections of coupled and uncoupled lines of different electrical length in contrast with phase shifters of class I which have only coupled sections. They published solution tables for a number of optimal designs. The advantages of class II phase shifters over the classical class I phase shifters were demonstrated in several publications [19, 20, 21]. However, class II phase shifters have a higher ripple value per optimized bandwidth and, due to the very high coupling ratio of adjacent sections, severe parasitic effects at the transitions. This limits the practical upper frequency of operation. The coupling values of class II phase shifters are on average

4% lower than class I networks, and the structure is also smaller. It was also noted that by making the coupling coefficients equal, the design is significantly simplified.

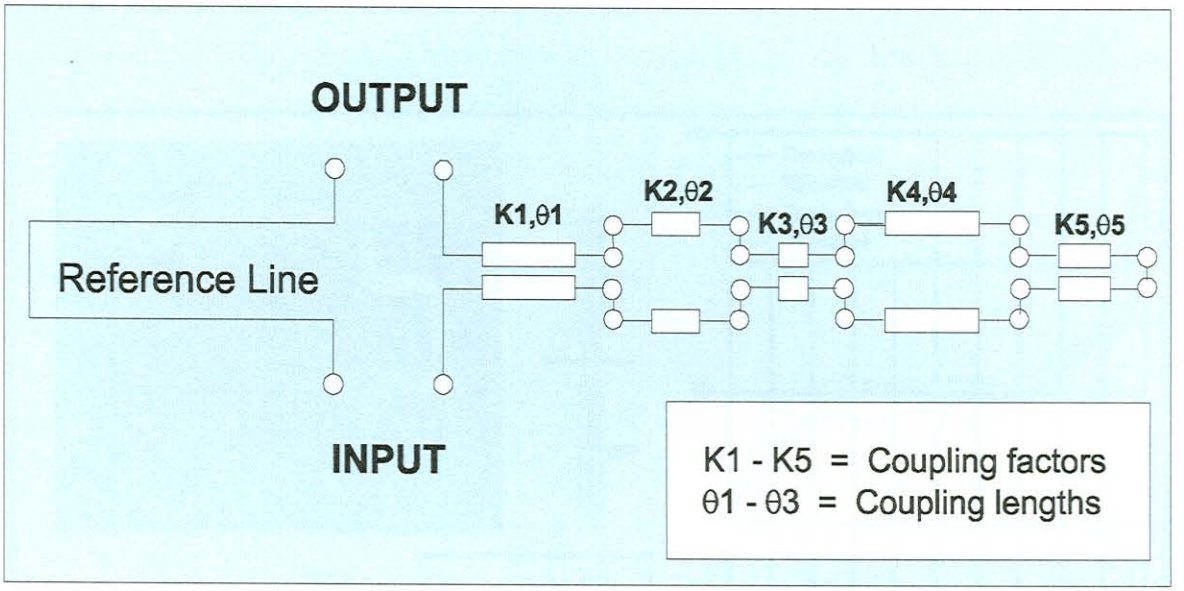

Figure 4 : Five-section phase shifter of class II

Equations for the synthesis of single-section Schiffman phase shifters were also presented in 1985 by Quirarte and Starski [22]. The equations enable the calculation of the bandwidth and phase ripple for a given coupling coefficient, or the coupling coefficient of the section for a given phase deviation and bandwidth.

In order to achieve larger bandwidth, it is necessary to use sections which are more tightly coupled. This is difficult to realise. In a paper titled "Novel Schiffman Phase Shifters", Quirarte and Starski [23] showed in 1993 how parallel-connected coupled sections of loosely coupled lines can obtain the same differential phase shift as a single tightly coupled section. This is shown in Figure 5. Another advantage is that the parallel section has approximately double the impedance of conventional sections. This reduces parasitic components at transitions and increases the coupling factor.

In 1994 Meschanov et al [24] published an article called " A new structure of microwave ultra-wideband differential phase shifter". Optimized designs of this new structure were tabulated, which is merely a Schiffman phase shifter of type C [15]. The type C network has a 6 : 1 bandwidth for a 1.2° ripple. It was concluded that the optimum type C network has a maximum coupling coefficient for the shortest section and a minimum coupling coefficient for the longest section. According to the

paper, a smaller phase ripple was achieved than for other stepped types, allowing wider bandwidth for the same ripple. The coupling values were found to be lower than other types. The disadvantage is that the structure is larger than other types.

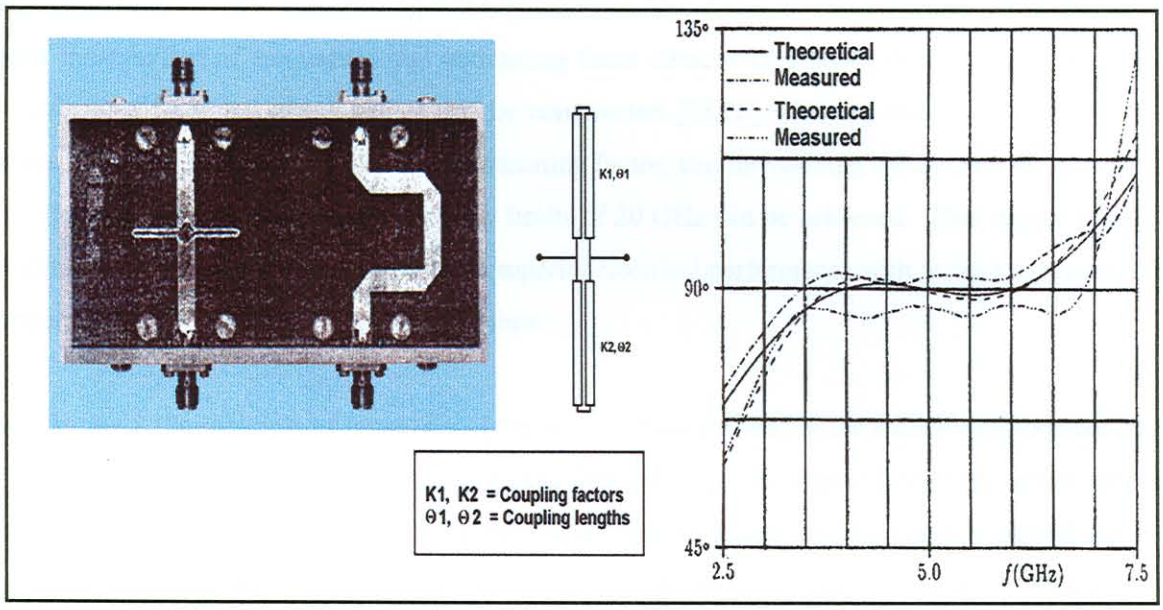

Figure 5 : Parallel-connected Schiffman sections with theoretical & measured results

From this study it was clear that virtually all work regarding wideband differential phase shifters was based on Schiffman's original work. No significant progress has been made except for some improvements on, or extensions of the classical Schiffman phase shifter.

1.2. Existing Shortcomings in Differential Phase Shifter Design

Up to the present a set of design rules linking size, coupling, structure type and class to realise the optimal ultra-wideband phase shifter has not yet been formulated. There has been no successful design or results published for a 2-18 GHz equi-ripple device. Only one researcher [17] notes that for ultra-wideband operation, it is essential to avoid section step transitions which cannot easily be accounted for in the mathematical model. This is an important fact that will be discussed in Section 3.3 in detail. The band limiting obstacle that could not be overcome was the interconnecting discontinuity at the far end of the coupled lines.

1.3. Contributions of this Thesis

It will be shown that all of these problems can be overcome by approaching the problem from an entirely different angle. By realising that a symmetric coupler has the unique property of quadrature split independent of frequency, and combining these devices in a novel configuration, an ultra-wideband differential phase shifter can be constructed [25,26]. Noting that the transitions and manufacturing tolerance will be the band limiting factor, and introducing the concept of symmetry to alleviate these effects, upper frequency limits of 20 GHz can be achieved. This unique class of microwave differential phase shifter offers superior electrical performance with respect to bandwidth, upper frequency limit, size and synthesis time.

In Chapter 2 the principle of operation of the novel ultra-wideband phase shifter will be presented. The coupler-based phase shifter and the classical Tresselt's tapered coupled-line phase shifter will be compared. In Chapter 3 the three main elements of the phase shifter are thoroughly analysed and the synthesis of each is discussed. Considerable attention is given to the unique semi-distributed splitter required to excite the coupler on both sides of the triplate centre substrate [27]. An in-depth sensitivity analysis is presented in Chapter 4 to provide insight into the sensitivity of the phase shifter's performance to manufacturing tolerances. General phase shifter synthesis guidelines are presented in Chapter 5, and processes and tolerance requirements are discussed. A typical ultra-wideband phase shifter is then synthesized and the theoretical and practical results are presented. The example is specifically chosen to be a 45° phase shifter, as the sensitivity analysis indicated this case to be the most sensitive to manufacturing tolerances. The document ends with a summary and general conclusions. All work presented in this thesis is the authors own, unless specified by means of reference.

References

[1] V. P. Meschanov, I. V. Metelnikova, and L. G. Fokeev, "Optimum synthesis of stepped phase shifters of class II", Radiotekhnika i Elektronika, vol. 28, no. 12, pp. 2341-2346, 1983.

[2] R. B. Dome, "Wideband phase shift networks", Electronics, vol. 19, pp. 112-115; Dec. 1946.

[3] S. Darlington, "Realisation of a constant phase difference", Bell Sys. Tech. J., vol. 29, pp. 94-104, Jan. 1950.

[4] H. J. Orchard, "Synthesis of wide-band two-phase networks", Wireless Eng., vol. 27, pp. 72-81, March 1950.

[5] D. K. Weaver, Jr., "Design of wide-band 90 degree phase-difference network", Proc. IRE, vol. 42, pp. 671-676, April 1954.

[6] D. G. C. Luck, "Properties of some wide-band phase-splitting networks", Proc. IRE, vol. 37, pp. 147-151, April 1949.

[7] H. Sohon, "Wide-band phase-delay circuit", Proc. IRE, vol. 41, pp. 1050-1052, Aug. 1953.

[8] E. M. T. Jones and J. T. Bolljahn, "Coupled strip-transmission-line filters and directional couplers", IRE Trans. Microwave Theory Tech., vol. MTT-4, pp 75-81, April 1956.

[9] S. B. Cohn, "Shielded coupled strip transmission line", IRE, vol. MII-3, no. 5, Oct. 1955.

[10] B. M. Schiffman "A new class of broadband microwave 90 degree phase shifters", IRE Trans. Microwave Theory Tech., vol. MTT-6, pp. 232-237, April 1958.

[11] W. J. D. Steenart, "The synthesis of coupled transmission line all-pass networks in cascades of 1 ton", IEEE Trans. Microwave Theory Tech., vol. MTT-11, pp. 23-29, Jan. 1963.

[12] C. I. Zysman and A. Matsumoto, "Properties of microwave C-sections", IEEE Trans. Circuit Theory, vol. CT-12, pp. 74-82, March 1965.

[13] E. G. Crystal, "Analysis and exact synthesis of cascaded commensurate transmission-line C-section pass networks", IEEE Trans. Microwave Theory Tech., pp. 285-291, June 1966.

[14] P. I. Richards, "Resistor transmission line circuits", Proc. IRE, vol. 36, pp. 217-220, Feb. 1948.

[15] B. M. Schiffman, "Multisection microwave phase shift network", IEEE Trans. Microwave Theory Tech., vol. MTT-14, pp. 209, April 1966.

[16] J. P. Shelton and J. A. Mosko, "Synthesis and design of wide-band equal-ripple TEM directional couplers and fixed phase shifters", IEEE Trans. Microwave Theory Tech., vol. MTT-14, pp. 462-473, Oct. 1966.

[17] C. P. Tresselt, "Broadband tapered-line phase shift networks", IEEE Trans. Microwave Theory Tech., vol. MTT-16, pp. 51-52, Jan. 1968.

[18] B. Schiek and J. Köhler, "A method for broad-band matching of microstrip differential shifters", IEEE Trans. Microwave Theory Tech., vol. 25, no. 8, pp. 666-671, Aug. 1977.

[19] V. P. Meshchanov, and A. L. Fel'dshtein, "Radiotekhnika i eletronika", vol. 18, no. 10, pp. 2039, 1976. (Radio Eng. Electron. Physics, vol. 18, no. 10, 1976)

[20] B. F. Bunimovich,, V. P. Meshchanov, and A. L. Fel'dshtein, " Radiotekhnika i elektronika," vol. 19, no. 8, pp. 1602, 1974. (Radio Eng. Electron. Physics, vol. 19, no. 8, 1974)

[21] A. L. Fel'dshtein, V. P. Meshchanov, and Yu. V. Kibirskii, "Antenny (Antennas)", Svyaz Press, Moscow, no. 21, 1975.

[22] J. L. R. Quirarte and J. Piotr Starski, "Synthesis of Schiffman phase shifters", IEEE Trans. Microwave Theory Tech., vol. 39, no.11, pp. 1885-1889, Nov. 1991.

[23] J. L. R. Quirarte and J. Piotr Starski, "Novel Schiffman phase shifters", IEEE Trans. Microwave Theory Tech., vol. 41, no. 1, pp. 9-14, Jan. 1993.

[24] V. P. Meshchanov, I. V. Metelnikova, V. D. Tupikin, and G. G. Chumaevskaya, "A new structure of microwave ultrawide-band differential phase shifter", IEEE Trans. Microwave Theory Tech., vol. 42, no. 5, pp. 762-765, May 1994.

[25] F. V. Minnaar, J. C. Coetzee and J. Joubert, "The analysis and synthesis of a novel ultra-wideband microwave differential phase shifter", in IEEE AP MTT - Symp., Pretoria, S.A., pp. 138 - 433.,Nov 1995.

[26] F. V. Minnaar, J. C. Coetzee, and J. Joubert," A novel ultra-wideband microwave differential phase shifter," IEEE Trans. Microwave Theory Tech., vol.45, pp.1249 - 1252, Aug 1997.

[27] F. V. Minnaar, J. C. Coetzee, and J. Joubert,'The development of an ultra-wideband via connected broadside coupled splitting structure," in IEEE AP MTT - Symp., Cape Town, S.A., pp.465 - 466.,Sept 1998.

CHAPTER 2. ULTRA-WIDEBAND PHASE SHIFTER PRINCIPLES OF OPERATION

2.1. Introduction

A novel class of phase shifter is discussed and the principle of operation is explained. The unique frequency-independent quadrature property of symmetric couplers is shown to be the foundation of the success of these devices. The phase-shift characteristic is related to the coupling performance by a derived set of transform equations. The same freedom with respect to bandwidth and ripple is achieved as with the coupling properties. The phase shifter is compared to the tapered Tresselt phase shifter, and the practical bandwidth-limiting obstacles are shown to be eliminated.

2.2. Proposed Novel Ultra-wideband Phase Shifter

Shelton and Mosko realised that multisection parallel coupled TEM directional couplers and phase shifters are very closely related, and published a paper [1] on the synthesis and design of wideband equal ripple TEM directional couplers and fixed phase shifters. Both components were described as four-port networks, matched at all ports. In the directional coupler, a change in relative amplitude of the outputs with respect to the inputs is achieved, while in the phase shifter, a change in the relative phase of the outputs in comparison to the inputs is achieved.

Both the coupler and phase shifter were analysed, consisting of any number of equal $\lambda/4$ centre-frequency coupled sections. The analysis was based on inter-sectional reflections, all added at a reference plane, to derive the transfer amplitude or phase characteristic of the two components. It was found that the coupling characteristic of the device is the resultant of contributions of odd harmonics in θ. The electrical length of the coupled sections is proportional to frequency. For the phase shifter, the overall phase dispersion characteristic was found to be the result of contributions of even harmonics in θ. The analysis and design tables were all based on these foundations.

Had Shelton and Mosko [1] constructed their phase shifter with the end section half the length of all the other sections, they would have found the phase shifter and coupler response to be the result of contributions by odd harmonics in θ. Both components could then be analysed and designed equivalently, and a single set of design tables would have been sufficient. Two identical phase shifters can be joined in symmetry at the high-coupling ends, producing a symmetric coupler. A simple transform then relates the coupler and phase shifter performance parameters.

Shortly after the publication of Shelton and Mosko [1], Tresselt, the founder of the non-uniform line technique application to directional couplers, suggested applying the same techniques to this class of phase shifters [2]. As with the couplers, it was realised that the spread in coupling values between adjacent sections was large enough to produce significant reactive discontinuities in practical TEM line geometries, adversely affecting VSWR and phase accuracy of the device. Tresselt's paper [2] described the design of these phase shifters, which considerably alleviates the effect by employing coupling which is continuously tapered through the length of the device. A phase shifter was designed and constructed to be a continuously tapered device, starting with the prototype from tables provided by Shelton and Mosko. The layout of a typical Tresselt phase shifter is shown in Figure 6. The design equal ripple was from 1 GHz to 11.5 GHz, but measured results deviated at the high frequency end. It was concluded that the interconnecting strap at the end of the taper added parasitic components which could not sufficiently be compensated for beyond 9 GHz.

The problem was finally overcome by the novel coupler phase shifter proposed in this thesis. By using a hybrid coupler as vector processing element, symmetry can be introduced to avoid the interconnecting strap. The phase shifter response can be extended to 20 GHz and beyond. The layout of the novel phase shifter is shown in Figure 7. Standard coupler design tables such as published by Crystal and Young [3] can be used instead of special calculated phase shifter design tables.

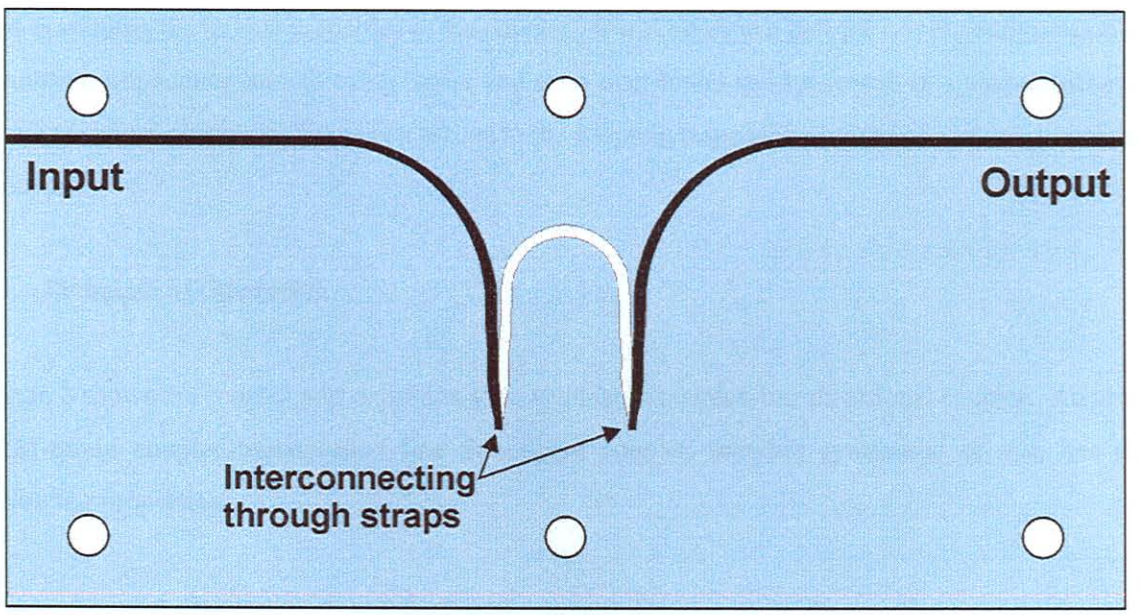

Figure 6 : Typical layout of Tresselt-based phase shifter

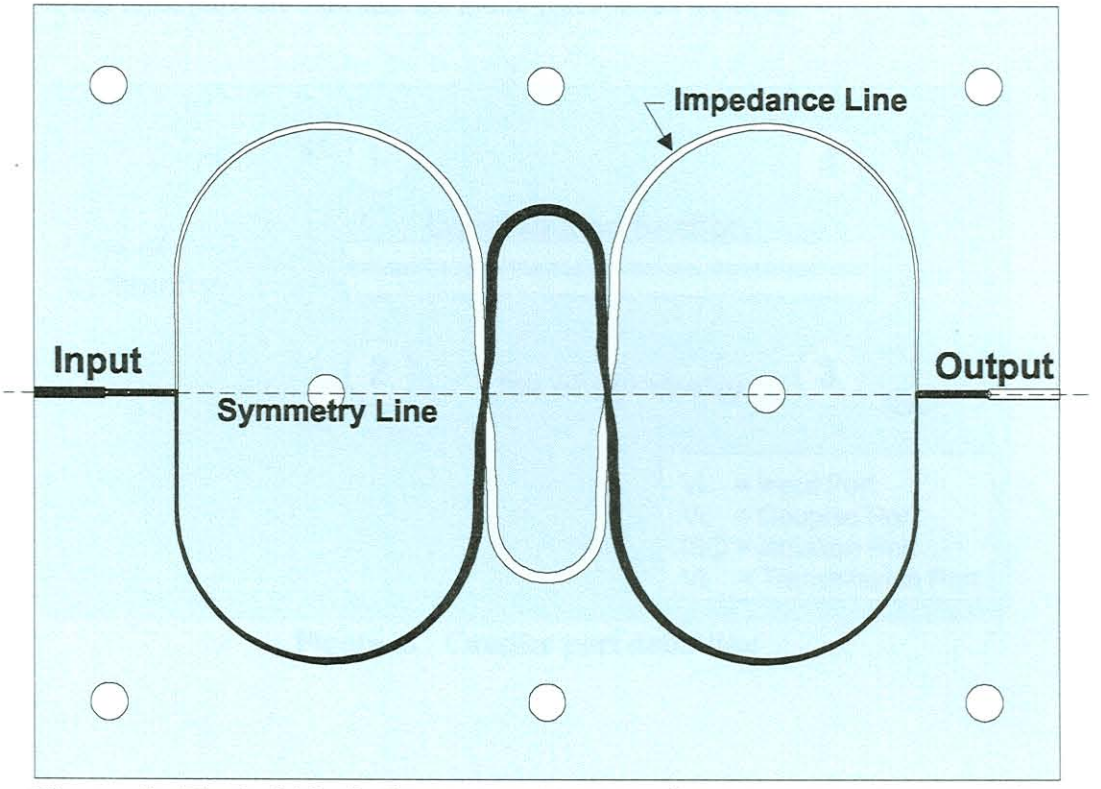

Figure 7 : Typical block diagram and layout of coupler-based phase shifter

The principle of operation of the proposed novel ultra-wideband phase shifter will be explained by first examining the unique properties of the coupler. It will be shown that the novel configuration of a coupler, impedance transforming tapers and semi-distributed splitters result in a phase shifter of which the phase characteristics can be related to the coupling response by means of a simple transform function.

2.3. Principle of Operation

Figure 8 shows the coupler port definition for a symmetric coupled-line directional coupler. An ideal TEM-mode coupled-transmission line directional coupler, whether symmetric or not, has the following properties:

- There is coupling of power from port 1 to port 2.
- There is transfer of power from port 1 to port 4.
- There is no transfer from port 1 to port 3 (isolation).

- If any three ports are matched, the fourth port appears matched.

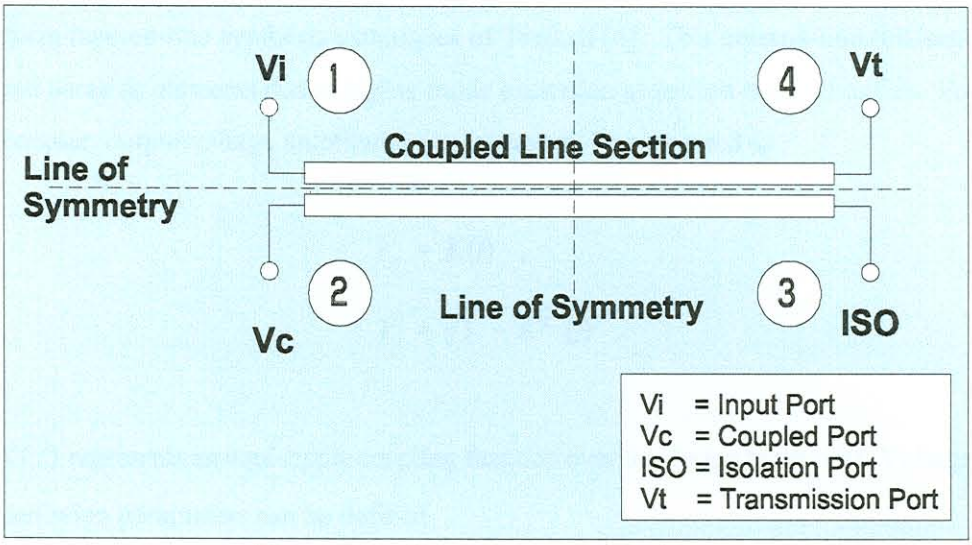

Figure 8 : Coupler port definition

Symmetric directional couplers have, in addition, the following unique and very valuable property:

- The coupled port (2) leads the transmission port (4) in quadrature at all frequencies [3, 4, 5].

This is the foundation on which the whole principle of operation is built. To fully understand the principle of operation of the phase shifter, it is necessary to review some relevant properties of symmetric directional couplers.

The coupling factor K of a coupler specifies the voltage ratio of coupled versus incident power . The coupling value (in decibel) can therefore be defined as

$$C = 20 \log (K) \quad . \tag{2.1}$$

A single section coupler only achieves this coupling coefficient over a limited band, depending on the ripple specification. However, by increasing the number of sections the bandwidth may be increased significantly. The number of sections and their coupling values depend on the bandwidth and ripple specification. Equal ripple Chebyshev multi-section coupler design tables, covering up to 20 : 1 bandwidth, have been tabulated by Crystal and Young [3].

Very high isolation and realisability into the mm-band can be achieved in stripline medium, using the non-uniform tapered-line synthesis techniques of Tresselt [4]. This tapered-line realisation avoids transitional parasitic elements due to higher mode excitation at section discontinuities. For a multi-section coupler, output voltage amplitudes can in general be expressed as

$$V_c = K(f) \quad , \tag{2.2}$$

$$V_t = \sqrt{1 - K^2(f)} \quad . \tag{2.3}$$

Where $K(f)$ represents an equi-ripple coupling function over the design bandwidth. Voltage coupling and transmission parameters can be defined

$$f_c = j e^{-j\theta} V_c \quad , \tag{2.4}$$

$$f_t = e^{-j\theta} V_t \quad . \tag{2.5}$$

Where the term $e^{-j\theta}$ accounts for the linear frequency dependant phase term caused by the physical length of the coupler. Examining the f_c and f_t functions, it is clear that f_c always leads f_t by 90°, independent of frequency. A coupler section is always a quarter wavelength long at the centre frequency. Symmetric couplers always have an odd number of sections. For a higher fractional bandwidth, more sections should be added to the coupler. As more sections are added to a wideband coupler of fixed lower cutoff frequency, the bandwidth and centre frequency are increased at roughly the same rate. As the centre frequency increases, the section lengths decrease. The physical length of a multi-sectional coupler therefore depends only on the lower cutoff frequency. The bandwidth and ripple (coupling deviation) is therefore fixed by the coupling nature of the device along its length.

For stripline couplers, the maximum achievable coupling over a broad band is practically about -6 dB. By connecting couplers in tandem, however, any coupling level can be achieved without compromising bandwidth or ripple. The electrical behaviour of a single ideal coupler as shown in Figure 9 may be described by an *S*-matrix

$$\begin{bmatrix} b_1 \\ b_2 \\ b_3 \\ b_4 \end{bmatrix} = \begin{bmatrix} 0 & f_c & 0 & f_t \\ f_c & 0 & f_t & 0 \\ 0 & f_t & 0 & f_c \\ f_t & 0 & f_c & 0 \end{bmatrix} \cdot \begin{bmatrix} a_1 \\ a_2 \\ a_3 \\ a_4 \end{bmatrix}, \tag{2.6}$$

where the f_c and f_t functions are as defined before in (2.4) and (2.5). The couplers discussed here may be single section narrow-band, or wideband tapered-line devices, in which case the coupling factors $K(f)$ in equations (2.2) and (2.3) become equi-ripple coupling functions. To interconnect the right ports of tandem connected couplers, it is necessary to cross the coupled lines as shown in Figure 9. From the figure it is also clear that the tightest coupling is in the middle of the coupler, and the slackest at the ends. Single section couplers, however, have the same coupling throughout the length of coupled lines such as shown in Figure 8.

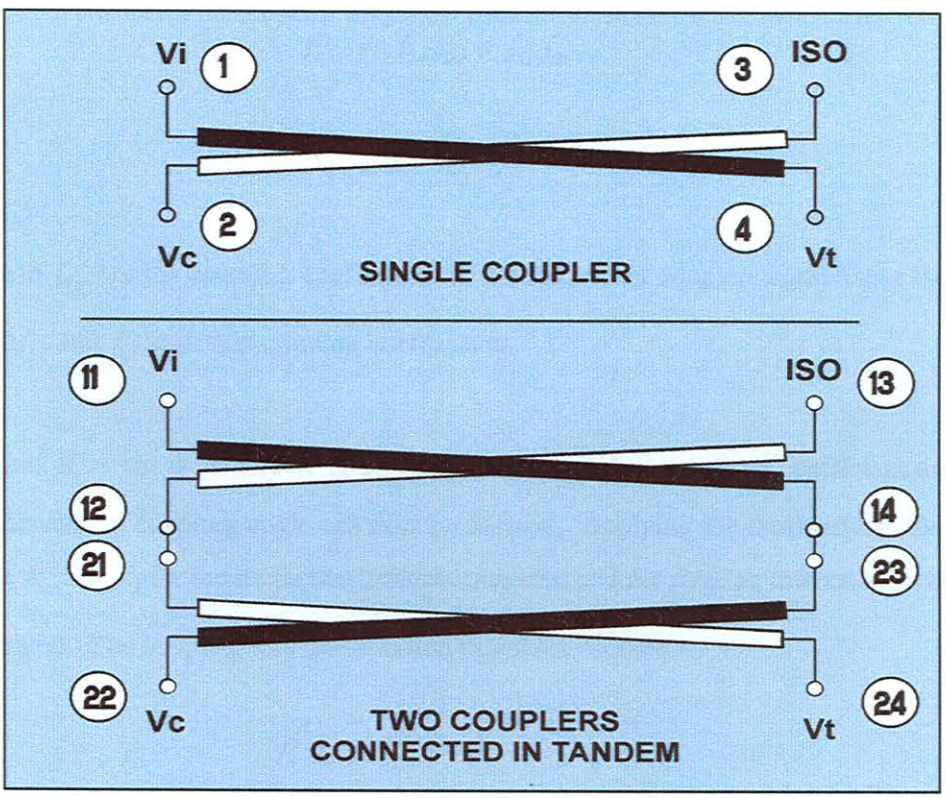

Figure 9 : Single and tandem connected couplers

Classical coupler theory can be presented in an alternative form to clarify the phase shifter principles. Let f_c' and f_t' represent the effective coupling and transmission coefficients of the tandem-connected coupler. Referring to Figure 9 it can be shown (Appendix A) that for the tandem-coupled case, the *S*-matrix becomes

$$\begin{bmatrix} b_{11} \\ b_{22} \\ b_{13} \\ b_{24} \end{bmatrix} = \begin{bmatrix} 0 & f_c' & 0 & f_t' \\ f_c' & 0 & f_t' & 0 \\ 0 & f_t' & 0 & f_c' \\ f_t' & 0 & f_c' & 0 \end{bmatrix} \cdot \begin{bmatrix} a_{11} \\ a_{22} \\ a_{13} \\ a_{24} \end{bmatrix} . \tag{2.7}$$

The tandem connected *S*-parameters f' can be written in terms of the separate coupler *S*-parameters f as

$$f_c' = f_{1c} f_{2c} + f_{1t} f_{2t} \ , \tag{2.8}$$

$$f_t' = f_{1c} f_{2t} + f_{1t} f_{2c} \ , \tag{2.9}$$

where f_{1c} and f_{2c} are the coupling coefficients of the individual couplers comprising the tandem coupler, and f_{1t} and f_{2t} their transmission coefficients.

The transform $K = \sin \phi$, where K is the frequency-dependent coupling coefficient and ϕ the frequency-dependent coupling angle can now be defined. Applying the transform to the original definition of V_c and V_t for the single and tandem-connected coupler case, an interesting concept can be demonstrated. The coupling and transmission functions become

$$f_c = j e^{-j\theta} \sin \phi \ , \tag{2.10}$$

$$f_t = e^{-j\theta} \cos \phi \ , \tag{2.11}$$

and for the tandem connected case in Figure 9, we find after substitution in equations (2.8) and (2.9) and simplifying,

$$f_c' = j e^{-j\theta} \sin(\phi_1 + \phi_2) \quad , \tag{2.12}$$

$$f_t' = e^{-j\theta} \cos(\phi_1 + \phi_2) \quad . \tag{2.13}$$

It can also be shown that, for n tandem-connected couplers of equal bandwidth,

$$f_{cn} = j e^{-j\theta} \sin(\phi_1 + \phi_2 + \ldots + \phi_n) \quad , \tag{2.14}$$

$$f_{tn} = e^{-j\theta} \cos(\phi_1 + \phi_2 + \ldots + \phi_n) \quad . \tag{2.15}$$

Therefore, adding equal-bandwidth couplers in tandem means adding their coupling angles. The compound coupling coefficient can then be calculated as follows: For couplers with individual coupling angles ϕ_1, ϕ_2 ... ϕ_n, the composite coupling angle with all connected in tandem, becomes

$$\phi_t = \phi_1 + \phi_2 \ldots + \phi_n \quad . \tag{2.16}$$

The resulting coupling coefficient becomes

$$K_t = \sin \phi_t \quad , \tag{2.17}$$

and the coupling decibel value is

$$C_t = 20 \log K_t \quad . \tag{2.18}$$

Another important result is that the coupling angle ripple, or tolerance, of identical tandem-connected couplers, can also be added. If, for two couplers to be connected in tandem,

$$\phi_1 = \phi_{01} \pm \delta\phi_1 \quad , \tag{2.19}$$

$$\phi_2 = \phi_{02} \pm \delta\phi_2 \quad . \tag{2.20}$$

Then the tandem connected couplers would yield a coupling angle of

$$\phi_t = (\phi_{01} + \phi_{02}) \pm (\delta\phi_1 + \delta\phi_2) \quad , \tag{2.21}$$

where ϕ_{01} and ϕ_{02} are the mean values, and $\delta\phi_1$ and $\delta\phi_2$ the ripple values of coupler 1 and coupler 2 respectively. Therefore, this forms a new coupler of added mean and ripple coupling angle values. The mean coupler angle and coupling coefficient can be related by the next equation:

$$C_0 = 20\log\left[\sin(\phi_0)\right] \quad . \tag{2.22}$$

The ripple-added values are defined by the following equation:

$$C_0 + \delta C = 20\log\left[\sin(\phi_0 + \delta\phi)\right] \quad . \tag{2.23}$$

and substituting equation (2.22) in (2.23), and solving for δC, yields

$$\delta C = 20\log\left[\frac{\sin(\phi_0 + \delta\phi)}{\sin(\phi_0)}\right] \quad . \tag{2.24}$$

It can also be demonstrated that by employing more couplers in tandem, the mean coupling value (C_0) and ripple specification (δC) of each individual coupler slackens, where C_0 and δC are the mean and ripple coupling values in dB, respectively. For n identical tandem-connected couplers, the resultant ripple coupling value is therefore

$$\delta C_n = 20\log\left[\frac{\sin(n\phi_0 + n\delta\phi)}{\sin(n\phi_0)}\right] \quad . \tag{2.25}$$

While the output phasors are always in perfect quadrature, their amplitude ratio depends on the coupling factor K. It follows directly from the principle of energy conservation that if one phasor amplitude increases, the other phasor amplitude will decrease. Therefore, the coupling ripple is amplitude- superimposed on these phasors and will be 180° out of phase, conserving input energy. These vectors are presented in Figure 10.

Realising this unique and important condition, phase shifters with ultra-wideband coverage can be synthesized [6,7]. A phase shifter is formed when the output voltages V_c and V_t of a coupler are vector-added and the result compared to the input of the coupler:

$$f_o = f_c + f_t \quad , \tag{2.26}$$

$$= e^{-j\theta}\cos\phi + j\, e^{-j\theta}\sin\phi \quad , \tag{2.27}$$

$$= 1\, e^{j\phi} e^{-j\theta} \quad . \tag{2.28}$$

Comparing the result to a reference line of electrical length θ, as is in the case of differential phase shifters, the term $e^{-j\theta}$ falls away. Therefore, if the output ports of a ϕ coupling-angle coupler are hard-wired, the output provides a vector with a phase shift ϕ relative to a reference line of same electrical length over the device bandwidth. The coupling angle ripple $\delta\phi$ becomes the phase shift ripple. To add phase shift ϕ^+, a coupler of coupling angle ϕ^+ must be added in tandem. By splitting the input signal and exciting both the input and isolated port with identical signals, a symmetric phase shifter evolves as shown in Figure 11. This improves high frequency operation due to the fact that the effect of small manufacturing errors tend to cancel in symmetric networks. This can be explained by the observation that errors generally occur in both phasors and do not contribute to phase shift errors of the combined result. This principle is demonstrated in APPENDIX B.

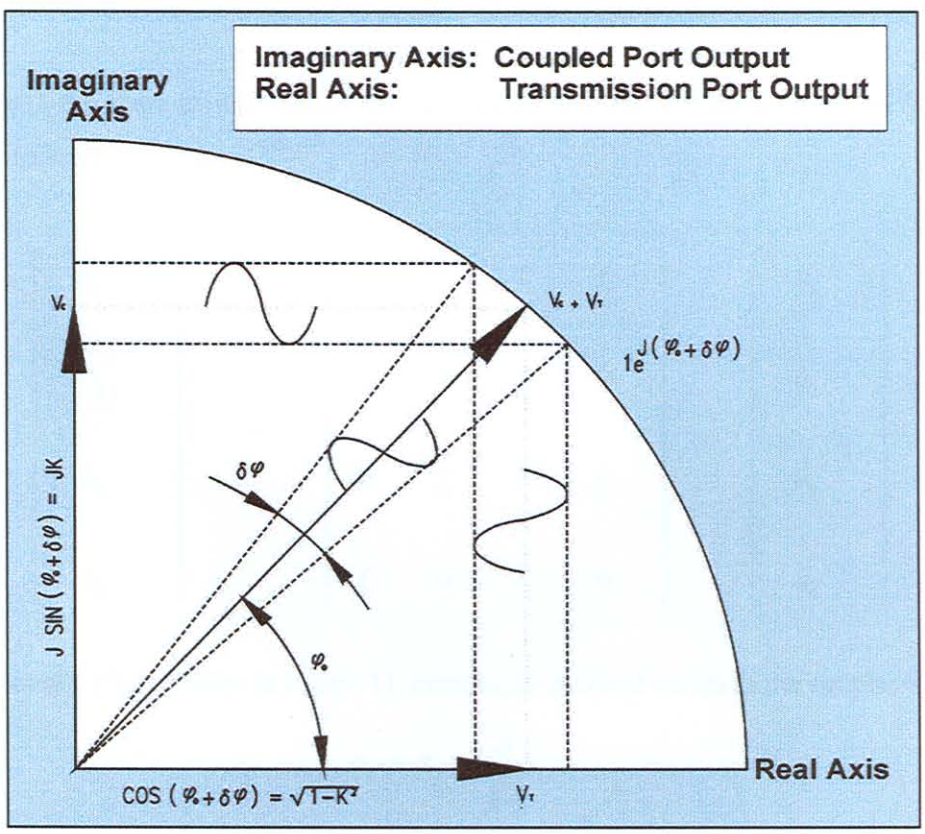

Figure 10 : Vector representation of coupler response

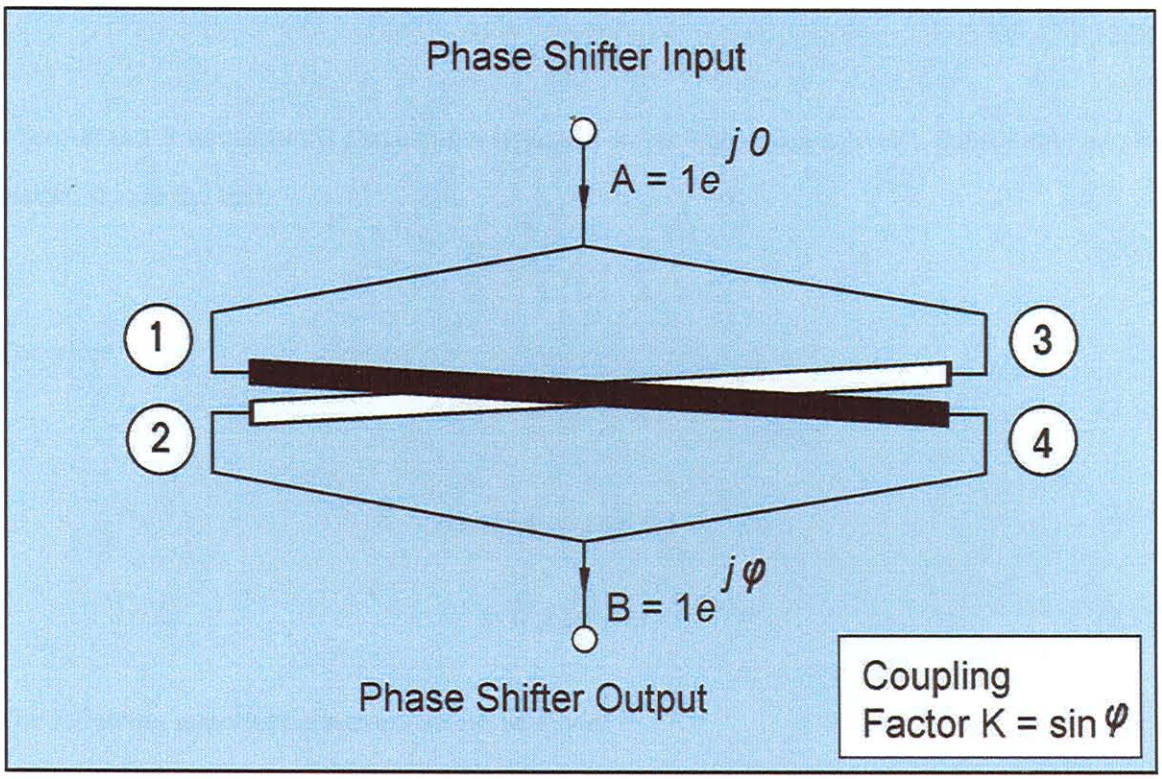

Figure 11 : Symmetric phase shifter

From Figure 11 the phase shifter transfer function can be derived. For the coupler, the *S*-parameter matrix is as follows:

$$\begin{bmatrix} b_1 \\ b_2 \\ b_3 \\ b_4 \end{bmatrix} = \begin{bmatrix} 0 & f_c & 0 & f_t \\ f_c & 0 & f_t & 0 \\ 0 & f_t & 0 & f_c \\ f_t & 0 & f_c & 0 \end{bmatrix} \cdot \begin{bmatrix} a_1 \\ a_2 \\ a_3 \\ a_4 \end{bmatrix} \qquad (2.29)$$

For the symmetric phase shifter in Figure 11, assume the incident waves to the coupler to be

$$a_1 = a_3 = \frac{A}{\sqrt{2}}, \qquad (2.30)$$

and the waves exiting the coupler to be

$$b_2 = b_4 = \frac{B}{\sqrt{2}} \quad , \tag{2.31}$$

where A and B represent the phase shifter input and output signals respectively. Substituting into the matrix, it is found that

$$\frac{B}{2} = \frac{A}{2} f_c + \frac{A}{2} f_t \quad . \tag{2.32}$$

Therefore

$$B = A(f_c + f_t) \quad , \tag{2.33}$$

$$B = A(\cos\phi + j\sin\phi)\, e^{-j\theta} \quad , \tag{2.34}$$

$$B = A e^{j\phi} e^{-j\theta} \quad . \tag{2.35}$$

The following important observations can be made:

- The circuit is throughout matched from point to point and operate reflection less.
- There is theoretically no energy loss, because $|B/A| = 1$.
- The frequency dependant term $e^{-j\theta}$ is balanced out by the reference line.
- The transfer function reflects a phase difference ϕ which is the coupling angle of the coupler.

Therefore, in principle, a lossless phase shifter with phase shift characteristics similar in shape and bandwidth to the coupling nature of the coupler has been constructed. The phase shift and coupling values can be related with a simple transform equation.

References

[1] J. P. Shelton and J. A. Mosko, "Synthesis and design of wide-band equal-ripple TEM directional couplers and fixed phase shifters", IEEE Trans Microwave Theory Tech., vol. MTT-14, no. 10, pp. 462-473, Oct. 1966.

[2] C. P. Tresselt, "Broadband tapered-line phase shift networks", IEEE Trans. Microwave Theory Tech., vol. MTT-16, pp. 51-52, Jan. 1968.

[3] E. G. Crystal and L. Young, "Theory and tables of optimum symmetric TEM-mode coupled-transmission-line directional couplers", IEEE Trans Microwave Theory Tech., vol. 13, no. 5, pp. 544-558, Sept. 1965.

[4] C. P. Tresselt, "The design and construction of broadband high-directivity, 90-degree couplers using non-uniform line techniques", IEEE Trans Microwave Theory Tech., vol. 14, no. 12, pp. 647-656, Dec. 1966.

[5] J. A. G.Malherbe,"Microwave transmission line couplers", Artech House, Norwood, 1988.

[6] F. V. Minnaar, J. C. Coetzee, and J. Joubert,"The analysis and synthesis of a novel ultra - wideband microwave differential phase shifter", in IEEE AP MTT - Symp., Pretoria, S.A., pp.138-433, Nov 1995.

[7] F. V. Minnaar, J. C. Coetzee, and J. Joubert,"A novel ultra - wideband microwave differential phase shifter," IEEE Trans. Microwave Theory Tech., vol. 45, pp.1249 - 1252, Aug 1997.

CHAPTER 3. DESIGN AND ANALYSIS OF PHASE SHIFTER ELEMENTS

3.1. Introduction

The newly proposed coupler based phase shifter consists of three basic building blocks or elements, namely a splitter, tapered-line impedance transformers and a coupler. The function of the splitter is to divide the incoming signal into equal amplitude and phase vectors (or twins) and to transfer one of these signal parts to the other side of the middle slab of the tri-plate structure. A second splitter recombines the resultant equal phasors at the output of the device to conserve energy. The coupler combines the two vectors in such a way that the output vectors have a fixed amplitude ratio and quadrature difference. After vector addition, the phase shift depends on the coupling nature of the coupler. The function of the four $\sqrt{2}:1$ transformer tapers is to match the phase shifter input and output ports to the coupler. The transformers could be neglected if the input impedance level could be reduced to half the coupler internal impedance level. This is impractical, however, because the centre high-coupling-value section of the coupler will become too narrow to etch accurately. These elements will be analysed in detail to reveal the nature and limitations to the performance of the phase shifter. The results will also be used in the sensitivity and tolerance analysis, which will follow in Chapter 4.

First, the sensitivity of asymmetric spaced stripline devices is investigated. Then the tapered-line transformers are analysed and the sensitivity of exponential tapers to tolerance variations is calculated. The analysis and synthesis of stripline couplers then follows. Special attention is paid to the semi-distributed stripline splitter. First, broadside coupled stripline properties and the nature of the via interconnection is analysed with a full-wave analysis procedure. After that, the single and multiple-via splitting structure is analysed and the resonance properties are investigated. The *S*-parameters of the splitter is derived and practical considerations are discussed. The chapter ends with general conclusions.

3.2. Tapered Stripline Impedance Transformers

Before the tapered-line impedance transformer design is discussed it is essential to investigate the sensitivity of the conduction medium of this element to manufacturing tolerance. Therefore, the sensitivity of asymmetric spaced stripline devices is first discussed in paragraph 3.2.1. Then the tapered line transformer design is discussed in paragraph 3.2.2 and an investigation into the sensitivity of these tapers to manufacturing tolerances follows in paragraph 3.2.3.

3.2.1. Sensitivity of Asymmetric Spaced Stripline Structures

There is a need to know the effect of variation in some parameters in the characterization of the transmission structures, such as the 50 Ω lines and the 50 Ω - 100 Ω impedance transforming tapers of a phase shifter. It is assumed that the line and tapers are realised in asymmetric-spaced stripline conductors such as shown in Figure 12.

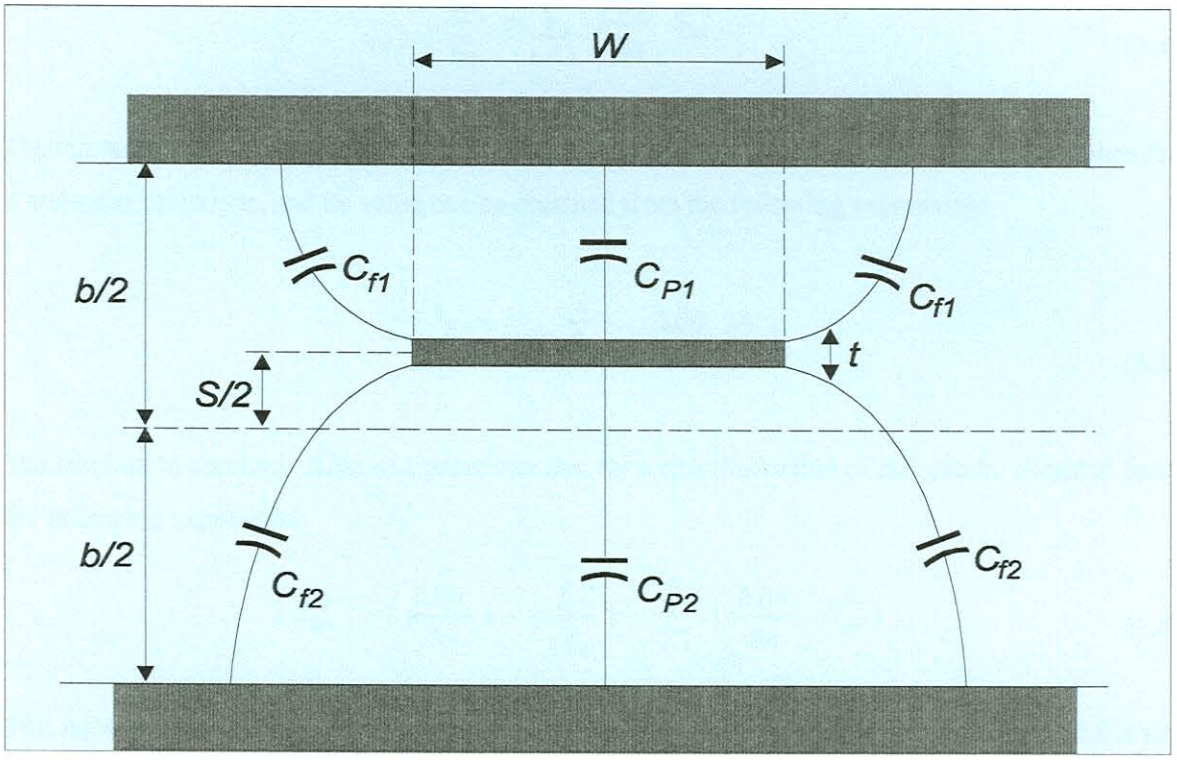

Figure 12 : Cross section of asymmetric spaced stripline devices

The normalized sensitivity of a function F with respect to a parameter x is defined as [1]

$$S_x^F = \lim_{\Delta x \to o} \frac{\Delta F/F}{\Delta x/x} , \tag{3.1}$$

$$= \frac{x}{F} \cdot \frac{\partial F}{\partial x} . \tag{3.2}$$

This is the ratio of the fractional change in the function F to the fractional change in the parameter x, referred to as the normalized sensitivity. The change in impedance ΔZ of a transmission line is related to the tolerance ΔB in parameter B by

$$\frac{\Delta Z}{Z_0} = \frac{\Delta B}{B} S_B^{Z_0} \quad , \tag{3.3}$$

where Z_0 is the impedance with ΔB equal to zero. When Z_0 is a function of several independent variables Bn, where $n = 1, 2 \ldots N$. The total change in Z_o is given by

$$\frac{\Delta Z}{Z_0} = \sum_{n=1}^{N} \frac{\Delta Bn}{Bn} S_{Bn}^{Z_0} \quad . \tag{3.4}$$

The tolerance ΔBn leads to a spread in value of ΔZ. The largest possible value of ΔZ determines the worst-case behaviour, and its value can be obtained from the following expression:

$$\frac{(\Delta Z)_{MAX}}{Z_0} = \pm \sum_{n=1}^{N} \left| \frac{\Delta Bn}{Bn} S_{Bn}^{Z_0} \right| \quad . \tag{3.5}$$

The fabrication accuracy ΔBm of a parameter Bm, for a specified value of ΔZ, can be obtained from the following expression:

$$\left| S_{Bm}^{Z_0} \right| \cdot \left| \frac{\Delta Bm}{Bm} \right| = \left| \frac{\Delta Z}{Z_0} \right| - \sum_{n \neq 1}^{N} \left| \frac{\Delta Bn}{Bn} \cdot S_{Bn}^{Z_0} \right| \quad . \tag{3.6}$$

This equation holds when the right-hand side is positive, otherwise the specified value of ΔZ is not realisable with the given set of ΔBn values. This analysis is useful in determining the trade-off between the tolerances and the performances. Before calculating the sensitivities of asymmetric spaced stripline structures, the impedance properties of these structures are reviewed. The impedance of asymmetric spaced stripline devices can be stated as follows (see Figure 12) [2]

$$Z_0 = \frac{120\pi}{\sqrt{\epsilon_r}} \cdot \frac{1}{C/\epsilon} \quad , \tag{3.7}$$

where

$$C/\epsilon = C_{P1}/\epsilon + C_{P2}/\epsilon + 2\, C_{f1}/\epsilon + 2\, C_{f2}/\epsilon \quad . \tag{3.8}$$

The total conductor unit-length capacitance C/ϵ is comprised of plate capacitances C_{P1}/ϵ and C_{P2}/ϵ and the fringe fields C_{f1}/ϵ and C_{f2}/ϵ. The fringe fields can be calculated from

$$C_{fi}/\epsilon = \frac{1}{\pi}\left[2\,\xi_i \ln(\xi_i + 1) - (\xi_i - 1)\ln(\xi_i^{\,2} - 1)\right] , \tag{3.9}$$

where

$$\xi_1 = \frac{1}{1 - \dfrac{t}{b - s}} , \tag{3.10}$$

and

$$\xi_2 = \frac{1}{1 - \dfrac{t}{b + s}} . \tag{3.11}$$

The plate capacitances can be calculated from the following equations:

$$C_{P1}/\epsilon = \frac{\dfrac{2w}{b - s}}{1 - \dfrac{t}{b - s}} , \tag{3.12}$$

and

$$C_{P2}/\epsilon = \frac{\dfrac{2w}{b + s}}{1 - \dfrac{t}{b + s}} . \tag{3.13}$$

For symmetric spaced stripline devices, the equation for Z_0 simplifies to

$$Z_0 = \frac{120\pi}{\sqrt{\epsilon_r}}\left[\frac{w}{b - t} + C_f/\epsilon\right]^{-1} , \tag{3.14}$$

and

$$C_f/\epsilon \fallingdotseq \frac{\ln(4)}{\pi} \qquad \text{for } t \ll b . \tag{3.15}$$

According to Getsinger [3], the width must be compensated for the loss of fringe field capacitances when

$$\frac{w}{b - t} \leq 0.35 . \tag{3.16}$$

The new width must become

$$w'/b = \frac{1}{1.2}\left[0.07\left(1 - \frac{t}{b}\right) + \frac{w}{b}\right] . \tag{3.17}$$

In a typical case where 5 mil substrate is sandwiched between two 20 mil substrates, this compensation adds 1 μm at 75Ω ($\pm$ 0. 4 mm) and gradually increases to a maximum of 50 μm where w approaches 0 (infinite impedance line). Since the effects of compensation is negligible in the tolerance analysis, it is neglected. The sensitivity of Z_0 with respect to $x = w, b, s, t$ and ϵ_r, may be calculated as follows:

$$S_x^{Z_0} = \frac{x}{Z_0} \cdot \frac{\partial Z_0}{\partial x} \quad , \tag{3.18}$$

$$= \frac{x}{120\pi} \cdot \sqrt{\epsilon_r} \cdot C/\epsilon \cdot \frac{\partial Z_0}{\partial x} \quad . \tag{3.19}$$

If $x = \epsilon_r$ then the sensitivity of the line impedance to the dielectric constant ϵ_r becomes

$$S_{\epsilon_r}^{Z_0} = -\,½ \quad \text{since} \quad \frac{\partial}{\partial \epsilon_r}\left[C/\epsilon \right] = 0 \quad . \tag{3.20}$$

If $x = w, b, s, t$ then we calculate (3.18) as

$$S_x^{Z_0} = \frac{-x}{C/\epsilon} \cdot \frac{\partial}{\partial x}\left[C/\epsilon \right] \quad . \tag{3.21}$$

Substituting equation 3.7 into 3.21, it is found that

$$S_x^{Z_0} = \frac{-xZ_0\sqrt{\epsilon_r}}{120\pi} \cdot \frac{\delta}{\delta x}\left[C/\epsilon \right] \quad . \tag{3.22}$$

From the definition of tolerance analysis in equation (3.3), it follows that

$$\Delta Z_0 = \Delta x \cdot \left[S_x^{Z_0} \cdot \frac{Z_0}{x} \right] \quad . \tag{3.23}$$

Equation 3.22 can be expanded to yield the following sensitivity equation:

$$S_x^{Z_0} = \frac{-x}{C/\epsilon}\left[\frac{\partial}{\partial x} C_{P1}/\epsilon + \frac{\partial}{\partial x} C_{P2}/\epsilon + 2\,\frac{\partial}{\partial x} C_{f1}/\epsilon + 2\,\frac{\delta}{\delta x} C_{f2}/\epsilon \right] \quad . \tag{3.24}$$

The following constants are defined, to simplify the expressions for the sensitivity analysis

$$A = \frac{1}{b - s - t} \qquad B = \frac{1}{b + s - t} \quad , \tag{3.25}$$

$$M = \frac{2/\pi}{(b - s - t)^2} \ln\left[2\left(\frac{b - s}{t}\right) - 1\right] \quad , \tag{3.26}$$

$$N = \frac{2/\pi}{(b + s - t)^2} \ln\left[2\left(\frac{b + s}{t}\right) - 1\right] \quad , \tag{3.27}$$

$$X = C_{f1}/\epsilon + C_{f2}/\epsilon \quad . \tag{3.28}$$

The sensitivity of the line impedance to the various parameters are then calculated as

$$S_{\epsilon_r}^{Z_0} = -\tfrac{1}{2} \quad , \tag{3.29}$$

$$S_t^{Z_0} = \frac{-t}{C/\epsilon} \cdot \left[2w\,(A^2 + B^2) + (b - s)\,M + (b + s)\,N\right] \quad , \tag{3.30}$$

$$S_w^{Z_0} = \frac{-2w}{C/\epsilon} \cdot \left[A + B\right] \quad , \tag{3.31}$$

$$S_s^{Z_0} = \frac{-s}{C/\epsilon} \cdot \left[2w\,(A^2 - B^2) + t\,(M - N)\right] \quad , \tag{3.32}$$

$$S_b^{Z_0} = \frac{-b}{C/\epsilon} \cdot \left[-2w\,(A^2 + B^2) - t\,(M + N)\right] \quad , \tag{3.33}$$

where

$$\frac{1}{C/\epsilon} = \frac{\sqrt{\epsilon_r}\,Z_0}{120\pi} \quad , \tag{3.34}$$

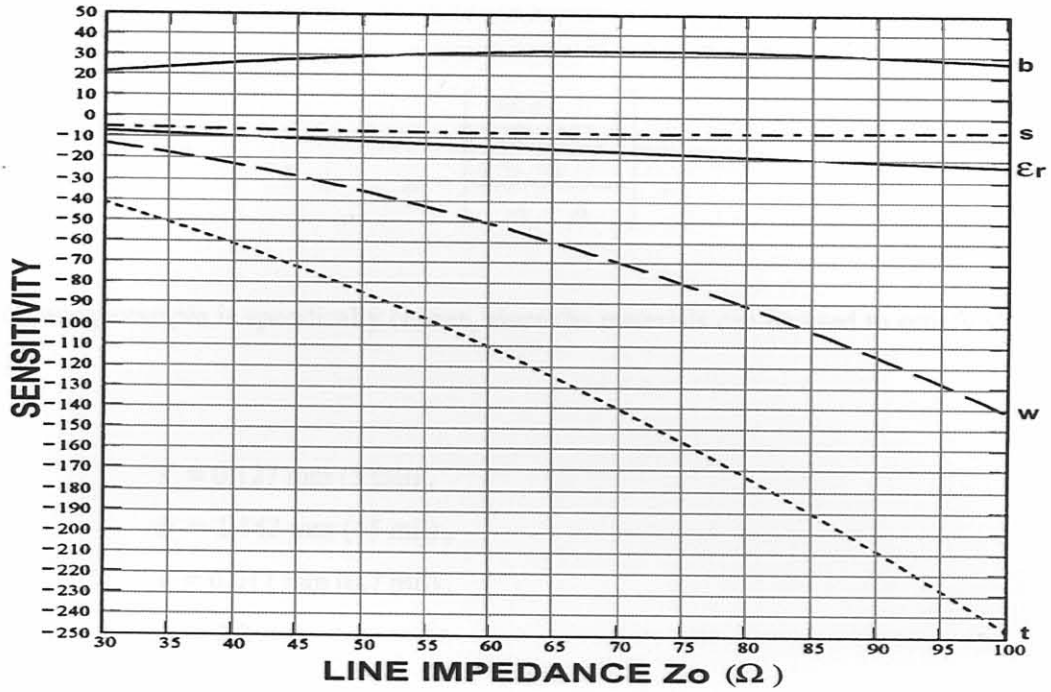

Figure 13 : Sensitivity of asymmetric spaced stripline

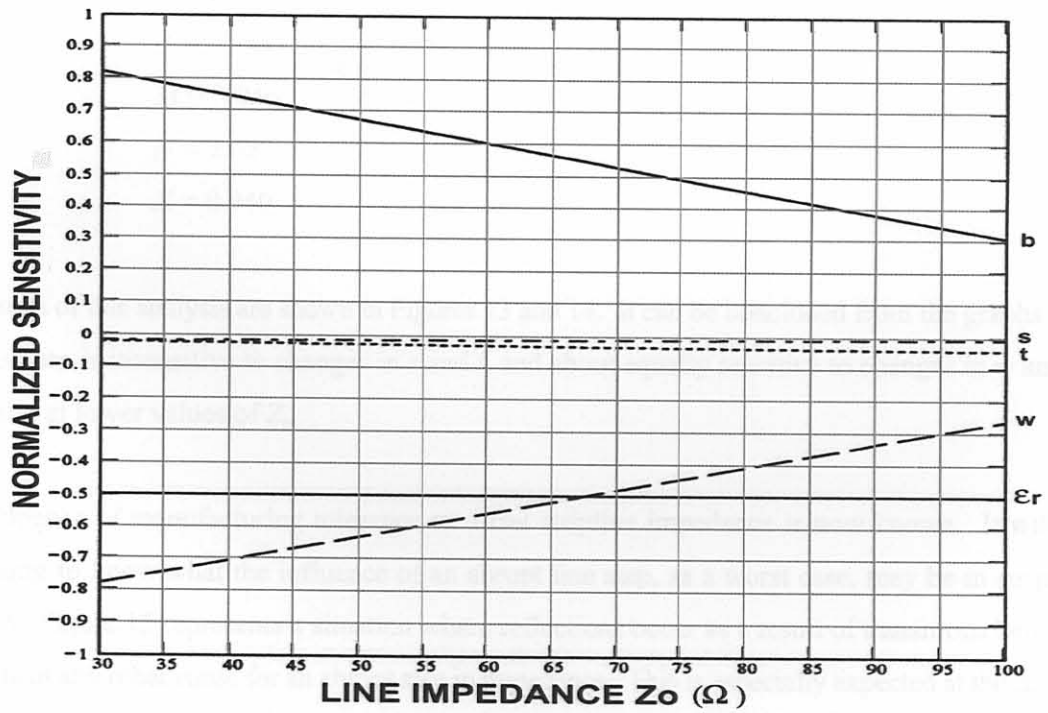

Figure 14 : Normalized sensitivity of asymmetric spaced stripline

and

$$w = \left[\frac{\frac{60\pi}{\sqrt{\epsilon_r}\, Z_0} - X}{A + B} \right] . \tag{3.35}$$

The following example is specifically chosen, since the materials can be used to satisfy almost all designs:

$s = 0.127$ mm (5 mil),
$b = 1.143$ mm (45 mil),
$t = 0.017$ mm (0.7 mil),
$\epsilon_r = 2.2$.

The previously defined constants, equations (3.25) - (3.28) are then:

$A = 1.001$
$B = 0.798$
$M = 3.046$
$N = 2.027$
$X = 0.940$

The results of this analysis are shown in Figures 13 and 14. It can be concluded from the graphs that the structure is insensitive to changes in s and t, and about equally sensitive to changes in w and b, especially at lower values of Z_0.

The influence of manufacturing tolerance to offset stripline impedance is now known. It will be interesting to know what the influence of an abrupt line step, as a worst case, may be in stripline medium. Figure 15 represents a situation where reflections occur as a result of transitions between elements or any other cause for an abrupt step in impedance. This is especially expected at the splitter ports, since the impedance tapers can be connected to the couplers in a smooth transition.

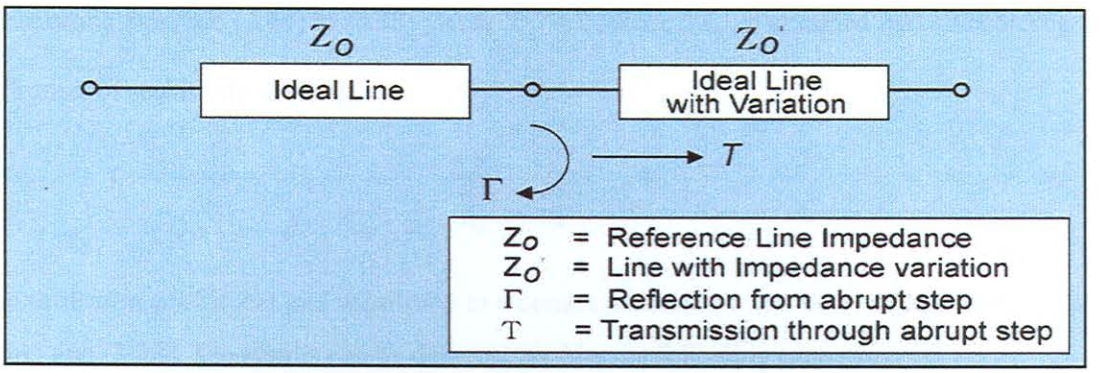

Figure 15 : Reflections due to an abrupt impedance step

Let the reflection and transmission coefficients be defined as

$$\Gamma = \frac{Z_0' - Z_0}{Z_0' + Z_0} \quad , \tag{3.36}$$

$$T = 1 + \Gamma = \frac{2\,Z_0'}{Z_0' + Z_0} \quad . \tag{3.37}$$

The error vector can be described as

$$V_e\, e^{j\Psi e} = T - 1 = \Gamma \quad . \tag{3.38}$$

Substituting (3.36) into (3.38) yields

$$V_e\, e^{j\Psi e} = \frac{Z_0' - Z_0}{Z_0' + Z_0} \quad , \tag{3.39}$$

where

$$Z_0' = Z_0 + \Delta Z_0 \quad . \tag{3.40}$$

Therefore, substituting (3.40) in (3.36) and simplifying, yields

$$\Gamma = \frac{\left(\frac{\Delta Z_0}{Z_0}\right)}{2 + \left(\frac{\Delta Z_0}{Z_0}\right)} \quad . \tag{3.41}$$

Substituting equation (3.41) in (3.38) yields $\Psi_e = 0$, since ΔZ_0 is assumed real. According to the definition of sensitivity in (3.3),

$$\frac{\Delta Z_0}{Z_0} = \frac{\Delta x}{x} \cdot S_x^{Z_0} \quad . \tag{3.42}$$

The reflection coefficient and sensitivity to a certain parameter x can be evaluated using equations (3.41) and (3.42). The results can be demonstrated by the following examples:

- A change of 10% in the ϵ_r parameter causes a -33 dB reflection coefficient, independent of Z_0.
- A change of 10μm in t causes a -38 dB reflection for 100 Ω lines, and -44 dB reflection for 30 Ω lines.
- A change of +0.2 mm in w causes a -15 dB reflection for 100 Ω lines and -28 dB reflection for 30 Ω lines. A negative change in w provides a slightly better situation.
- A change of 0.05 mm in s causes a -48 dB reflection for 30 Ω lines and -57 dB for 100Ω lines.
- A change of 0.1 mm in b causes a -29 dB reflection for 30 Ω lines and a -38 dB reflection or 100 Ω lines.

3.2.2. Tapered-Line Transformer Design

We now present the design of the tapered-line impedance transformers. The reflection coefficient from any tapered line, assuming small internal reflections, can be described by the following integral [4]:

$$\Gamma = \tfrac{1}{2} \int_0^L e^{-j2\beta z} \cdot \frac{d}{dz} (\ln Z)\, dz \quad . \tag{3.43}$$

where L represents the taper length, z the distance variable along the taper, and Z the taper impedance as a function of z. The best choice of taper would be the well-known Klopfenstein taper [5], since it has a minimum equal ripple reflection coefficient magnitude in the pass band for a specified taper length. RP Hecken [6] offers design procedures for a "near-optimum" taper, which avoids the small impedance steps required by the optimum taper at the ends of the taper. These steps could possibly add asymmetric parasitic components at the coupler inputs, and should be avoided.

To relieve the phase shifter designer of time-consuming taper synthesis, the straight-forward exponential taper is recommended. In an exponential taper the impedance is tapered in an exponential fashion along the length of the device. This also considerably simplifies the sensitivity and tolerance analyses of the taper. Due to internal reflections, a tapered line is not entirely dispersionless. However, test results in chapter 5 suggest that this effect is small enough to approximate linear behaviour and allow compensation via the reference line. For exponential tapers, the normalized impedance takes the form

$$Z(z) = \alpha^{z/L} \qquad \text{where} \qquad \alpha = Z_2/Z_1 \ . \tag{3.44}$$

Substitution in the integral (3.43), and simplification yields

$$\Gamma = \tfrac{1}{2}\, e^{-j\beta L} \cdot \ln \alpha \cdot \left[\frac{\sin(\beta L)}{\beta L}\right] \ . \tag{3.45}$$

For a 50-100 Ω taper, equation (3.45) yields

$$|\Gamma|\,(dB) = 20 \log\left[\ln\sqrt{2} \cdot \frac{\sin(\pi x)}{\pi x}\right] , \tag{3.46}$$

where

$$x = \frac{2L}{\lambda} \ . \tag{3.47}$$

The theoretical reflection minima occur where $\beta L = n\pi$ ($n = 1, 2, 3 \ldots$), and maxima where $\beta L = 0$ and $\beta L = m$ ($m = 3, 5, 7 \ldots$). The maximum reflection occurs (out of band) at 0GHz and is theoretically -9.2dBc. The maximum in-band reflection occurs at 3GHz and is expected to be -22.6dBc, as seen in Figure 16.

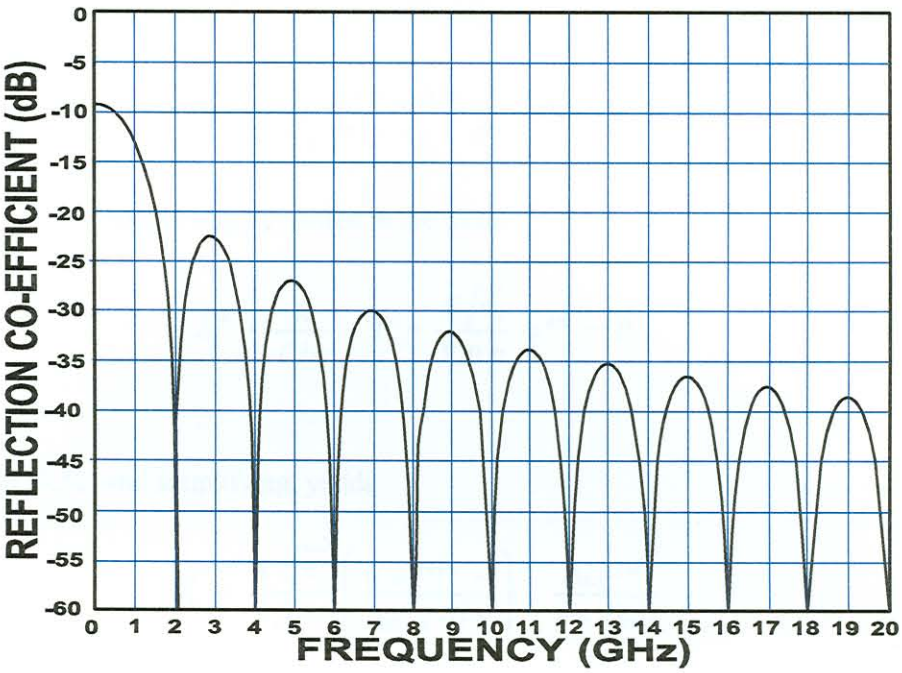

Figure 16 : Impedance taper theoretical reflection coefficient

It can be concluded therefore that the reflection maxima is exceptionally low, even at the highest in-band lobe (lobe #2). The taper length can be related to lower cutoff frequency as

$$L\ (f_L) = \frac{\lambda_L}{2} = \frac{C}{2\sqrt{\epsilon_r}\, f_L} \quad , \tag{3.48}$$

$$L = \frac{150}{\sqrt{\epsilon_r}\, f_L} \quad . \tag{3.49}$$

where the length is in millimetres and the frequency in Gigahertz.

3.2.3. The Sensitivity of Exponential Tapers

The theory can be extended to calculate the sensitivity of the impedance transforming tapers to material and manufacturing tolerance. Using the mathematical description of the reflection coefficient of a taper in general, and the definition of sensitivity for Γ with respect to any parameter x,

$$S_x^{\Gamma} = \frac{x}{\Gamma_0} \cdot \frac{\partial \Gamma}{\partial x} \quad . \tag{3.50}$$

Then, after substituting in equation (3.43) and simplifying, yields

$$S_x^{\Gamma} = \frac{x}{2\Gamma_0} \int_0^{L} e^{-j2\beta z} \frac{\partial}{\partial z} \left(S_x^{z} \right) dz \quad . \tag{3.51}$$

The sensitivity of impedance can be written in the form

$$S_x^{z} = \frac{K}{C/\epsilon} + P = \frac{K\sqrt{\epsilon_r}}{120\,\pi}\, \alpha^{\,z/L} + P \quad . \tag{3.52}$$

Substitution in (3.51) and simplifying, yields

$$S_x^{\Gamma} = \frac{K\sqrt{\epsilon_r}}{120\,\pi} \left(\frac{\alpha\, e^{-j2\beta L} - 1}{\ln \alpha^{\,j2\beta L}} \right) \cdot \frac{\beta L e^{j\beta L}}{\sin(\beta L)} \quad , \tag{3.53}$$

where α represents the impedance ratio of the taper. If $\alpha = 2$ (50 Ω - 100 Ω taper) and $2\beta L > \ln \alpha$ (in the passband) then

$$S_x^{\Gamma} \simeq \frac{K\sqrt{\epsilon_r}}{240\,\pi} (3 + j \cot \beta L) \quad . \tag{3.54}$$

To find the frequency βL at which S_x^{Γ} is maximum, we solve for

$$\frac{\partial \mid S_x^{\Gamma} \mid}{\partial (\beta L)} = 0 \quad . \tag{3.55}$$

Therefore

$$\beta L = \pm n\pi; \qquad n = 0, 1, 2 \ldots \tag{3.56}$$

i.e. in the dips (minima) of Γ. The peaks of Γ occur at:

$$\beta L = \frac{\pi}{2} \pm n\pi; \quad n = 0, 1, 2 \ldots \tag{3.57}$$

The first lobe of Γ is the maximum, where

$$\beta L = \frac{3\pi}{2} \quad . \tag{3.58}$$

This is therefore where the maximum influence of tolerance variations is expected. Therefore

$$S_x^{\Gamma}\,/_{\beta L = \frac{3\pi}{2}} = \frac{K\sqrt{\epsilon_r}}{80\pi} \quad . \tag{3.59}$$

Now

$$\Gamma_{New} = \Gamma_0 + \Delta\,\Gamma \quad , \tag{3.60}$$

$$= \Gamma_0 \left[1 + \frac{\Delta x}{x}\, S_x^{\Gamma}\right] \quad . \tag{3.61}$$

The maximum reflection from the impedance taper transformer due to manufacturing tolerance is therefore

$$|\,\Gamma_{MAX}\,| = \frac{ln2}{3\pi}\left[1 + \frac{\Delta x}{x} \cdot \frac{K\sqrt{\epsilon_r}}{80\pi}\right] \quad . \tag{3.62}$$

Substituting equation (3.52) in (3.29) to (3.33) and solving for the value of K, it can be shown that

$$K_{\epsilon_r} = 0 \quad , \tag{3.63}$$

$$K_t = 2X\,t\,\frac{(A^2 + B^2)}{A + B} - t\,[\,(b - s)\,M + (b + s)\,N] \quad , \tag{3.64}$$

$$K_w = 2X \quad , \tag{3.65}$$

$$K_s = 2sX\,(A - B) - ts\,(M - N) \quad , \tag{3.66}$$

$$K_b = -2bX\,\frac{(A^2 + B^2)}{A + B} + bt\,(M + N) \quad , \tag{3.67}$$

where the constants A, B, M, N and X are as defined before in equations (3.25) - (3.28). This analysis infers the following:

- A perfect taper has a first in-band lobe reflection of -22.68 dB.
- A worst case taper reflection of -22.6 dB is expected for a combined tolerance of 10% on parameters w, b, s, t or ϵ_r .

- The taper is most sensitive to variations in parameters t and w.
- The taper is not sensitive to material or manufacturing tolerances.

3.3. Stripline Coupler Design and Practical Considerations

3.3.1. Analysis and Synthesis of Stripline Couplers

Coupler design tables were presented by Crystal and Young in 1965 [7]. Equal-ripple polynomials were determined and applied to the synthesis of symmetric TEM-mode coupled transmission line directional couplers using exact analysis. The tables of symmetric couplers of various nominal coupling values over a range of ripple and bandwidths were published. An optimization program was written to iteratively derive the impedances of any number of section couplers over any specific bandwidth and equal-ripple value. Using the tables published by Crystal and Young, or the optimization program, a coupler with arbitrary specification can be synthesized.

When such a multi-section coupler is implemented, Tresselt found that the spread in coupling values required in adjacent quarter-wave sections is large enough to produce substantial differences in physical line dimensions [8]. Furthermore, a finite length of transition is required to realise these junctions. These transitions then excite higher order modes which can be represented by reactive parasitic components. The effects of these parasitic elements are especially noticeable at higher frequencies where VSWR and directivity are degraded.

Tresselt wrote a paper [8] in 1966 on the synthesis and design of high-directivity 90° couplers using non-uniform line techniques. The design employs a continuously-tapered coupling coefficient, resulting in a nonuniform coupler having optimum bandwidth for a given coupler length. It is interesting to note that these nonuniform couplers are a quarter-wavelength longer at centre frequency than the stepped equivalent prototype, and requires a somewhat tighter maximum coupling coefficient at the coupler centre. In effect, the Tresselt procedure provides a means of smoothing out a discrete section coupler. Kammler [9] demonstrated that the Tresselt procedure does not always give rise to the optimal continuously tapered coupler. Kammler presented a computer-aided design procedure employing a special optimization process to produce the optimum coupling response. Standard

parametric forms based on an approximate Fourier analysis as well as a more general spline parametric form were developed and illustrated. He could, however, only demonstrate very small differences between his optimal design and the Tresselt procedure.

The author of this thesis used Tresselt's design procedure to design several couplers, and very good practical results were obtained. Shelton's paper [10] on impedances of offset parallel-coupled strip transmission lines were used continuously to calculate physical line dimensions of the tapered lines. The assumption was made (and proved valid) that the non-uniform line couplers taper so gradual, that it permits usage of physical coupling data based on infinitely long, uniformly-coupled line calculations.

After confidence was gained in the analysis and synthesis of these couplers, a program was compiled to automate all the labourious calculations. The number of sections, coupling, triplate dimensions and permittivity are specified along with the centre frequency. The program calculates the coupling required at the centre of the coupler where the coupler is completely over-coupled, i.e. the lines are broadside coupled. The line dimensions are calculated to satisfy the coupling value and to approach the 50 Ω system impedance as closely as possible. The impedance, defined as the square root of the product of the even - and odd - mode impedances, is usually within 5 Ω from the system impedance at the input of the coupler. The coupler impedance is then tapered in a linear fashion from the centre impedance value to the 50 Ω system impedance at the input of the coupler. This impedance taper, along with the coupling taper, is used as input to the program section which calculates the taper of the physical dimensions of the coupler. The program produces a text file with the coupling, even and odd mode impedances, and line width and offset as a function of distance, in tabular form. It also creates an AutoCad-format graphical file which can be used to generate the photolithographic mask needed to etch the coupler.

A 5-section coupler was designed with the aid of the program, and practically evaluated. The designed physical taper was then divided into 100 incremental sections, each with an average line width and coupling offset. The *S*-parameters of each incremental section was evaluated by two different methods; Shelton's closed-form equations, and a full-wave FEM analysis computer program. The *S*-parameter files were cascaded and the theoretical performance of the coupler was analysed and evaluated. The results were so closely matched that no difference was visible on overlay graphs up to 18GHz. The frequency behaviour of a typical 9-section test coupler is shown in Appendix E.

3.3.2. Tolerance Analysis of Stripline Couplers

The sensitivity and tolerance analysis of a single-section coupler is described in detail by Srigiripuram et al. [11]. Since mathematical equations describing the sensitivity and tolerance of multi-section couplers is a complex issue worthy of an entire separate treatise, the analysis is simplified by dividing it into a material tolerance analysis and an etching alignment analysis.

The dual, tandem-connected 3dB coupler is divided into a large amount of equal-length sections. A single parameter of these sections is then independently randomly adjusted within certain tolerances and the coupling and phase responses of the coupler are optimized for worst performance. To avoid the publication of numerous results, the worst case numbers are recorded and summarized in Table 3.1.

- Over- and Under-Etching

All line widths were simultaneously adjusted by up to twice the tolerance of over- or under-etching. All other parameters were fixed. For a tolerance of 25 micron, a 0.45 dB coupling deviation was observed. Since the structure remained symmetric, no phase distortion was recorded. The bandwidth of the coupler remained unchanged (See Table 3.1).

- Photolithography Scaling Errors

All layout dimensions such as lengths, widths and offsets, were scaled by fixed percentages. For a -5% scaling tolerance, a 0.48 dB coupling deviation was recorded, and for a +5% scaling tolerance, a 0.15 dB coupling deviation was recorded. Since the structure remained symmetric, no phase distortion occurred. In general, amplitude distortion was worse at higher frequencies. The bandwidth also changed with the same percentage as the scaling error (Table 3.1).

- Mask Alignment Errors

The etching masks can be misaligned in three ways. When a small misalignment occurs in the direction of the length of the coupling sections, only negligible errors are caused. When the misalignment occurs in the direction transverse to the length of the coupled sections, the effect is that

of moving the over-coupled area of the coupler to one side, increasing the coupling of all sections to that side, and decreasing the coupling of all sections on the opposite side. For a 70 μm misalignment error, errors of 0.6 dB in coupling and 5.6° in phase were recorded. The bandwidth of the coupler remained unchanged.

- Rotational Alignment Errors

When one etch mask is rotated with respect to the other by 3.5°, 12.5 dB of coupling error and 7° of phase distortion are caused. For a 1° rotational misalignment, errors of 0.8 dB in coupling and 0.3° in phase were recorded. The bandwidth was virtually unaffected (Table 3.1).

- Material Tolerances

The analysis results for certain parameter tolerances are summarized in Table 3.1. ($\mathcal{P}$ is a scaling factor of the resistivity of the cladding material relative to copper):

Table 3.1 : Effect of material tolerances on couplers

Parameter	Tolerance	δC (dB)	ΔP (deg)	ΔBandwidth
s	±10 μm	0.55	-	-
b	+100/-100 μm	0.4/0.25	-	+0.4 GHz./-0.5GHz
t	±15 μm	0.01	-	-
ϵ_r	+20% / -20%	-	-	-1.6 GHz./+2 GHz
ρ	+100% / -100%	-	0.12/0.25	-
Roughness	±10 μm	0.18	3.9	-

Regarding the tolerance analyses of stripline couplers, the following conclusions can be summarized:

- Symmetric couplers have no phase balance distortion. Material tolerances do not influence phase behaviour.
- Over- or under-etching and scaling errors also does not influence phase behaviour.

- Coupler amplitude and phase response are very sensitive to alignment, especially rotational errors.

- Amplitude behaviour is sensitive to virtually all errors, especially variations in s. Measured values should be used in design, as supplier tolerance is typically 12 μm.

- Phase and amplitude response are very sensitive to random surface errors, or roughness.

3.4. Semi-Distributed Stripline Splitter

3.4.1. Introduction

The function of the splitter is to divide an incoming signal into two signal twins, very closely matched in amplitude, and especially phase. Likewise, it must also recombine two signal twins into a single output signal. The symmetric stripline coupler utilized in the phase shifter has its input ports on opposite sides of the centre dielectric slab of the triplate structure. This complicates the splitter to the extent that the divided signals must also appear on opposite sides of the triplate structure, to enter the coupler. The same geometrical problem occurs at the output of the coupler, where recombination of the signal twins occurs.

An ideal splitter is presented in Figure 17. If one of the splitter output signals is routed to the other side of the substrate, the symmetry is destroyed. The interconnection via introduces a series inductance which cannot be avoided. After much consideration, many experiments and simulations, the semi-distributed stripline splitter was developed [12]. The properties of an ideal splitter are now derived, after which the semi-distributed splitter is introduced.

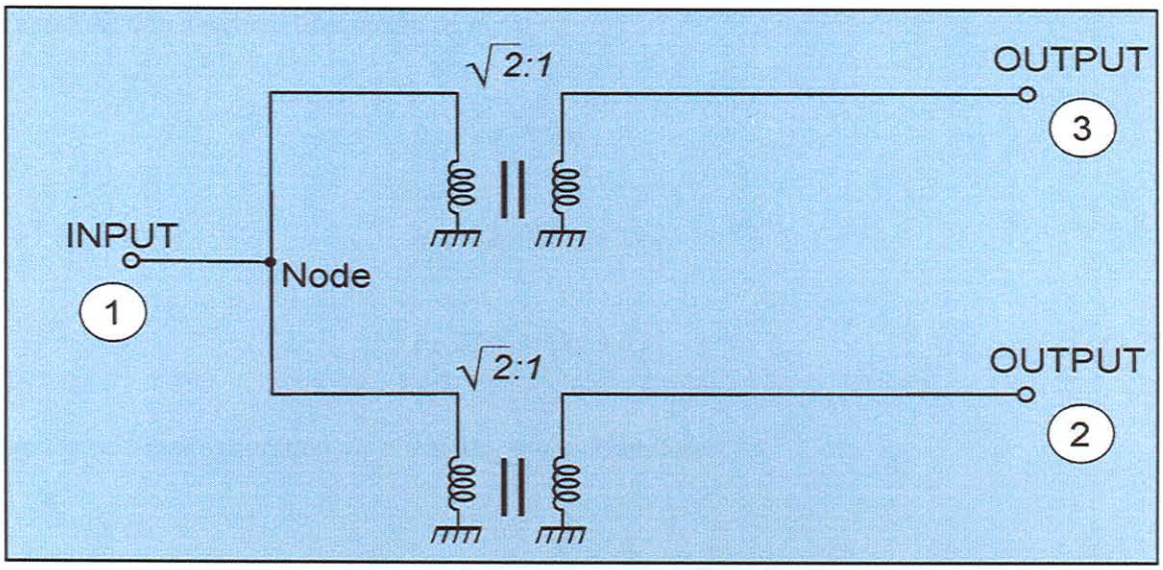

Figure 17 : The ideal splitter schematic

The three port splitter *S*-parameter matrix can be represented as

$$[S] = \begin{bmatrix} S_{11} & S_{12} & S_{13} \\ S_{21} & S_{22} & S_{23} \\ S_{31} & S_{32} & S_{33} \end{bmatrix} . \tag{3.68}$$

Let

$$T = S_{21} = S_{12} = S_{31} = S_{13} \quad \text{(Equal Split)} , \tag{3.69}$$

$$\Gamma = S_{22} = S_{33} \quad \text{(Output Match)} , \tag{3.70}$$

$$C = S_{23} = S_{32} \quad \text{(Isolation)} . \tag{3.71}$$

If the input port is matched at all conditions, the *S*-parameter matrix can be simplified to

$$[S] = \begin{bmatrix} 0 & T & T \\ T & \Gamma & C \\ T & C & \Gamma \end{bmatrix} . \tag{3.72}$$

Therefore, when written in equation form,

$$b_1 = Ta_2 + Ta_3 , \tag{3.73}$$

$$b_2 = Ta_1 + \Gamma a_2 + Ca_3 , \tag{3.74}$$

$$b_3 = Ta_1 + Ca_2 + \Gamma a_3 . \tag{3.75}$$

For the odd-mode condition, $a_1 = 0$ and $a_2 = -a_3$. Therefore

$$b_1 = 0; \qquad \frac{b_2}{a_2} = \frac{b_3}{a_3} = \Gamma - C \quad . \tag{3.76}$$

The odd-mode reflection and transmission coefficients can therefore be defined as

$$\rho_0 = \Gamma - C \qquad \text{(Reflection)} , \tag{3.77}$$

$$\tau_0 = 0 \qquad \text{(Transmission)} . \tag{3.78}$$

For the even-mode condition, $a_1 = 0$ and $a_2 = a_3$. Therefore

$$b_1 = 2\ Ta_2 \quad , \tag{3.79}$$

$$\frac{b_2}{a_2} = \frac{b_3}{a_3} = \Gamma + C \quad , \tag{3.80}$$

$$\frac{b_1}{a_2} = 2T \quad . \tag{3.81}$$

The even-mode refection and transmission coefficients can therefore be defined as

$$\rho_e = \Gamma + C \qquad \text{(Reflection)} , \tag{3.82}$$

$$\tau_e = 2T \qquad \text{(Transmission)} . \tag{3.83}$$

Solving for the unknown *S*-parameters, yields

$$\Gamma = \frac{\rho_e + \rho_o}{2} \quad , \tag{3.84}$$

$$C = \frac{\rho_e - \rho_o}{2} \quad , \tag{3.85}$$

$$T = \frac{\tau_e}{2} \quad . \tag{3.86}$$

But

$$\tau_e = \sqrt{2} \qquad \text{(lossless combination of ports 2 \& 3)} \, , \tag{3.87}$$

$$\rho_0 = \frac{0 - Z_0}{0 + Z_0} = -1 \qquad \text{(virtual short circuit at node)} \, , \tag{3.88}$$

$$\rho_e = 0 \qquad \text{(all ports matched in even mode)} \, . \tag{3.89}$$

$$\therefore \ \Gamma = -1/2 \quad , \tag{3.90}$$

$$C = 1/2 \quad , \tag{3.91}$$

$$T = 1/\sqrt{2} \quad . \tag{3.92}$$

Assuming a transmission phase angle θ, the ideal phase shifter splitter *S*-parameter matrix can therefore be represented by

$$[S] = \begin{bmatrix} 0 & \frac{1}{\sqrt{2}} e^{-j\theta} & \frac{1}{\sqrt{2}} e^{-j\theta} \\ \frac{1}{\sqrt{2}} e^{-j\theta} & -1/2 e^{-j2\theta} & 1/2 e^{-j2\theta} \\ \frac{1}{\sqrt{2}} e^{1j\theta} & 1/2 e^{-j2\theta} & -1/2 e^{-j2\theta} \end{bmatrix} . \tag{3.93}$$

After much consideration, it was realised that an electrically short splitter will always add a phase lag to the signal split off to the other side of the centre slab of the practical triplate structure. This is due to the extra physical path length added by the interconnecting via, or any other interconnecting device. The solution was to use a semi distributed splitter, consisting of a length of broadside coupled stripline (BCS) structure with a number of interconnecting vias to distribute the split over an electrically longer structure, as shown in Figure 18.

To simplify the analysis, the vias are chosen to be of identical diameter and equal spacing. The via diameter is also chosen to be small compared to the BCS width, in order to prevent even-mode fringe field disturbance. In the even mode, the overlapping lines of the BCS structure are excited in phase, and out of phase in the odd mode.

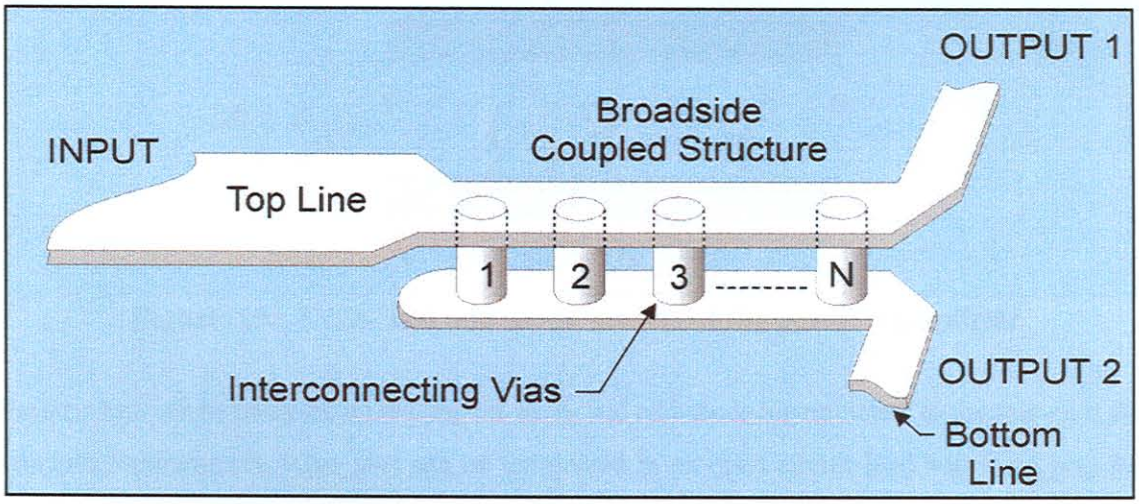

Figure 18 : The semi-distributed splitter

Figure 19 shows the periodical BCS-via structure models in even and odd mode. In the even mode, the voltage across each via is zero, therefore no current flows through the vias. The *S*-parameters of the even-mode model is therefore simply the even-mode *S*-parameters of the BCS structure without the vias.

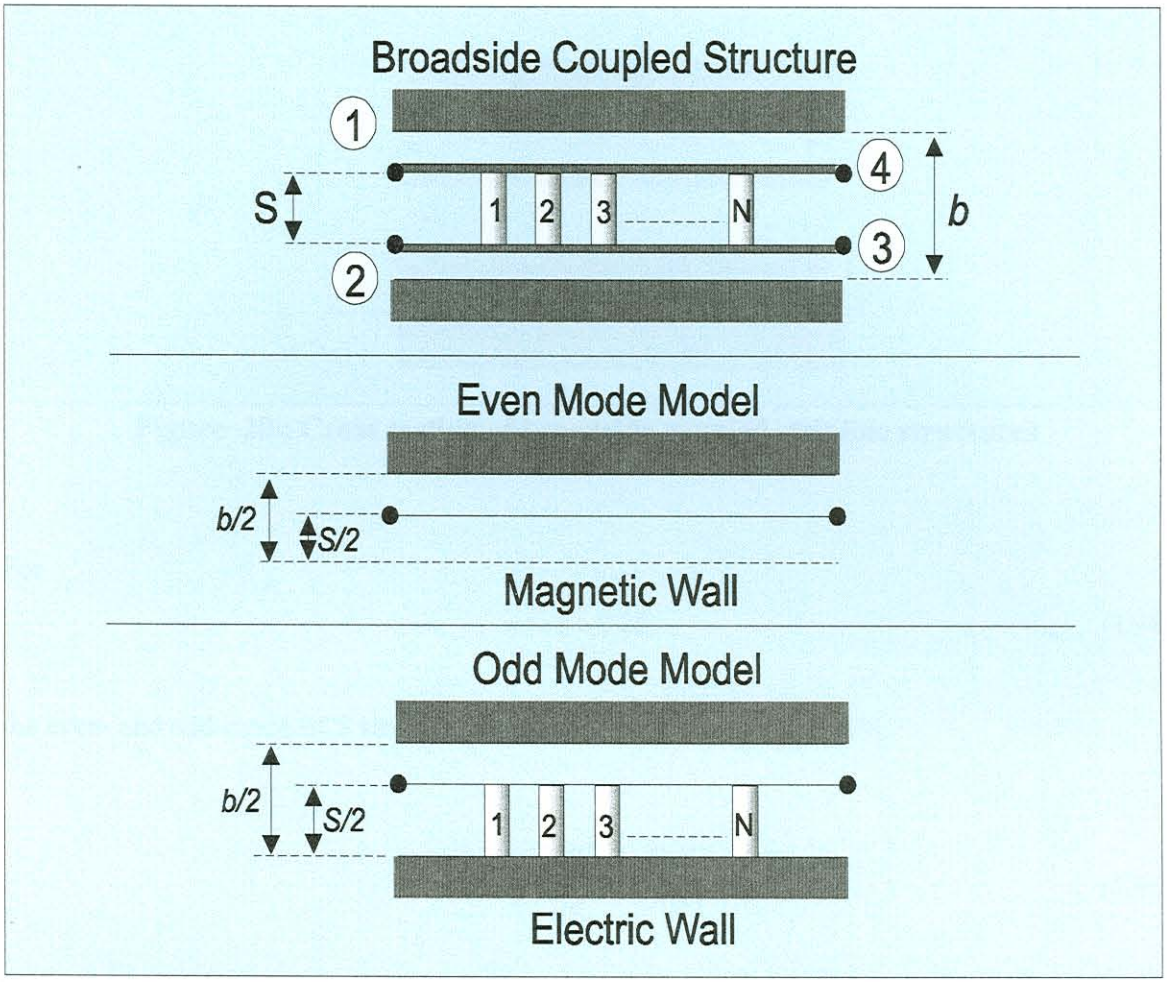

Figure 19 : Even- and odd mode models of the periodical splitter

The structure can be analysed by relating the even- and odd-mode *S*-parameters to the four-port BCS structure *S*-parameters. One port can be terminated in an open circuit load and the 4 port BCS structure *S*-parameters can be reduced to the 3 port splitter *S*-parameters. The splitter can then be evaluated over a broad band for various numbers of vias and via spacings. This investigation will then lead to general design criteria for splitters employed in ultra-wideband coupler-based phase shifters.

3.4.2. Broadside Coupled Stripline Properties

The semi-distributed splitter is realized in homogeneous BCS structure. In this section, the structure properties are discussed. Closed form solutions were published by Cohn [13] for the impedances of BCS structures in homogenious dielectric media. The solutions were presented in terms of complete elliptic integrals *K(k)*, of the first kind. The terminology is clarified in Figure 20.

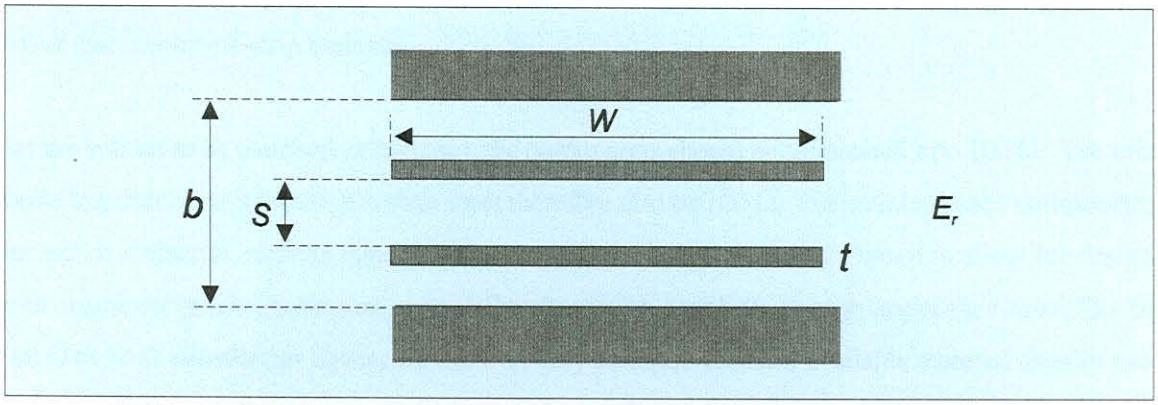

Figure 20 : Cross section of broadside coupled stripline structures

For

$$w/s \geq 0.35, \tag{3.94}$$

the even- and odd-mode BCS stripline impedances are given by Cohn [13].

$$Z_{oe} = \frac{188.3}{\sqrt{\epsilon_r}} \cdot \frac{K(k')}{K(k)} \quad , \tag{3.95}$$

$$Z_{oo} = \frac{296.1}{\sqrt{\epsilon_r} \cdot \frac{b}{s} \tanh^{-1} k} \quad , \tag{3.96}$$

$$k' = \sqrt{1 - k^2} \quad , \tag{3.97}$$

where k is a real number. The normalized strip width is given by

$$w/b = \frac{2}{\pi}\left(\tanh^{-1}\left[\sqrt{\frac{k \cdot \frac{b}{s} - 1}{\frac{1}{k} \cdot \frac{b}{s} - 1}}\right] - \frac{s}{b} \tanh^{-1}\left[\frac{1}{k}\sqrt{\frac{k \cdot \frac{b}{s} - 1}{\frac{1}{k} \cdot \frac{b}{s} - 1}}\right]\right) . \tag{3.98}$$

Cohn [13] found that the finite copper thickness affects the odd-mode impedance the most. For copper thickness less than 1.5 mil, the fringe fields are very close to those of zero thickness.

Normally 0.7 mil (½ ounce copper) is used. Also, s should be taken as the distance between the strips rather than centre-of-strip distance.

For the splitter to be matched to the input, the output arms should be terminated into 100 Ω. The even mode impedance of the BCS-structure must therefore also be 100 Ω. For coupler-based components, the lowest dielectric constant material commercially available is usually chosen to allow for designs with comfortable line dimension, especially where high coupling, or high impedance lines, like the 100 Ω to 50 Ω transformer tapers, are used. A very common standard available material usually used is the PTFE ($\epsilon_r = 2.2$) substrate. Substituting these values into equation (3.95) and solving, we find

$$\frac{K(k')}{K(k)} = 0.7877 \quad , \tag{3.99}$$

and solving for k yields

$$k = 0.8621 \quad . \tag{3.100}$$

Substituting the value of k into equation (3.98), and simplifying, yields

$$Z_{oo} = 153.4 \cdot \frac{s}{b} \quad . \tag{3.101}$$

The designer would then choose s/b and calculate w/b and Z_{oo} using equations (3.98) and (3.101). As an example, a very general choice for a tightly coupled line would be

$$s = 5 \text{ mil} \; ; \; b = 45 \text{ mil}; \quad \epsilon_r = 2.2 \; .$$

Solving equation (3.98) and (3.101) yields:

$$Z_{oo} = 17.0 \; \Omega \quad \text{and} \quad w = 0.602 \text{ mm} \; .$$

Verifying with a full-wave analysis program [14], it is found that

$$w = 0.602 \text{ mm} \; ,$$
$$Z_{oo} = 18.3 \; \Omega \; .$$

It can be concluded that Cohn's closed-form equations [13] are quite accurate and that the equations can be generalized into a more simple form to aid in the design of the semi-distributed splitter.

3.4.3. Via Through-hole Interconnection Properties

In order to accurately analyse the splitter, it is necessary to first analyse the via as an element. This is only needed in the odd-mode analysis, as discussed in 3.4.1. The *S*-parameters of a single via in the odd mode, as in Figure 21, are calculated from 0 to 20 GHz, for various via diameters. A full-wave analysis was used, as described by Jansen [14], which was verified against measurements up to 40 GHz.

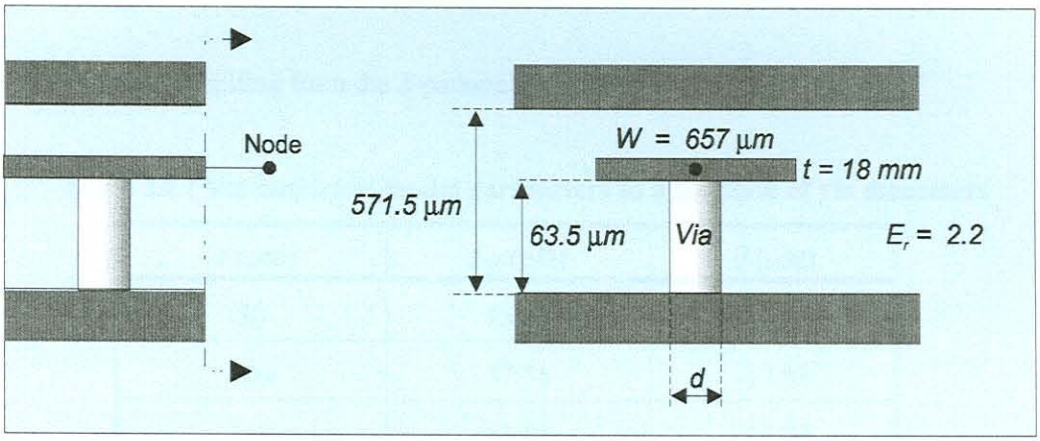

Figure 21 : Odd mode single via full-wave analysis physical structure

It is assumed that the via is perfectly conducting and cylindrical. To analyse the structure, 6 mm line lengths were used to clear the excitation ports from the via. The via model *S*-parameters were printed into a file, for diameters of d = 50, 100, . . . 600 μm from 1 to 20 GHz. The *S*-parameters were de-embedded by 6mm plus half the via diameter. The *S*-parameters were imported into a mathematical CAD program where a model was optimized to fit the *S*-parameters.

After many models were considered, it was found that the *S*-parameters could be very closely fitted to a model comprised of series transmission lines of negative length, and a shunt inductor. The impedance of these lines were chosen to be the same as the BCS structure odd-mode impedance, to allow simple application of the model into the BCS-via structure. The line length can simply be added to the via separation distance, simplifying the BCS-via structure to a length of BCS line, interconnected periodically by inductors. The via empirical model is shown in Figure 22.

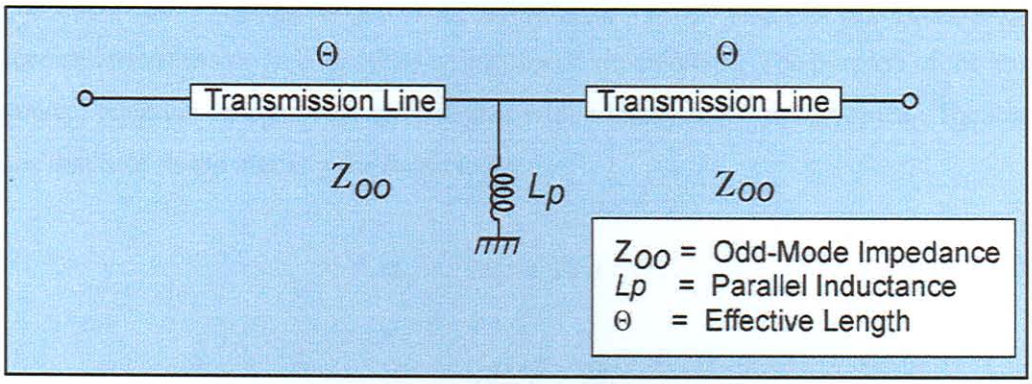

Figure 22 : Odd mode single via empirical model

The element values resulting from the *S*-parameter fit are presented in Table 3.2.

Table 3.2 : Via empirical model parameters as a function of via diameters

d (μm)	*Lp* (pH)	θ (μm)
50	45.64	-13.41
100	37.55	-17.98
150	33.81	-22.46
200	31.41	-26.82
250	30.58	-31.97
300	29.03	-35.72
350	27.44	-39.28
400	27.47	-43.96
450	27.41	-48.55
500	26.99	-52.58
550	26.71	-56.65
600	26.16	-60.42

When compared to the results of the full wave analysis, the *S*-parameters of the equivalent network were found to fit exactly at 0 GHz and about 14 GHz. The worst deviation occurred at about 7 GHz and 20 GHz. The equivalent circuit model reflection coefficient amplitude was a maximum of 0.2 dB higher at 7 GHz and 0.2 dB lower at 20 GHz compared with the full-wave analysis values. The maximum phase difference was 0.5 degrees. It can therefore be concluded that a very accurate model

for the via was found. An empirical equation was derived, with the help of a CAD program, for the inductance and transmission line length as a function of via diameter. The purpose of the empirical mathematical equation is to provide the designer with a handy set of design rules. The empirical equations that best fit the model were found to be

$$L_p = 26.5 + 28\, e^{-8.5d}, \tag{3.102}$$

and

$$\theta = -[855d + 98], \tag{3.103}$$

Where

d represents the via diameter in mm ,
L_p is the shunt inductance in pH ,
θ is the series line length in μm .

The models derived for the via can be used for any 5-mil-spaced BCS structure where the line is wide enough (or the via diameter small enough), to ensure that the via does not interfere with the line fringe field. It was found that the condition was met when

$$w/d > 1.2 . \tag{3.104}$$

These models are accurate to within 1 pH and 7.5 μm. Since this tolerance falls well within the etching material tolerance values, it may be neglected. It can be concluded that an accurate set of empirical equations was derived to assist with the design of ultra-wideband phase shifter splitters.

3.4.4. Semi-Distributed Splitter Odd Mode Analysis

3.4.4.1. Introduction

To simplify the analysis of the splitter, the concept of even and odd mode of operation is utilized, as discussed before. The even-mode analysis is relatively simple because the vias can be excluded from the even-mode model. In the odd-mode analysis, the BCS structure is first assumed to be infinitely long. The reflection and transmission properties of such a structure with a single via interconnection are first determined. The analysis is then extended to a BCS system with n equally spaced vias. It is shown that the structure acts as a filter which resonates under certain conditions, where the odd

mode is not rejected. The criteria to avoid this situation are determined. The general *S*-parameters of the odd mode BCS-via structure are then calculated and discussed.

3.4.4.2. Single-Via Splitter Odd-Mode Properties

The transmission and reflection properties of a single via in BCS, in the odd mode, is derived. The model is shown in Figure 23.

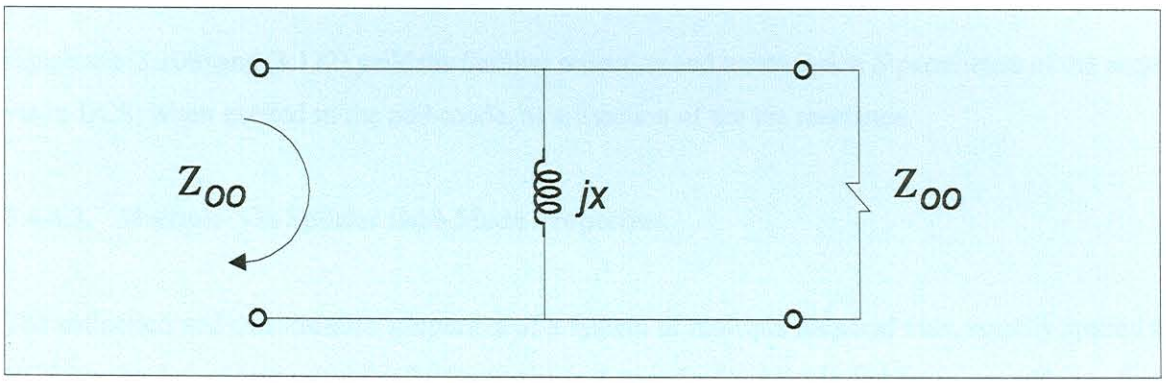

Figure 23 : Odd-mode model of single via in BCS

The transmission line parts of the via model are absorbed in the BCS line, which is chosen to be of the same impedance. The reflection from the via is given by

$$\Gamma = \frac{-1 + 2jx}{1 + 4x^2} \quad , \tag{3.105}$$

where

$$x = \frac{X}{Z_{oo}} \quad . \tag{3.106}$$

For lossless networks, the two general conditions of energy conservation are applied.

$$\sum_{j=1}^{2} | S_{ij} |^2 = 1 \quad , \tag{3.107}$$

$$\sum_{j=1}^{2} S_{jm} \cdot S_{jn}^{*} = 0 \qquad m \neq n \quad . \tag{3.108}$$

Therefore

$$|\Gamma|^2 + |T|^2 = 1 \quad , \tag{3.109}$$

$$\Gamma T^* + T\Gamma^* = 0 \quad , \tag{3.110}$$

$$T = \frac{4x^2 + j\,2x}{1 + 4x^2} \quad , \tag{3.111}$$

$$\therefore \quad T = 1 + \Gamma \quad . \tag{3.112}$$

Equations (3.106) and (3.112) yield the familiar reflection and transmission *S*-parameters of the single via in BCS, when excited in the odd-mode, as a function of the via reactance.

3.4.4.3. Multiple-Via Splitter Odd-Mode Properties

The reflection and transmission properties of a system of multiple identical vias, equally spaced in BCS, can be determined using a reflectogram as in Appendix C. All relevant terms are added to form a mathematical series of terms representing the reflection or transmission coefficient of a n-via system, where $n = 1, 2, 3 \ldots$. Unfortunately the reflectogram complicates rapidly for $n > 3$. The results are as follows:

For a single via ($n = 1$), the reflectogram analysis yields

$$\Gamma_1 = \Gamma \,, \tag{3.113}$$

$$T_1 = T\,\Psi \,. \tag{3.114}$$

For two vias ($n = 2$), the reflectogram analysis yields

$$\Gamma_2 = \Gamma + T^2\,\Psi^2\,\Gamma + T^2\,\Psi^4\,\Gamma^3 + T^2\,\Psi^6\,\Gamma^5 + T^2\,\Psi^8\,\Gamma^7 + \ldots \quad , \tag{3.115}$$

$$= \frac{T^2\,\Psi^2\,\Gamma}{(1 - \Psi^2\,\Gamma^2)} + \Gamma \quad . \tag{3.116}$$

$$T_2 = T^2 \Psi^2 + T^2 \Psi^4 \Gamma^2 + T^2 \Psi^6 \Gamma^4 + T^2 \Psi^8 \Gamma^6 + \ldots \,, \tag{3.117}$$

$$= \frac{T^2 \Psi^2}{(1 - \Gamma^2 \Psi^2)} \,. \tag{3.118}$$

For three vias ($n = 3$), the reflectogram analysis yields

$$\Gamma_3 = \Gamma_2 + \frac{\dfrac{T^4 \Psi^4 \Gamma}{(1 - \Psi^2 \Gamma^2)^3}}{1 - \dfrac{T^2 \Psi^4 \Gamma^2}{(1 - \Psi^2 \Gamma^2)^2}} \,, \tag{3.119}$$

$$T_3 = \frac{\dfrac{T^4 \Psi^4 \Gamma}{(1 - \Psi^2 \Gamma^2)^3}}{1 - \dfrac{T^2 \Psi^4 \Gamma^2}{(1 - \Psi^2 \Gamma^2)^2}} \,. \tag{3.120}$$

Γ, T and Ψ represent the reflection, transmission and phase coefficients of a single via in BCS. It is a simple matter to calculate the close form equations from the infinite series. After much consideration, attempts to write closed-form general equations for a system of n vias from the above results were abandoned, as no arithmetic pattern could be discerned for the results with n as variable. The alternative was to derive a set of recursive equations for the reflection and transmission properties of the general case of n vias in BCS. The reflectogram now consists of only two elements, namely a single via and a set of n vias. The complete reflectogram is shown in Appendix D. The series can be written in closed form as

$$\Gamma_{n+1} = \Gamma + \frac{T^2 \Psi^2 \Gamma_n}{1 - \Gamma \Psi^2 \Gamma_n} \,, \tag{3.121}$$

$$T_{n+1} = \frac{T \Psi T_n}{1 - \Gamma \Psi^2 \Gamma_n} \,. \tag{3.122}$$

It can be shown that these equations can be used iteratively to calculate the S-parameter properties of any number of vias in BCS.

3.4.4.4. Semi-Distributed Splitter Resonance

The semi-distributed splitter has an inherent resonance due to its periodic construction. The splitter application is therefore similar in nature to an odd-mode bandpass filter, used in the rejection frequency band. A typical plot of a BCS-via structure odd-mode transfer characteristic is shown in Figure 24.

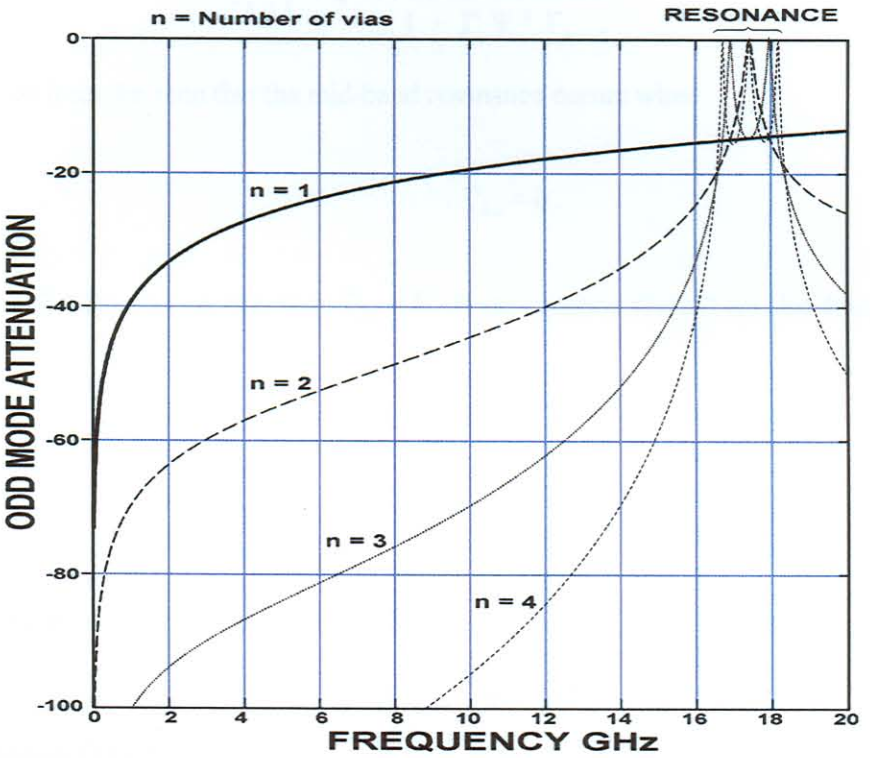

Figure 24 : Odd mode transfer characteristic of the splitter structure

It is clear that, at lower frequencies, the odd mode is rejected, permitting the splitter to be close to ideal. The odd mode causes the twin voltage vectors to be unequal in amplitude and / or phase. At a certain frequency range, the structure resonates or becomes an odd mode passing structure, causing severe splitter imbalance. This frequency band should be avoided. The frequency at which the structure resonates, can be determined in general, when $\Gamma_n = 0$. In graphs of transfer characteristics of BCS-via structures, as shown in Figure 24, it can be seen that exact points of resonance occur when the odd mode attenuation peaks at 0 dB. The graphs peak at the same point at mid-band when

$$\Gamma_k = \Gamma_{k-2} \quad K = 4, 6, 8 \ldots \tag{3.123}$$

Substituting into the equations of section 3.4.4.3, we find the following prediction of resonance. Substitute equation (3.123) into equation (3.121)

$$\Gamma_k = \Gamma + \frac{T^2 \Psi^2 \Gamma_{k-1}}{1 - \Gamma \Psi^2 \Gamma_{k-1}} \quad , \tag{3.124}$$

therefore

$$\Gamma_{k-1} = \Gamma + \frac{T^2 \Psi^2 \Gamma_{k-2}}{1 - \Gamma \Psi^2 \Gamma_{k-2}} \quad . \tag{3.125}$$

From Figure 24 it can be seen that the mid-band resonance occurs when

$$\Gamma_{k-2} = 0 \, . \tag{3.126}$$

From equation (3.125) we conclude that: $\Gamma_{k-1} = \Gamma$. From equation (3.125) we also find, for k even

$$\Gamma_k = 0 \quad , \tag{3.127}$$

and for k odd

$$\Gamma_k = \Gamma \quad . \tag{3.128}$$

Substituting equation (4.124) into (4.126) yields

$$1 + \Psi^2 [T^2 - \Gamma^2] = 0 \quad . \tag{3.129}$$

But from equation (3.112)

$$T = 1 + \Gamma \quad . \tag{3.130}$$

Substituting (3.130) into (3.129) and solving for phase yields

$$\Psi^2 = \frac{-1}{1 + 2\Gamma} \quad . \tag{3.131}$$

For short vias, $x \ll 1$ and $\Gamma \simeq -1$. (3.132)

For example, assume that

$$L_{MAX} = 30pH \quad \text{and} \quad f_{MAX} = 20 \; GHz, \; x \leq 0.2 \quad .$$

Equation (3.105) yields

$$\Gamma = -0.862 + j \; 0.3$$
$$\Gamma \simeq -1 \quad .$$

From equation (3.131), the phase angle between vias at the mid-band resonance condition can be determined from

$$\Psi^2 = \cos 2\theta - j \sin 2\theta \simeq 1 .$$

Therefore

$$\theta = m\,\pi; \qquad m = 1, 2, 3 .... \qquad m \neq 0 . \tag{3.133}$$

Therefore, to avoid the first resonance, the via spacing should be chosen so that, at the highest frequency of operation, $\theta < \pi$. Translating into a simple design guide, we find

$$L_{MAX} = \frac{150}{\sqrt{\epsilon_r}\, f_{MAX}} . \tag{3.134}$$

where L_{MAX} is the maximum via separation in mm and f_{MAX} the frequency, in GHz, when the first resonance occurs.

$$\text{If} \quad \epsilon_r = 2.2 , \quad \text{and} \quad f_{MAX} = 20 \text{ GHz} , \quad \text{then} \quad L_{MAX} = 5.06 \text{ mm} .$$

For the splitter to operate properly at 20 GHz, the via spacing should therefore be considerably less than 5 mm. Typically, a via spacing of 2 or 3 mm is chosen to avoid resonance up to 20GHz.

3.4.5. Semi-Distributed Splitter *S*-parameters

It was demonstrated in section 3.4.1 that the effect of the BCS-coupled structure with n identical equal-spaced via interconnections can be analysed by introducing the well-known even- and odd-mode analysis. The analysis is complicated by the fact that the BCS- via structure *S*-parameters are derived in the odd-mode impedance. These parameters need to be converted to system impedance Z_o at the input and $2Z_o$ at the output ports 3 and 4. The even-mode *S*-parameters can easily be derived in Z_o; $2Z_o$ system-impedance format.

If Γ'_{01}, Γ'_{02} and T'_0 are the input reflection coefficient, output reflection coefficient and transmission *S*-parameters measured in the odd-mode system impedance, it can be shown [15] that these coefficients can be converted to input impedance Z_o at port 1 and 2 and output impedance $2Z_o$ at ports 3 & 4 using the transforms

$$\Gamma_{01} = \frac{(1 - r_0 \Gamma'_{02})(\Gamma'_{01} - r_i) + r_0 (T'_0)^2}{k} , \tag{3.135}$$

$$\Gamma_{02} = \frac{(1 - r_i \Gamma'_{01})(\Gamma'_{02} - r_0) + r_i (T'_0)^2}{k} , \tag{3.136}$$

$$T_0 = \frac{AT'_0}{k} , \tag{3.137}$$

where

$$r_i = \frac{Z_0 - Z_{00}}{Z_0 + Z_{00}} = 0.4641 , \tag{3.138}$$

$$r_o = \frac{2Z_0 - Z_{00}}{2Z_0 + Z_{00}} = 0.6906 , \tag{3.139}$$

$$A = \frac{\sqrt{32}\, Z_0 Z_{00}}{(Z_0 + Z_{00})(2Z_0 + Z_{00})} = 0.6406 , \tag{3.140}$$

$$k = (1 - r_i \Gamma'_{01})(1 - r_o \Gamma'_{02}) - r_i r_0 (T'_0)^2 . \tag{3.141}$$

Using simple energy conservation principles, it can be shown that the even-mode *S*-parameter can be represented by

$$[S_E] = \begin{bmatrix} \Gamma_{E1} & T_E \\ T_E & \Gamma_{E2} \end{bmatrix} = \begin{bmatrix} \frac{1}{3} & \frac{\sqrt{8}}{3} e^{-jn\theta} \\ \frac{\sqrt{8}}{3} e^{-jn\theta} & \frac{-1}{3} e^{-j2n\theta} \end{bmatrix} . \tag{3.142}$$

where $n\theta$ represents the total electrical length of the n sections of θ length of line between the $n + 1$ vias in the four port BCS structure. Using general even- and odd-mode analysis on the four-port BCS structure it can be verified that the scattering parameters $[S']$ are given by

$$S'_{11} = S'_{22} = \frac{\Gamma_{01} + \Gamma_{E1}}{2} = \Gamma_1 \quad , \tag{3.143}$$

$$S'_{33} = S'_{44} = \frac{\Gamma_{02} + \Gamma_{E2}}{2} = \Gamma_2 \quad , \tag{3.144}$$

$$S'_{12} = S'_{21} = \frac{\Gamma_{E1} - \Gamma_{01}}{2} = C_1 \quad , \tag{3.145}$$

$$S'_{43} = S'_{34} = \frac{\Gamma_{E2} - \Gamma_{02}}{2} = C_2 \quad , \tag{3.146}$$

$$S'_{23} = S'_{14} = S'_{41} = S'_{32} = \frac{T_0 + T_E}{2} = T \quad , \tag{3.147}$$

$$S'_{13} = S'_{31} = S'_{24} = S'_{42} = \frac{T_E - T_0}{2} = X \quad . \tag{3.148}$$

The symmetric four-port structure *S*-parameters can be reduced to that of the three port splitter, by leaving one port open, e.g. $b_2 = a_2$ and eliminating b_2.

$$S_{11} = \frac{C_1^2}{(1 - \Gamma_1)} + \Gamma_1 \quad , \tag{3.149}$$

$$S_{22} = \frac{T^2}{(1 - \Gamma_1)} + \Gamma_2 \quad , \tag{3.150}$$

$$S_{33} = \frac{X^2}{(1 - \Gamma_1)} + \Gamma_2 \quad , \tag{3.151}$$

$$S_{12} = S_{21} = \frac{T\,C_1}{(1 - \Gamma_1)} + X \quad , \tag{3.152}$$

$$S_{13} = S_{31} = \frac{X\,C_1}{(1 - \Gamma_1)} + T \quad , \tag{3.153}$$

$$S_{23} = S_{32} = \frac{XT}{(1 - \Gamma_1)} + C_2 \quad . \tag{3.154}$$

Therefore the splitter *S*-parameter matrix can be represented in matrix form as

$$[S] = \begin{bmatrix} \left(\Gamma_\Theta + \frac{C_\Theta^{\,\theta}}{1-\Gamma_\Theta}\right) & \left(X + \frac{TC_\Theta}{1-\Gamma_\Theta}\right) & \left(T + \frac{XC_\Theta}{1-\Gamma_\Theta}\right) \\ \left(X + \frac{TC_\Theta}{1-\Gamma_\Theta}\right) & \left(\Gamma_\theta + \frac{T^\theta}{1-\Gamma_\Theta}\right) & \left(C_\theta + \frac{TX}{1-\Gamma_\Theta}\right) \\ \left(T + \frac{XC_\Theta}{1-\Gamma_\Theta}\right) & \left(C_\theta + \frac{TX}{1-\Gamma_\Theta}\right) & \left(\Gamma_\theta + \frac{X^\theta}{1-\Gamma_\Theta}\right) \end{bmatrix} . \quad (3.155)$$

Port match, transmission loss and amplitude- and phase-match equations were derived and verified against the full-wave analysis. The results were found to be virtually identical from DC to 20GHz.

Device match:

$$S_{\theta\theta} = \Gamma_\Theta + \frac{C_\Theta^{\,\theta}}{1-\Gamma_\Theta} , \quad (3.156)$$

$$S_{\theta\theta} = \Gamma_\theta + \frac{T^\theta}{1-\Gamma_\Theta} , \quad (3.157)$$

$$S_{II} = \Gamma_\theta + \frac{X^\theta}{1-\Gamma_\Theta} . \quad (3.158)$$

Device transfer:

$$S_{\theta\Theta} = X + \frac{TC_\Theta}{1-\Gamma_\Theta} , \quad (3.159)$$

$$S_{I\Theta} = T + \frac{XC_\Theta}{1-\Gamma_\Theta} . \quad (3.160)$$

Device amplitude tracking:

$$\delta_{\hat{a}} = 20 \log \left[\frac{|S_{\theta\Theta}|}{|S_{I\Theta}|}\right] . \quad (3.161)$$

Device phase tracking:

$$ANG_X = Arg \left[\frac{S_{\theta\Theta}}{S_{I\Theta}}\right] . \quad (3.162)$$

3.4.6. Semi-Distributed Splitter Practical Considerations

In realising a test splitter, a 30 micron etching tolerance with very smooth, sharply defined edges could be achieved. The vias could however not be realised satisfactorily by through-hole plating or electro-sputtering techniques, due to their length-to-diameter ratios. Conductive epoxy vias proved to be more capacitive in nature at low frequencies, whereas through-ribbons were found to be more inductive due to the extra length to the point of adhesion. The best vias were realised by a combination of conductive epoxy and ribbons. The splitter is shown in Chapter 5.

The structure resonance for the test splitter was deliberately chosen to be at about 17 GHz, where the theory clearly shows sharp spiky *S*-parameter characteristics as shown in Figure 24. The measured results reveal smoother bump or wavy disturbance due to slight variance in practical via nature and spacing. From the analysis it is apparent that if the via diameter is increased, the odd-mode rejection also increases. However, if the via diameter becomes comparable to the line width, it starts to interfere with the line fringe field, causing even-mode mismatch. A good choice seems to be $d < (w\text{-}s)$. It is also important that the via spacing be close enough so that the circuit will remain far from resonance at the highest operating frequency.

From the *S*-parameter plots of the test splitter it is apparent that the splitter match is virtually independent of via diameter and number. The splitter results are summarised in Table 3.3.

Table 3.3 : Test Splitter Evaluation Results

Parameter	Theory	Practice
S_{11}	Better than -30 dB, rising gradually until resonance	Better than -15 dB up to resonance, about -10 dB at resonance
S_{22}, S_{33}	Within 0.3 dB from -6 dB	Within 0.3 dB from -6 dB
$P\Delta$	Within 0.3 dB up to resonance for all n, improving as n increases	1 via 1.4 dB max @ 20 GHz 2 via 0.6 dB max @ 20 GHz 3 via 0.4 dB max @ 20 GHz
$\Delta\phi$	4.2° at 20 GHz for single via, 2° max up to resonance for $n > 1$	1 via 7.5° max @ 20 GHz 2 via 5° max @ 20 GHz 3 via 3° max @ 20 GHz

From the sensitivity analysis and the results in table 3.3, it is clear that the phase imbalance is the most compelling reason to implement multiple vias. Referring to the sensitivity analysis in Chapter 4, these results will typically cause phase and amplitude errors for a 45° phase shifter constructed from the tandem connection of two couplers, as in table 3.4.

Table 3.4 : Predicted Phase Shifter Tolerance due to Splitter Tolerance

n	Phase Error	Amplitude Error	Phase Shift Deviation	Loss Deviation
1 via	7.5 Deg	1.4 dB	0.8 Deg	0.2 dB
2 vias	5 Deg	0.6 dB	0.3 Deg	0.04 dB
3 vias	3 Deg	0.4 dB	0.2 Deg	0.03 dB

3.5. Conclusion

The three elements comprising the phase shifter were analysed in depth. A general impedance transformer was developed in the form of an impedance-transforming tapered line, to best conserve symmetry. It was concluded that these tapers are relatively immune against material variations. The coupler design was then discussed at length and the tolerance analysis of stripline couplers was discussed. It was found that the rotational alignment of stripline couplers is critical to the symmetry of the device. Both the phase and amplitude characteristics are shown to be important for the performance of the phase shifter. A critical element to the phase shifter is the splitter. From the sensitivity analysis it follows that the signal should be split into equal amplitude and phase vectors. An ultra-wideband splitting structure was developed to split incoming signals into twin vectors. It has been demonstrated mathematically, and verified in practise, that for a splitter with close spacing of three or more through-vias, very good results can be obtained. The splitting amplitude and phase balance are virtually independent of BCS line width tolerances and via nature, as long as resonance is avoided.

References

[1] K. C. Gupta, R. Garg, and R. Chadha, "Computer aided design of microwave circuits", Artech House, Massachusetts, 1981.

[2] J. A. G. Malherbe, "Microwave transmission line filters", Artech House, Massachusetts, 1980.

[3] W. J. Getsinger, "Coupled rectangular bars between parallel plates", IRE Trans. MTT, vol. MTT-10, no. 1, pp. 65-72, Jan. 1972.

[4] R. E. Collin, "Foundations for microwave engineering", McGraw-Hill, New York, 1966.

[5] R. W. Klopfenstein, "A transmission line taper of improved design", IRE Proc., vol. 44, pp. 31-35, Jan. 1956.

[6] R. P. Hecken, "A near-optimum matching section without discontinuities", IEEE Trans. Microwave Theory Tech., vol. 20, pp. 734-739, Nov. 1972.

[7] E. G. Crystal and L. Young, "Theory and tables of optimum symmetric TEM-mode coupled-transmission-line directional couplers", IEEE Trans Microwave Theory Tech., vol. 13, no. 5, pp 544-558, Sept. 1965.

[8] C. P. Tresselt, "The design and construction of broadband high-directivity, 90-degree couplers using non-uniform line techniques", IEEE Trans Microwave Theory Tech., vol. 14, no. 12, pp. 647-656, Dec. 1966.

[9] D. W. Kammler, "The design of discrete N-section and continuously tapered symmetrical microwave TEM directional couplers ", IEEE Trans Microwave Theory Tech., vol. 17, no. 8, pp. 577-589, Aug. 1969.

[10] J. P. Shelton and J. A. Mosko, "Synthesis and design of wide-band equal-ripple TEM directional couplers and fixed phase shifters", IEEE Trans Microwave Theory Tech., vol. MTT-14, pp. 462-473, Oct. 1966.

[11] D. Srigiripuram, Shamasundara, and K. C. Gupta, "Sensitivity analysis of coupled microstrip directional couplers ", IEEE Trans Microwave Theory Tech., vol. 26, no. 10, pp. 788-794, Oct. 1978.

[12] F. V. Minnaar, J. C. Coetzee, and J. Joubert, "The development of an ultra-wideband via connected broadside coupled splitting structure", in IEEE AP MTT - Symp., Cape Town, S.A., pp. 465 - 466, Sept 1998.

[13] S. B. Cohn, "Characteristic impedances of broadside-coupled strip transmission lines", IRE Trans. Microwave theory Tech., vol. MTT-8, no. 6, pp. 633-647, Nov. 1960.

[14] R. H. Jansen, "A full-wave electromagnetic model of cylindrical and conical via hole grounds for use in interactive MIC/MMIC design", Proc. of the IEEE International Symposium, pp. 1233-1236, Albuquerque, USA, June 1992.

[15] K. Kurokana, "Generalized 2-port scattering parameters for arbitrary load and generator impedances", IEEE Trans Microwave Theory Tech., pp. 194, March 1965.

CHAPTER 4. PHASE SHIFTER SENSITIVITY ANALYSIS

4.1. Introduction

In this chapter the practicality of the proposed novel class of phase shifter is investigated. Equations will be derived to enable a designer to assign tolerances to various element parameters in order to yield a component that satisfies certain specifications. On the other hand the requirements of a fabrication technology suitable for achieving a given circuit performance may be specified. A sensitivity analysis is the best way to examine the trade-offs between specifications and tolerances.

An analysis of the effect of changes in the values of various element parameters on the component performance parameters is called a sensitivity analysis of the component. The sensitivities of the elements comprising the phase shifter yield information as to how design parameter tolerances affect the electrical specifications of the elements. Linking this information with the sensitivity analysis of the phase shifter, the sensitivity of the phase shifter performance parameters with respect to the design parameters is obtained [1]. First the error parameters and transfer functions of the phase shifter will be defined. Then the effect of the error parameters on the component performance, classified as amplitude and phase errors, is investigated. General guidelines will be presented to provide a feel for the sensitivity of certain performance parameters with respect to tolerance errors.

4.2. Error Parameters and Transfer Functions

A convenient way to do a sensitivity analysis is to model the component, in this case the phase shifter, as a combination of elements (here the splitter, impedance transformers and coupler). The sensitivity analysis may be simplified by modelling each element as an ideal element, with an additional multiplicative error voltage element, to represent any tolerance or another non-ideal electrical behaviour due to material or manufacturing tolerance. These error voltage elements, in general, will consist of amplitude and phase components. It will be shown that these error elements can be cascaded to represent the general case of four phase shifter error elements.

The error voltage elements of the splitters, tapers, and couplers may be called E_{si}, E_{ti} and E_{ci} respectively. The subscript will be used to distinguish between different splitters, tapers and couplers, to maintain generality. As seen in Figure 25, these errors may be cascaded to form four generic error elements in the phase shifter.

$$E_i = E_{si} \cdot E_{ti} \cdot E_{ci} \qquad i = 1, 2, 3, 4. \tag{4.1}$$

where these error vectors may be defined as

$$E_{ki} = |E_{ki}| e^{j\theta ki} \qquad k = s,t,c\,. \tag{4.2}$$

$$\therefore E_i = |E_i| e^{j\theta i}\,. \tag{4.3}$$

The amplitude factors may be cascaded in multiplication $|E_i| = |E_{si}| \cdot |E_{ti}| \cdot |E_{ci}|$, (4.4)

and the phase angles may be added in summation $\theta_i = \theta_{si} + \theta_{ti} + \theta_{ci}$. (4.5)

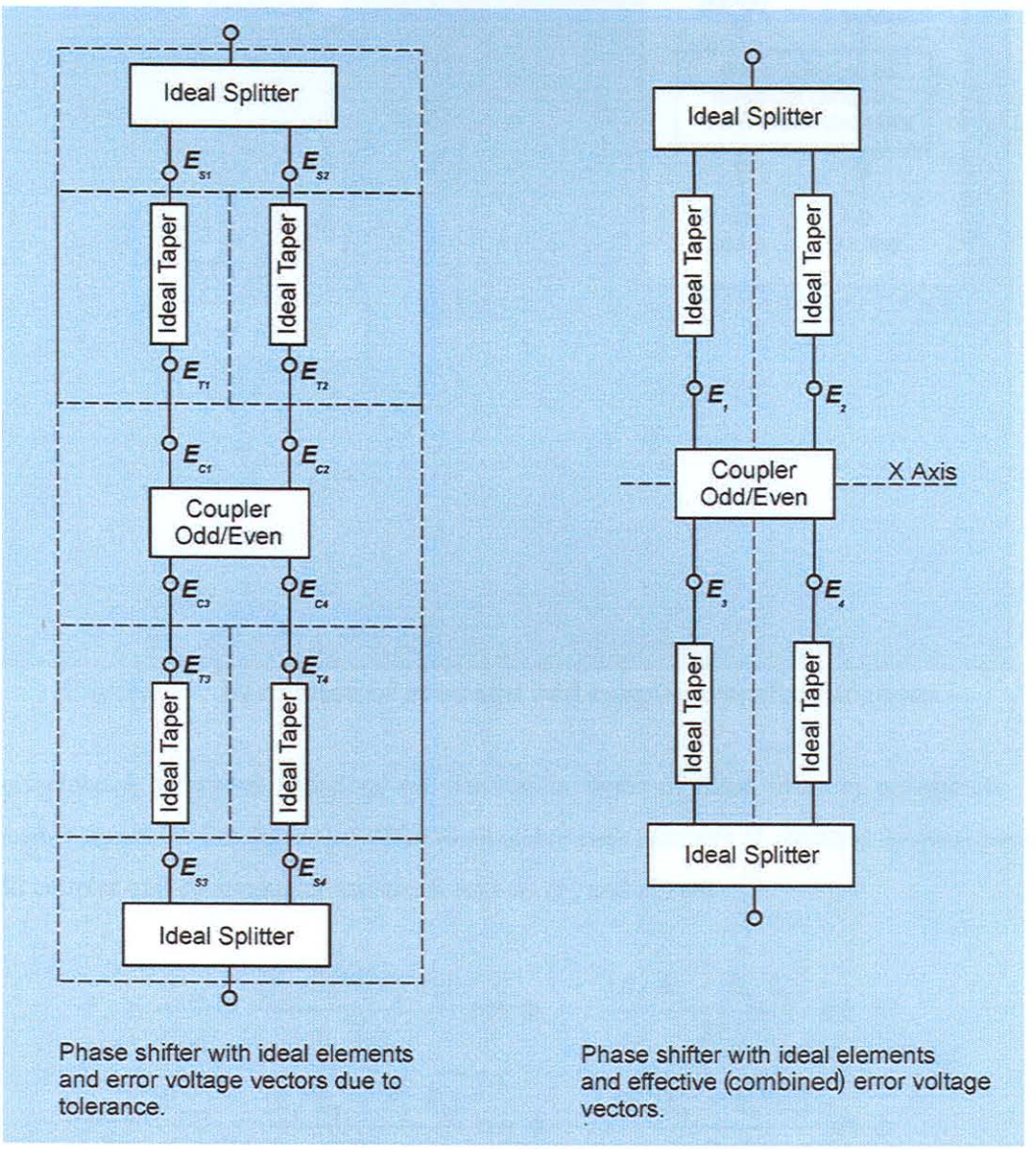

Figure 25 : Phase shifter with ideal elements and error voltage

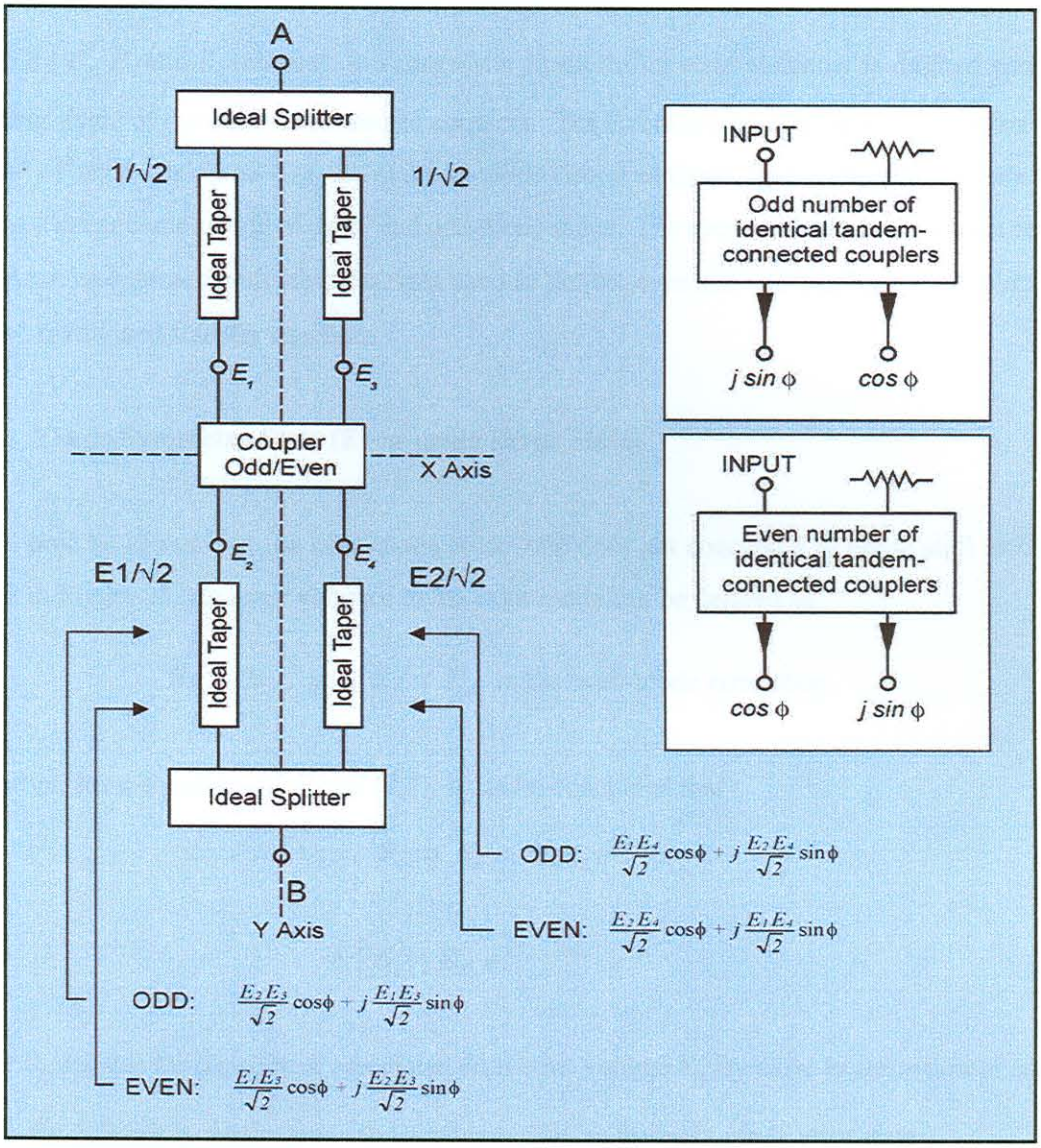

Figure 26 : Derivation of even and odd coupler transfer functions

The performance parameter functions are derived in terms of these element parameters. The performance parameter functions also differ when odd or even numbers of cascaded couplers are used. The odd coupler and even coupler transfer functions (F_o and F_e) are

$$F_o = \frac{B_{odd}}{A_{odd}} = \frac{[E_1\ E_4 + E_2\ E_3]}{2}\cos\phi + j\frac{[E_1\ E_3 + E_2\ E_4]}{2}\sin\phi\ , \tag{4.6}$$

$$F_e = \frac{B_{even}}{A_{even}} = \frac{[E_1\ E_3 + E_2\ E_4]}{2}\cos\phi + j\frac{[E_1\ E_4 + E_2\ E_3]}{2}\sin\phi\ . \tag{4.7}$$

where E_1, E_2, E_3 and E_4 represent the composite phase shifter error elements as defined and ϕ the coupling angle of the tandem-connected couplers. The errors can be seen as a combination of two "states" of error, analogous to even- and odd-mode circuit analyses, where any general state can be seen as a linear combination of even- and odd-mode states. The even- and odd-mode circuit analyses should not be confused with the subscripts used to denote even and odd numbers of couplers in the above- mentioned transfer functions.

4.2.1. Y-axis Symmetry State (Even-mode Error State)

It will now be shown that the even-mode error state does not contribute to phase shift errors. As shown in Figure 25, the error voltages in the even-mode can be derived as

$$E_1 = E_2 \text{ , and } E_3 = E_4 \text{ in the even-mode error state.} \tag{4.8}$$

Therefore, from equations (4.6) and (4.7), it can be concluded that

$$F_o = F_e = E_1 E_3 e^{j\phi} \text{ ,} \tag{4.9}$$

$$= |E_1||E_3| e^{j(\theta 1 + \theta 3)f} . e^{j\phi} \text{ .} \tag{4.10}$$

where θ_i denotes the phase error associated with error voltage E_i. By close examination of equation (4.10), the following conclusions can be made regarding the even-mode error state:

- The gain distortion equals the cascaded losses of the elements comprising the phase shifter.
- The phase distortion, presumed to be a linear function of frequency, can be eliminated by the addition or subtraction of a small length of line in the reference line. This is only true if the phase distortion is caused typically by a small distance offset
- It can therefore be concluded that the state of Y-axis symmetry does not contribute to phase shifter errors, and only to small losses.

4.2.2. X-axis Symmetry State (Odd-mode Error State)

It will now be shown that the odd-mode error state causes complex amplitude and phase errors. As shown in Figure 25, the error voltages in the odd-mode can be defined as

$E_1 = E_3$, and $E_2 = E_4$ in the odd-mode error state.

Therefore, from equations (4.6) and (4.7), it can be concluded that

$$F_o = E_1 E_2 \cos \phi + j \tfrac{1}{2} [E_1^2 + E_2^2] \sin \phi \quad , \tag{4.11}$$

$$F_e = \tfrac{1}{2} [E_1^2 + E_2^2] \cos \phi + j E_1 E_2 \sin \phi \quad . \tag{4.12}$$

By close examination of equations (4.11) and (4.12) it is clear that x-axis imbalance errors create complex phase and amplitude errors which need to be thoroughly investigated.

4.3. Derivation of Error Functions

Since it was demonstrated in paragraph 4.2.1 that even-mode imbalance has no effect on the phase shift response, only the odd mode error functions need to be derived. For this purpose an odd-mode amplitude imbalance of δ dB and a phase imbalance of θ degrees are assumed. The voltage imbalance factor can be defined as

$$D = 10^{\delta/20} \quad . \tag{4.13}$$

Let

$$E_1 = \sqrt{P_1}\, e^{j\theta/2} \quad , \tag{4.14}$$

and

$$E_2 = \sqrt{P_2}\, e^{-j\theta/2} \quad . \tag{4.15}$$

be the error voltages, with P_1 and P_2 representing power factors. The power imbalance and energy conservation relations are specified as

$$P_1 / P_2 = D^2 \quad , \tag{4.16}$$

$$P_1 + P_2 = 2 \quad . \tag{4.17}$$

Solving for P_1 and P_2 in terms of D yields

$$P_1 = \frac{2D^2}{D^2 + 1} \quad , \tag{4.18}$$

$$P_2 = \frac{2}{D^2 + 1} \quad . \tag{4.19}$$

Substituting in equations (4.14) and (4.15) yields

$$E_1 = \sqrt{\frac{2\,D^2}{D^2 + 1}}\, e^{j\theta/2} \quad , \tag{4.20}$$

$$E_2 = \sqrt{\frac{2}{D^2 + 1}}\, e^{-j\theta/2} \quad . \tag{4.21}$$

Equations (4.20) and (4.21) can be written in the more convenient form

$$E_1 = \sqrt{2} \sin (\arctan D)\, e^{j\theta/2} \quad , \tag{4.22}$$

$$E_2 = \sqrt{2} \cos (\arctan D)\, e^{-j\theta/2} \quad . \tag{4.23}$$

It can be shown that $$E_1 E_2 = \sin (2 \arctan D) = S_D \quad , \tag{4.24}$$

and $$\frac{E_1^2 + E_2^2}{2} = \cos\theta - j \sin\theta \cos (2 \arctan D) \tag{4.25}$$

$$= \cos\theta - jC_D \sin\theta \quad , \tag{4.26}$$

where $$C_D = \cos (2 \arctan D) \quad . \tag{4.27}$$

The odd and even coupler transfer functions associated with the odd-mode error state are therefore

$$F_o (\phi, \theta, \delta) = (S_D \cos\phi + C_D \sin\phi \sin\theta) + j \cos\theta \sin\phi \quad , \tag{4.28}$$

$$F_e (\phi, \theta, \delta) = \cos\theta \cos\phi + j (S_D \sin\phi - C_D \sin\theta \cos\phi \quad . \tag{4.29}$$

The important phase shifter performance parameters, namely phase shift and gain response, associated with imbalance errors δ dB and θ degrees, can now be defined.

$$P_o(\phi, \theta, \delta) = |S_{21}|_o^2 = \cos^2\theta \sin^2\phi + (S_D \cos\phi + C_D \sin\phi \sin\theta)^2 \quad , \tag{4.30}$$

$$P_e(\phi, \theta, \delta) = |S_{21}|_e^2 = \cos^2\theta \cos^2\phi + (S_D \sin\phi - C_D \cos\phi \sin\theta)^2 \quad , \tag{4.31}$$

$$\phi_o(\phi, \theta, \delta) = arg(S_{21_o}) = \arctan\left[\frac{\tan\phi \cos\theta}{S_D + C_D \tan\phi \sin\theta}\right] \quad , \tag{4.32}$$

$$\phi_e(\phi, \theta, \delta) = arg(S_{21_e}) = \arctan\left[\frac{S_D \tan\phi - C_D \sin\theta}{\cos\theta}\right] \quad . \tag{4.33}$$

From the phase shift, the phase shift errors can be derived as

$$\Psi_o(\phi, \theta, \delta) = \phi - \phi_o \tag{4.34}$$

$$= \arctan\left[\frac{C_D \tan^2\phi \sin\theta + \tan\phi (S_D - \cos\theta)}{\tan^2\phi \cos\theta + C_D \tan\phi \sin\theta + S_D}\right] \quad , \tag{4.35}$$

$$\Psi_e(\phi, \theta, \delta) = \phi - \phi_e \tag{4.36}$$

$$= \arctan\left[\frac{\tan\phi (\cos\theta - S_D) + C_D \sin\theta}{S_D \tan^2\phi - C_D \sin\theta \tan\phi + \cos\theta}\right] \quad . \tag{4.37}$$

Expressions (4.30), (4.31), (4.35) and (4.37) can be used to evaluate the phase shifter sensitivity with respect to element changes, in the odd-mode error state, referred to as imbalance. The remainder of this chapter will deal with the tracking requirement of elements comprising the phase shifter, using the above results.

4.4. Sensitivity Analysis Results

4.4.1. Amplitude Errors

For amplitude-only errors, we set $\theta = 0$ in the phase shifter performance parameter functions as derived in the previous section. Amplitude errors due to amplitude imbalance, for an odd and even number of tandem-connected couplers, are calculated as

$$P_{Ao}(\phi, \delta) = S_D^2 + C_D^2 \sin^2 \phi \quad , \tag{4.38}$$

and

$$P_{Ae}(\phi, \delta) = 1 - C_D^2 \sin^2 \phi \quad . \tag{4.39}$$

Phase shift errors due to amplitude imbalance, for an odd and even number of tandem-connected couplers, are as follows:

$$\Psi_{Ao}(\phi, \delta) = \arctan\left[\frac{\tan\phi\,(S_D - 1)}{\tan^2\phi + S_D}\right] \quad , \tag{4.40}$$

and

$$\Psi_{Ae}(\phi, \delta) = \arctan\left[\frac{\tan\phi\,(1 - S_D)}{S_D \tan^2\phi + 1}\right] \quad . \tag{4.41}$$

To find the phase shift range over which the phase shifter is least sensitive to amplitude imbalance we derive the un-normalized sensitivities of the performance parameters with respect to phase:

a) In the odd number of tandem-connected coupler case, amplitude sensitivity can be calculated by solving the following derivative:

$$\frac{\partial}{\partial\phi} P_{A,o}(\phi,\delta) = 0 \tag{4.42}$$

$$\therefore \phi = \pm 90° \cdot n \qquad n = 0, 1, 2... \tag{4.43}$$

Most sensitive to amplitude imbalance:

$$\phi = \pm 180°\, n \qquad n = 0, 1, 2... \tag{4.44}$$

Least sensitive to amplitude imbalance:

$$\phi = \pm (2n + 1) \cdot 90° \qquad n = 0, 1, 2... \tag{4.45}$$

b) In the even number of tandem-connected coupler case, amplitude sensitivity can be calculated by solving the following derivative:

$$\frac{\partial}{\partial \phi} P_{A,e}(\phi,\delta) = 0 \qquad \therefore \phi = \pm 90° \cdot n \qquad n = 0, 1, 2... \tag{4.46}$$

Most sensitive to amplitude imbalance:

$$\phi = \pm (2n + 1) \cdot 90° \qquad n = 0, 1, 2... \tag{4.47}$$

Least sensitive to amplitude imbalance:

$$\phi = \pm 180° \cdot n \qquad n = 0, 1, 2... \tag{4.48}$$

c) In the odd and even number of tandem-connected coupler cases, the two derivative equations yield the same solution for phase sensitivity:

$$\frac{\partial}{\partial \phi} \Psi_{A,o}(\phi,\delta) = 0 \quad , \tag{4.49}$$

and

$$\frac{\partial}{\partial \phi} \Psi_{A,e}(\phi,\delta) = 0 \quad . \tag{4.50}$$

$$\therefore \phi = \pm 45° \cdot n \qquad n = 0, 1, 2... \tag{4.51}$$

Most sensitive to amplitude imbalance:

$$\phi = \pm (2n + 1) \cdot 45° \qquad n = 0, 1, 2... \tag{4.52}$$

Least sensitive to amplitude imbalance:

$$\phi = \pm 90° \cdot n \qquad n = 0, 1, 2... \tag{4.53}$$

d) In a worst case analysis, to determine maximum amplitude imbalance errors we observe that maximum amplitude errors occur when $\sin\phi = 0$ in the odd number of tandem-connected coupler case, and $\sin\phi = 1$ in the even coupler number case.

$$P_{A,\,MAX}(\delta) = P_{A,o\,MAX}(\delta) = P_{A,\,e\,MAX}(\delta) = S_D^2 \tag{4.54}$$

Maximum phase shift errors occur when $\tan\phi = 1$ in the case of both even and odd number of tandem connected couplers.

$$| \Psi_{A,\,MAX}(\delta) | = | \Psi_{A,e\,MAX}(\delta) | = | \Psi_{A,o\,MAX}(\delta) | = | \arctan\left[\frac{S_D - 1}{S_D + 1}\right] | \qquad (4.55)$$

From Figure 27, which shows the graphs of amplitude errors, it is clear that these errors do not severely affect the phase shifter performance. In the odd number of tandem-connected coupler case, these errors affect the phase shifter gain most at low values of ϕ, while in the even coupler number case, the phase shifter gain is more sensitive to these errors for phase shift values closer to 90°.

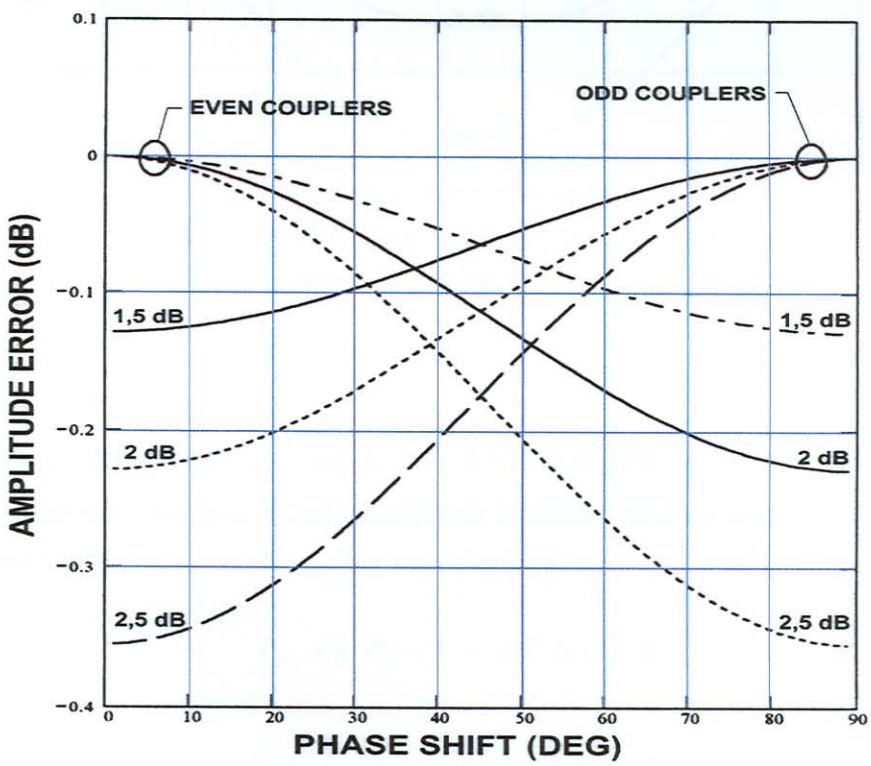

Figure 27 : Amplitude error due to amplitude imbalance

Values of amplitude imbalance as high as 2.5 dB cause a phase shifter insertion loss of only 0.35 dB. The phase shift is most sensitive for amplitude imbalance at phase shift values of 45°, but a 2.5 dB imbalance causes a phase shift error of only 1.2°. From the results as displayed in Figure 28, it is clear that the phase shifter performance parameters are insensitive to amplitude imbalance errors.

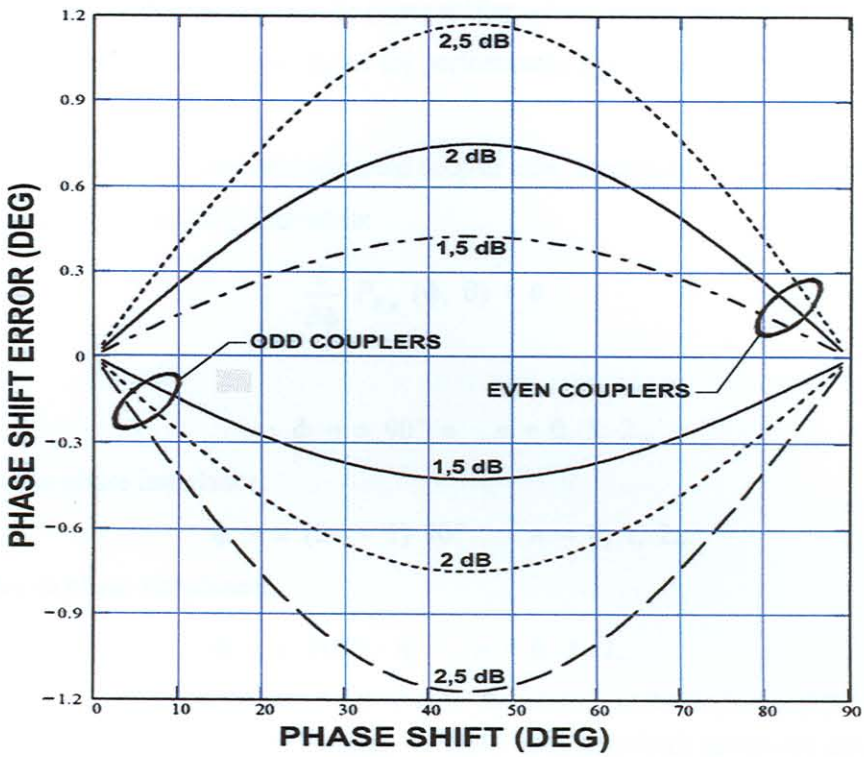

Figure 28 : Phase shift error due to amplitude imbalance

4.4.2. Phase Errors

To analyse phase errors, we set $C_D = 0$ and $S_D = 1$ ($\delta = 0$) in the phase shifter performance parameter functions, derived in the previous section. Amplitude errors due to phase imbalance, for an odd and even number of tandem-connected couplers, are calculated as

$$P_{P,o}(\phi, \theta) = 1 - \sin^2 \phi \sin^2 \theta \quad , \tag{4.56}$$

and

$$P_{P,e}(\phi, \theta) = 1 - \cos^2 \phi, \sin^2 \theta \quad . \tag{4.57}$$

Phase shift errors due to phase imbalance, for an odd and even number of tandem-connected couplers, are as

$$\Psi_{P,o}(\phi, \theta) = \arctan\left[\frac{\tan \phi \,(1 - \cos \theta)}{\tan^2 \phi \cos \theta + 1}\right] \quad , \tag{4.58}$$

and

$$\Psi_{P,e}(\phi, \theta) = \arctan\left[\frac{\tan \phi \cdot (\cos \theta - 1)}{\tan^2 \phi + \cos \theta}\right] \quad . \tag{4.59}$$

To find the phase shift range over which the phase shifter is least sensitive to phase imbalance errors we derive the un-normalized sensitivities of the performance parameters with respect to phase:

a) In the odd number of tandem-connected coupler case, amplitude sensitivity can be calculated by solving the following derivative:

$$\frac{\partial}{\partial \phi} P_{P,o}(\phi, \theta) = 0 \tag{4.60}$$

$$\therefore \phi = \pm 90^\circ n \quad n = 0, 1, 2... \tag{4.61}$$

Most sensitive to phase imbalance:

$$\phi = \pm (2n + 1)\, 90^\circ \quad n = 0, 1, 2... \tag{4.62}$$

Least sensitive to phase imbalance:

$$\phi = \pm 180^\circ \cdot n \quad n = 0, 1, 2... \tag{4.63}$$

b) In the even number of tandem-connected coupler case, amplitude sensitivity can be calculated by solving the following derivative:

$$\frac{\partial}{\partial \phi} P_{P,e}(\phi, \theta) = 0 \tag{4.64}$$

$$\therefore \phi = \pm 90^\circ n \quad n = 0, 1, 2... \tag{4.65}$$

Least sensitive to phase imbalance:

$$\phi = \pm (2n + 1)\, 90^\circ \quad n = 0, 1, 2... \tag{4.66}$$

Most sensitive to phase imbalance:

$$\phi = \pm 180^\circ \cdot n \quad n = 0, 1, 2... \tag{4.67}$$

b) In the odd and even number of tandem-connected coupler case, the two derivative equations yield the same solution for phase sensitivity:

$$\frac{\partial}{\partial \phi} \Psi_{P,o}(\phi, \theta) = 0 \ , \tag{4.68}$$

and

$$\frac{\partial}{\partial \phi} \Psi_{P,e}(\phi, \theta) = 0 \ . \tag{4.69}$$

$$\therefore \phi = \pm n \cdot 45^\circ \quad n = 0, 1, 2... \tag{4.70}$$

Most sensitive to phase imbalance:

$$\phi = \pm (2n + 1) \cdot 45^\circ \; n \qquad n = 0, 1, 2... \tag{4.71}$$

Least sensitive to phase imbalance:

$$\phi = \pm n \cdot 90^\circ \qquad n = 0, 1, 2... \tag{4.72}$$

c) In a worst case analysis, to determine maximum phase imbalance errors we observe that maximum amplitude errors occur when $\sin\phi = 1$ in the odd number of tandem connected coupler case, and $\cos\phi = 1$ in the even coupler number case.

$$P_{P,\,MAX}(\theta) = P_{P,o\,MAX}(\theta) = P_{P,e\,MAX}(\theta) = \cos^2\theta \tag{4.73}$$

Maximum phase shift errors occurs when $\tan\phi = 1$ for both even and odd number of tandem connected couplers.

$$|\,\Psi_{P\,MAX}(\theta)\,| = |\,\Psi_{P,0\,MAX}(\theta)\,| = |\,\Psi_{P,e\,MAX}(\theta)\,| \;,$$

$$= \left|\arctan\left[\frac{1 - \cos\theta}{1 + \cos\theta}\right]\right| = \left|\arctan\left[\tan^2\left(\frac{\theta}{2}\right)\right]\right| \;. \tag{4.74}$$

From the graphs of phase errors in Figure 29, it is clear that these errors severely affect the phase shifter performance. In the odd number of tandem-connected coupler case, these errors affect the phase shifter gain most at phase shift values close to 90°. The even number of tandem-connected coupler case, the phase shifter gain is more sensitive to these errors for low phase shift values. Phase imbalance errors of 45° cause a 3 dB loss. The phase shift shown in Figure 30 is most sensitive for phase imbalance at phase shift value of 45°, where a 45° imbalance causes a 10° phase shift error. From these results, it is clear that the phase shifter performance parameters are quite sensitive to phase imbalance errors. Application of symmetry to phase shifters is therefore a very important measure to enhance the performance of ultra-wideband devices.

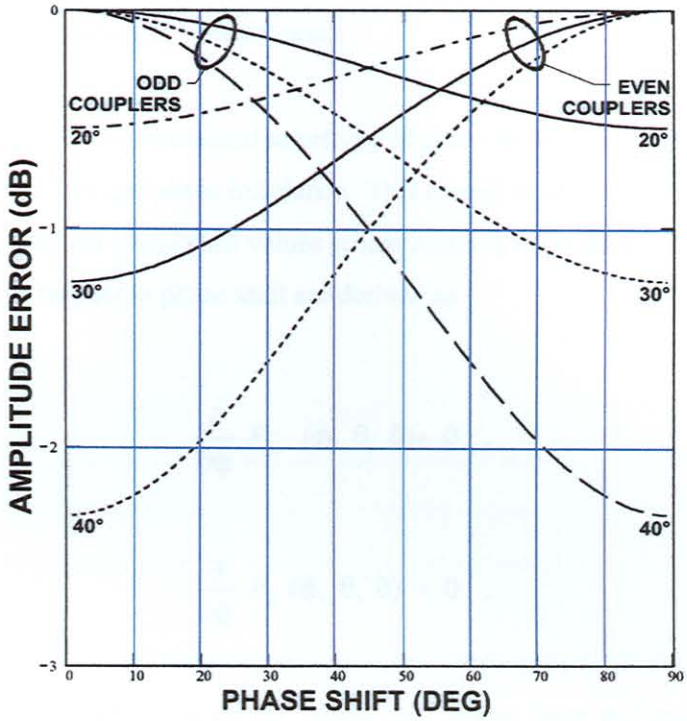

Figure 29 : Amplitude error due to phase imbalance

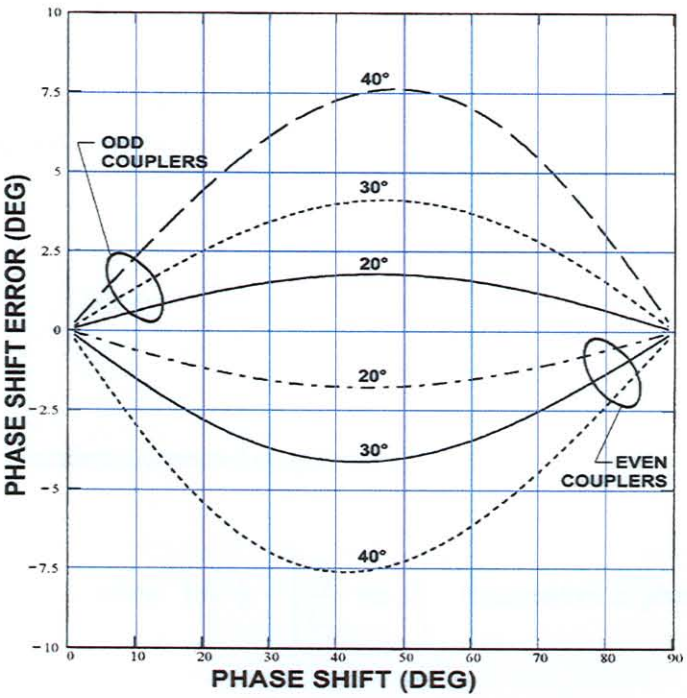

Figure 30 : Phase shift error due to phase imbalance

4.4.3. Combined Amplitude and Phase Errors

The next step is to derive the un-normalized sensitivity of phase shifter loss error with respect to phase shift, for combined amplitude and phase imbalance. This is used to derive expressions for maximum loss distortion, and to find the phase shift values where losses is most sensitive to these errors. The derivatives of loss with respect to phase shift are derived as

$$\frac{\partial}{\partial \phi} P_o \ (\phi, \theta, \delta) = 0 \quad , \tag{4.75}$$

and

$$\frac{\partial}{\partial \phi} P_e \ (\phi, \theta, \delta) = 0 \quad . \tag{4.76}$$

The solution of these derivatives yields the phase shift values least and most sensitive to both amplitude and phase imbalance. The derivatives yield the same solutions:

$$\tan^2 \phi + \left[\frac{S_D^2 - C_D^2 \sin^2 \theta - \cos^2 \theta}{S_D C_D \sin \theta} \right] \tan\phi - 1 = 0 \tag{4.77}$$

Two solutions are found when solving equation (4.77):

$$\tan \phi = \left[\frac{S_D}{C_D} \sin \theta \right]^{-1} \quad \text{or} \quad - \left[\frac{S_D}{C_D} \sin \theta \right] \quad . \tag{4.80}$$

For the odd number of tandem-connected coupler case:

$$P_{o,\,MAX} \ (\theta, \delta) = 1 \text{ when } \tan \phi = \left[\frac{S_D}{C_D} \sin \theta \right]^{-1} \text{ (unsensitive to phase imbalance)} \tag{4.81}$$

$$= S_D^2 \cos^2 \theta \text{ when } \tan \phi = -\left[\frac{S_D}{C_D} \sin \theta \right] \text{ (sensitive to phase imbalance)} \tag{4.82}$$

For the even coupler case:

$$P_{e\,MAX}\,(\theta,\,\delta) = 1 \text{ when } \tan\phi = -\left[\frac{S_D}{C_D}\sin\theta\right] \text{ (completely unsensitive)}, \tag{4.83}$$

$$= S_D^2\cos^2\theta \text{ when } \tan\phi = \left[\frac{S_D}{C_D}\sin\theta\right]^{-1} \text{ (most sensitive)}. \tag{4.84}$$

From the graphs of maximum loss distortion in Figures 31 and 32, it is clear that even for severe amplitude imbalance errors, the curve does not change significantly. Depending on odd or even number of tandem-connected couplers, the error curve shifts slightly left or right. This confirms that these phase shifters are relatively insensitive to amplitude distortion.

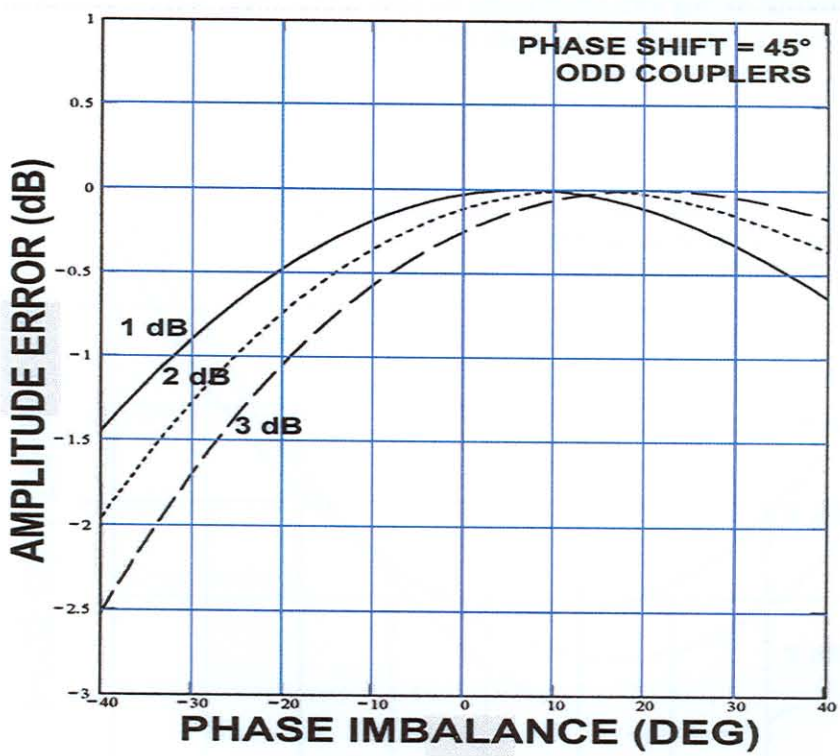

Figure 31 : Amplitude error due to amplitude and phase imbalance - odd couplers

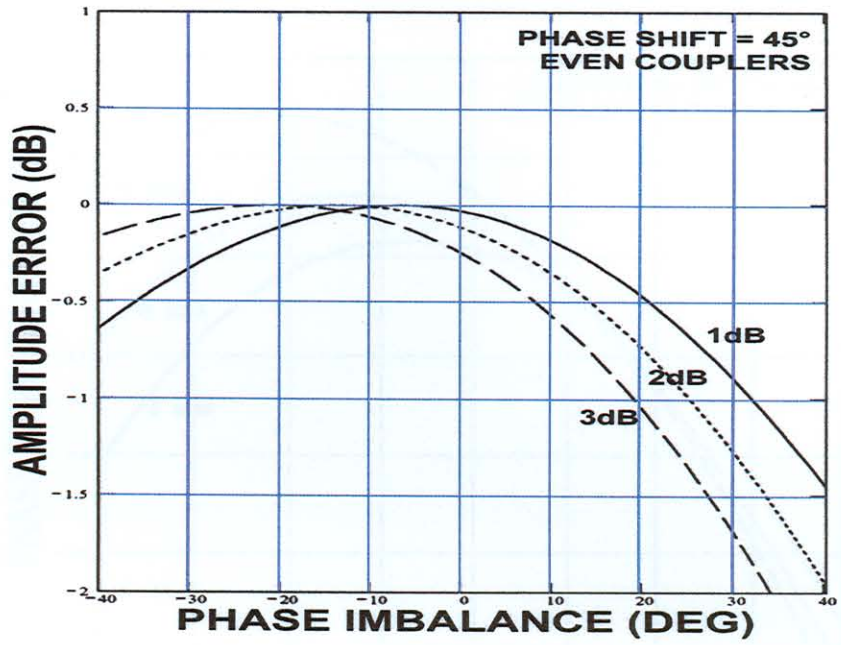

Figure 32 : Amplitude error due to amplitude and phase imbalance - even couplers

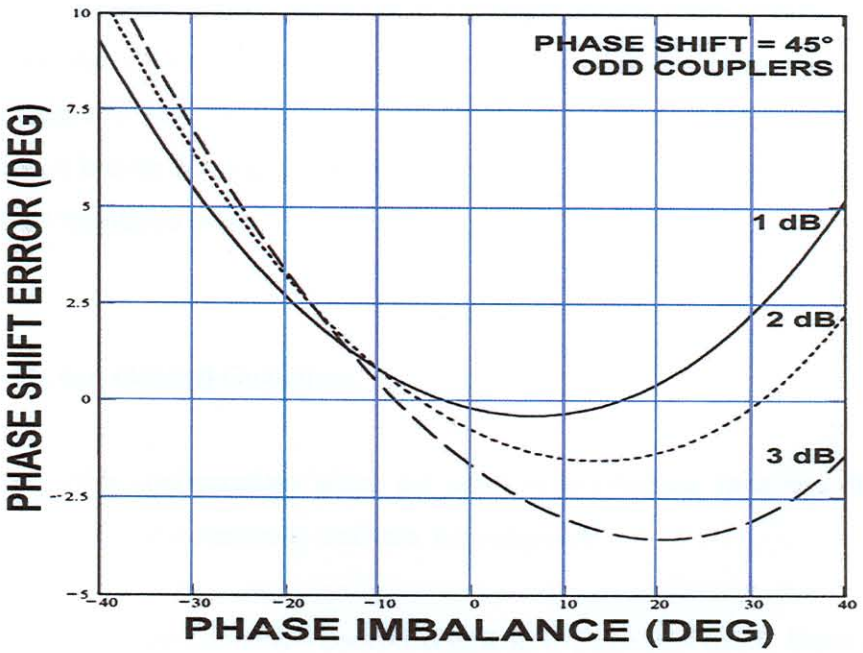

Figure 33 : Phase shift error due to amplitude and phase imbalance - odd couplers

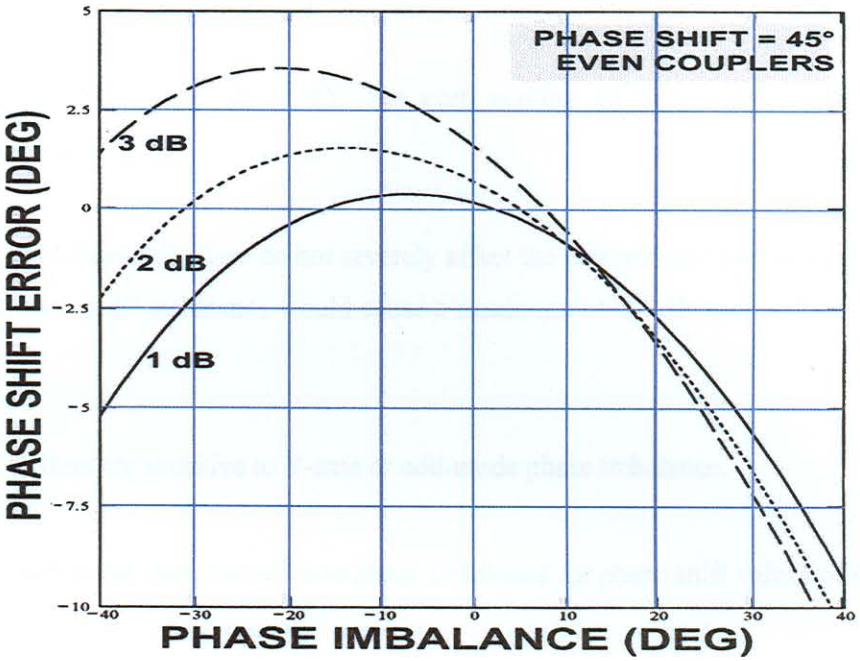

Figure 34 : Phase shift error due to amplitude and phase imbalance - even couplers

In Figures 33 and 34 graphs of phase shift error due to amplitude and phase imbalance can be seen. The error curves of the odd and even number of tandem-connected couplers form mirror pairs around the zero phase shift error line. As a parasitic element can even introduce a 20° phase imbalance at some frequencies, it is clear that large phase shift errors can be caused. The phase shifter is, therefore, sensitive to phase imbalance errors.

4.5. Conclusion and General Guidelines

To avoid phase shifter configurations which are sensitive to tolerance variations, the following guidelines, derived using the sensitivity analyses, are suggested:

- X-axis or even-mode asymmetry does not contribute to phase shift errors. Phase shifter losses are equal to the cascade of the amplitude errors.

- For phase shift values below 45°, an odd number of tandem-connected couplers is recommended.

- For phase shift values above 45°, an even number of tandem-connected couplers is recommended.

- Amplitude imbalance errors do not severely affect the performance parameters of the phase shifter. A 2.5 dB imbalance would cause a maximum of 0.4 dB loss and 1.2° phase shift error.

- Phase shifters are sensitive to Y-axis or odd-mode phase imbalance.

- Phase shifters are most sensitive to phase imbalance for phase shift values of 45°. A 45° imbalance cause a 10° phase shift error.

References

[1] K. C. Gupta, R. Garg, and R. Chadha, "Computer aided design of microwave circuits", Artech House, Massachusetts, 1981.

CHAPTER 5. PHASE SHIFTER SYNTHESIS

5.1. Introduction

For completeness, it was decided to synthesize a 45° phase shifter, due to the sensitivity analysis highlighting it as the most sensitive to tolerance variations. Firstly, a general synthesis procedure is presented to aid future designers in realising any ultra-broadband phase shifter of the newly proposed type. Restrictions to the developed theory are also highlighted. Critical manufacturing requirements and process tolerances are discussed to provide a feel for the ability to manufacture large quantities of these devices. Well-known state-of-the-art materials are chosen and the trade-offs are discussed. From a typical electrical performance specification, the device is designed and realised. The theoretical and measured performance figures are then presented and compared.

5.2. General Phase Shifter Synthesis Guidelines

The design of a wideband phase shifter starts with a specification of phase shift, ripple and bandwidth. The synthesis is restricted to homogeneous triplate media such as PTFE stripline structures, for optimum bandwidth.

- The mean and ripple coupling values of the coupler are calculated from the specification, using the phase shifter transform equations. If the coupling exceeds about 6 dB, two or more couplers should be used in tandem to relax the coupling specification per coupler. To simplify the design, tandem connected couplers are chosen to be identical. For phase shifts lower than 45°, an odd number of couplers is recommended to de-sensitize the phase shifter to tolerance variations. For phase shifts higher than 45°, an even number of tandem-connected couplers is recommended.

- For narrow-band or low frequency phase shifters, it is not always necessary to taper the couplers continuously. For wideband and high frequency operation, (eg exceeding 10 GHz) Tresselt's continuously tapered coupler principles [1] should be applied to improve directivity. Select the spacing s to be as small as possible (eg 5 mil) to minimize the via lengths and improve splitter performance. The ground plane spacing b is selected to best fit the fixed coupling value at the centre of the couplers for an internal impedance of 50 Ω. The couplers are then designed as discussed in Section 3.3.

- Exponential tapers are easily designed as in Section 3.2.2 and were found to be very successful, since taper performance is very insensitive to tolerance as calculated in Section 3.2.3. However, any taper, for example the Hecken taper, can be applied successfully.

- To design the splitter, calculate the BCS splitter width from Cohn's equations as discussed in Chapter 3. Choose the via diameter to be about half this width to avoid fringe field interference. The spacing of the vias should be selected to be as low as possible to avoid in-band resonance as discussed in Section 3.4.4.4 (typically 2mm). For frequencies below 10 GHz, two or three vias should be sufficient. Use of four vias extends the splitter performance to the millimetre wave band.

The via analysis reveals that small changes in via nature does not affect the performance of the splitter. The most typical material choices were used in the thorough analysis of the via splitter, but other materials are also expected to yield acceptable splitter results. To ensure smooth transitions between the elements comprising the phase shifter, it is important to avoid additional parasitical components internal to the phase shifter which could add to asymmetry.

5.3. Processes and Tolerance Requirements

A material that is very commonly used in the industry for accurate stripline microwave components, is the well-known RT/Duroid 5880 glass fibre reinforced polytetrafluoroethylene (PTFE) composite supplied by Rogers corporation. The fibres are randomly oriented to ensure a highly homogeneous substrate, and the dielectric constant is also found to be constant from panel to panel, over a wide frequency range. The substrate also has excellent machinability.

The dielectric constant of RT/Duroid 5880 composite is 2.2 ± 0.02 at 10 GHz at a temperature of 30°C and has a 0.78% tolerance at 0°C and 100°C. Therefore it is expected that the taper performance will not be affected significantly by temperature variations. All lines will have an added reflection coefficient of less than -45 dB and the bandwidth of the coupler (and therefor of the phase shifter) may change by a maximum of 200 MHz at 20 GHz. The material loss factor (tan δ) is specified at 0.0009 at 10 Ghz, which is very low. Regarding the substrate thickness tolerances, the 5 mil centre slab thickness s is expected to be within 13 μm and the GPS within 64 μm. Again the lines and tapers are virtually unaffected but the combined worst case may cause a coupling deviation

of 0.24 dB and a bandwidth change of 300 MHz at 20 GHz. While it is difficult to verify the dielectric constant, measured substrate thickness should be used in design calculations.

The expected copper thickness t is 18μm. The copper can be either rolled foil or electro-deposited onto the PTFE. Electro-deposited copper is prone to thermal stress cracks, especially for thin lines, but has a better adhesion to PTFE than rolled copper foil. Since it is desired to etch high-impedance lines accurately, rolled copper proves to be the better choice, especially since the surface roughness of rolled copper is the lowest. A roughness of 1.4 μm is expected, causing a 0.03 dB coupling value deviation in the coupler. Rolled copper also has much lower losses at high frequencies. The lines and taper are only slightly affected.

Over- or under-etching of 25 μm can cause a 0.45 dB coupling error, and should be compensated for by adding line-width to the mask. A 10 μm accuracy can be expected, leading to a 0.18 dB coupling tolerance. Scaling errors of 5% can also cause a 0.48 dB coupling tolerance, but less than 0.05% scaling error can be expected when the mask is laser-plotted and scaling verified by microscope. The top and bottom etch mask alignment at the photolythographic process proves to be the critical factor. Linear alignment errors of 70 μm and rotational errors of 1° cause 0.6 dB and 0.8 dB coupling errors respectively and 5.6° and 0.3° of phase errors respectively.

The splitter performance, as discussed previously, can be expected to be within 0.4 dB and 3° providing that the vias are realised by bonding gold ribbons through the via holes and filling the through holes with conductive epoxy.

Considering all processes and the associated tolerances, a coupler coupling error of about 0.8 dB and phase accuracy of 8.5° can be expected. These figures dominate the phase shifter performance, and a phase shift accuracy of 0.7° and amplitude deviation of 0.15 dB can be expected.

5.4. Phase Shifter Practical Example

As an example, a 45° ± 5° phase shifter over a 2-18 GHz band will be synthesised. The coupling for 45° phase shift can be calculated by equation (2.22).

$$C_0\,(dB) = 20\log[\sin 45°] = -3.01dB \tag{5.1}$$

The phase ripple is ± 5°. The corresponding coupling ripple is then, according to equation (2.24)

$$\delta_0\ (dB) = 20\ \log\left[\frac{\sin\ (45° + 5°)}{\sin\ (45°)}\right] = 0.695\ dB\ . \tag{5.2}$$

Since the mean coupling C_0 is too tight for a single coupler, the tandem connection of two identical couplers may be implemented, their coupling and ripple values being

$$C_0\ (dB) = 20\ \log\ [\sin\ (22.5°)] = -8.343\ dB\ , \tag{5.3}$$

$$\delta_0 = 20\ \log\left[\frac{\sin\ (22.5° + 2.5°)}{\sin\ (22.5°)}\right] = 0.862\ dB\ . \tag{5.4}$$

When designing coupler sections for optimal performance, it was found that a 5-section coupler will meet these specifications. The optimal normalized impedance levels as calculated by the optimization program described in section 3.3.1, were found to be

$$Z_1 = 1.09218\ ,$$

$$Z_2 = 1.26492\ ,$$

$$Z_3 = 2.09984\ .$$

The coupler design program described in paragraph 3.3.1 was run to synthesize the coupler. Typical measured *s*-parameter results of a 9-section test coupler is shown in Appendix E. The computer text file of the synthesis of the phase shifter coupler is also found in Appendix E. The graphical file which is also generated by the design program was stored to generate the etch-mask.

The splitter width was found to be 0.602 mm to ensure a 100 Ω even-mode impedance. A 0.3 mm via diameter was chosen, causing a 29.03 pH and -357.2 μm phase model for the via. The via spacing should be less than 5.06 mm to avoid resonance. Four vias were chosen with a 2 mm spacing.

The results of the sensitivity analysis are applied to the example in the last chapter to obtain acceptable splitter-coupler-taper imbalance and asymmetry tolerance figures for a desired phase shifter performance. Alternatively, the measured amplitude and phase tolerance of the practical phase shifter may be applied to the sensitivity analysis equations to quantify achieved imbalance.

In the practical example case, two tandem-connected couplers are synthesized to yield a 45° phase shifter. The equations for the even number of tandem-connected couplers are used at 45°.

$$S = \sin\left[2 \arctan\left(10^{\delta/20}\right)\right] , \tag{5.5}$$

$$C = \cos\left[2 \arctan\left(10^{\delta/20}\right)\right] . \tag{5.6}$$

where δ represents the amplitude imbalance, in dB. Let θ be the phase imbalance of the phase shifter. Then the associated amplitude and phase errors are

$$P_e(\delta,\theta) = 20 \log\left[\frac{\cos\theta^2 + (S_D - C_D \sin\theta)^2}{2}\right] , \tag{5.7}$$

$$\Psi_e(\delta, \theta) = \arctan\left[\frac{\cos\theta - S_D + C_D \sin\theta}{\cos\theta + S_D - C_D \sin\theta}\right] . \tag{5.8}$$

The results are presented graphically, for $-40° < \theta < 40°$ and $\delta = 1, 2, 3$ dB in Figures 32 and 34. The next table summarises the results for up to three vias:

Table 5.1 : Expected performance of phase shifters with up to 3 vias

Via No.	θ (deg)	δ (*dB*)	*A* err (*dB*)	Ψ err (deg)
1	7.5	15	2	8
2	5	6	0.4	3
3	2.5	3	0.3	2

An improved grasp of performance deviations that can be expected for a certain imbalance caused by manufacturing tolerance, was obtained. The sensitivity analysis was applied to the practical phase shifter example. The phase shifter seems to be fairly insensitive to manufacturing tolerances.

The tapers were synthesised as described by section 3.2.1. The photomask of the phase shifter is shown in Figure 35. Compensation of 35 μm was added to the line width to counteract the effect of over-etching.

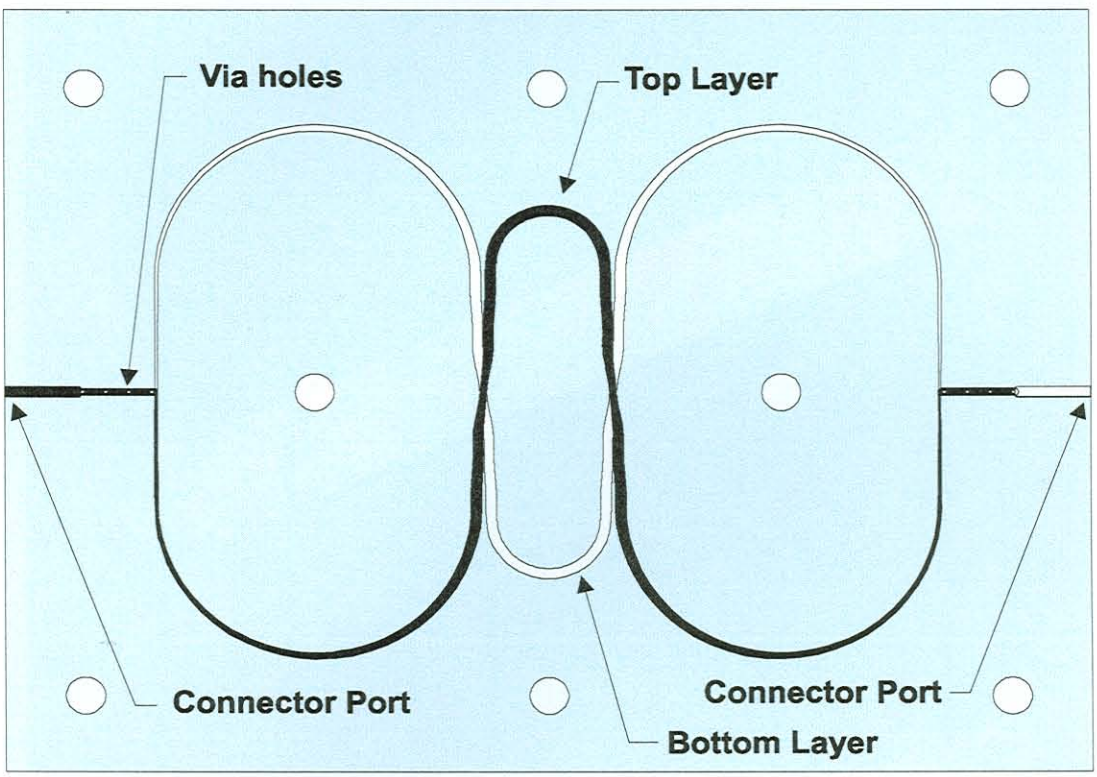

Figure 35 : Photomask of a 45° phase shifter

5.5. Practical Phase Shifter Results

The practical results of the phase shifter synthesized in 5.4 are now briefly discussed. Figure 36 shows a 20 : 1 microscope photo of the splitter, and a closer 50 : 1 photo of a ribbon-epoxy constructed via.

The sharp edge definition and 25μm tolerance suggests an excellent etching process control. The gold ribbons were mounted and the epoxy filled in a class 100 cleanroom.

A photo of the pre-assembled phase shifter is shown in Figure 37. The 100-50 Ω tapered transformer lines and tandem-connected couplers can clearly be seen. To prevent corrosion, a flush of gold was plated on the circuit tracks.

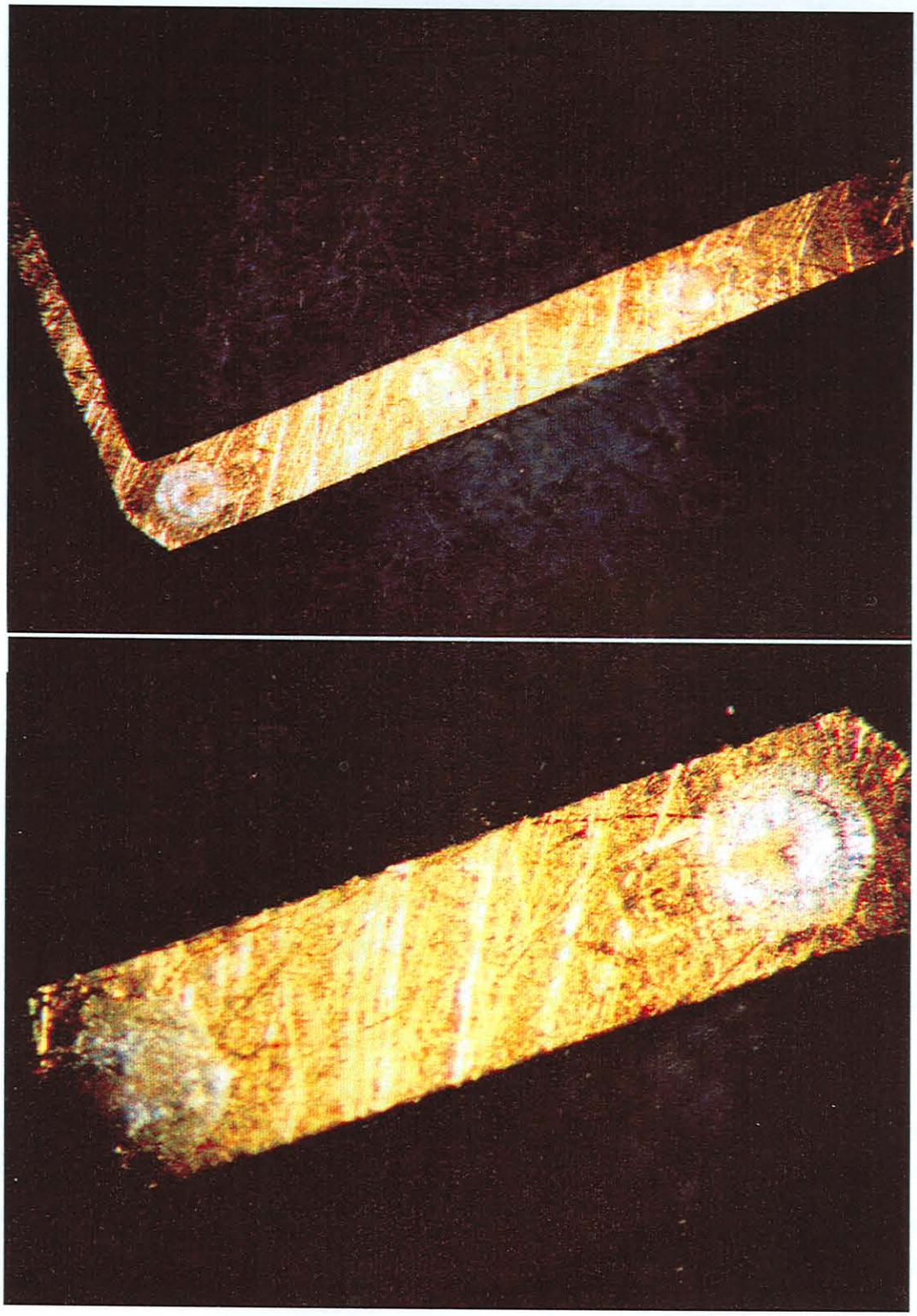

Figure 36 : The practical splitter and via

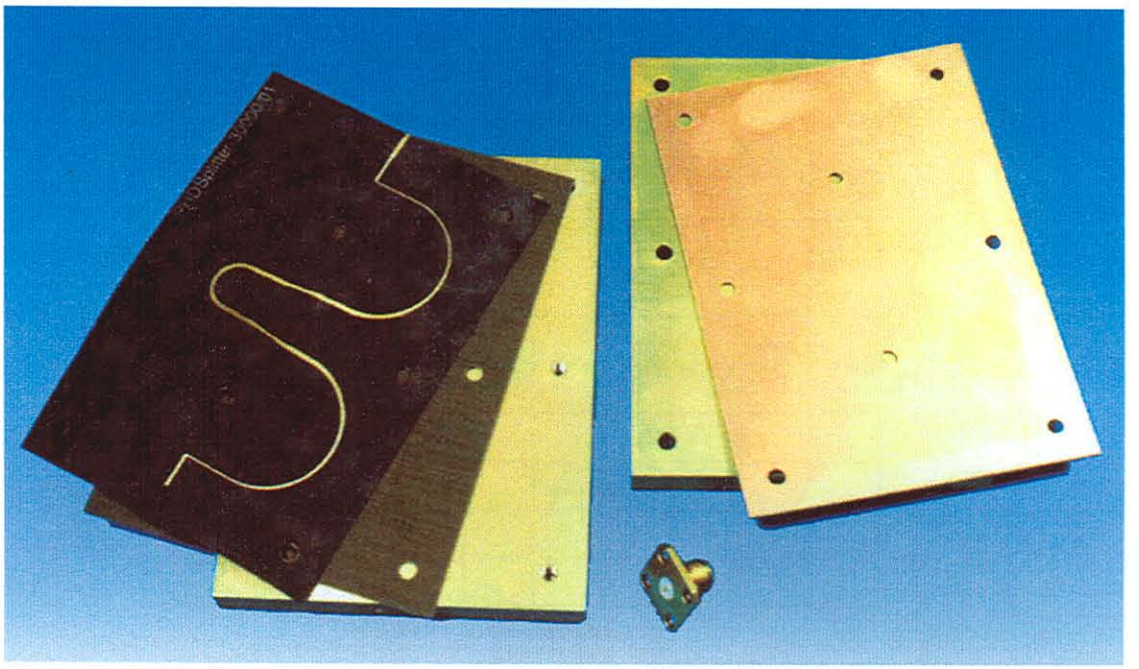

Figure 37 : The practical phase shifter

To measure the electrical performance of the phase shifter, the "through" calibration was done including the connectorized reference line, but measurements were conducted by substitution of the reference line by the phase shifter. The theoretical and measured phase shift versus frequency responses are superimposed on one graph (Figure 38). The excellent agreement of these responses demonstrate the theory to be very accurate. From Figure 38 it can be seen that the theoretical and practical phase shift agrees to within three degrees in the 2-18 GHz range. The sensitivity and tolerance analysis can be applied to this specific case and a graph of the expected production tolerance can be generated as in Figure 39. The measured phase shift response is superimposed on this graph to demonstrate the validity of the analysis, and the practicality of the novel phase shifter.

For completeness, Figure 40 shows the measured reflection and insertion loss response of the phase shifter. The results also agree with expected values. The reflection coefficient is below -15dBc from 2-18GHz except for the peak at 2.5GHz, and the maximum loss is only 1.7dB at 18GHz. The 0.602 mm lines in the 100 Ω tapered lines contribute most of the losses experienced at high frequency.

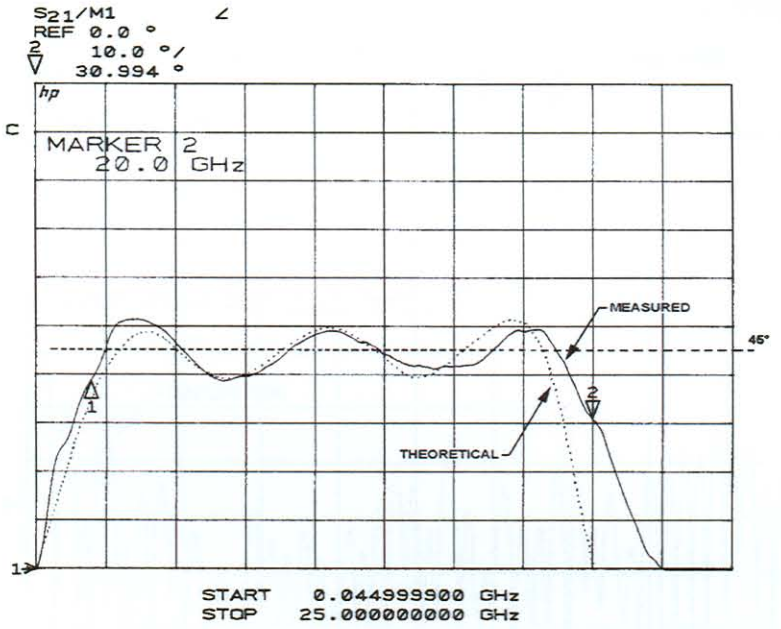

Figure 38 : Measured and theoretical phase shift response

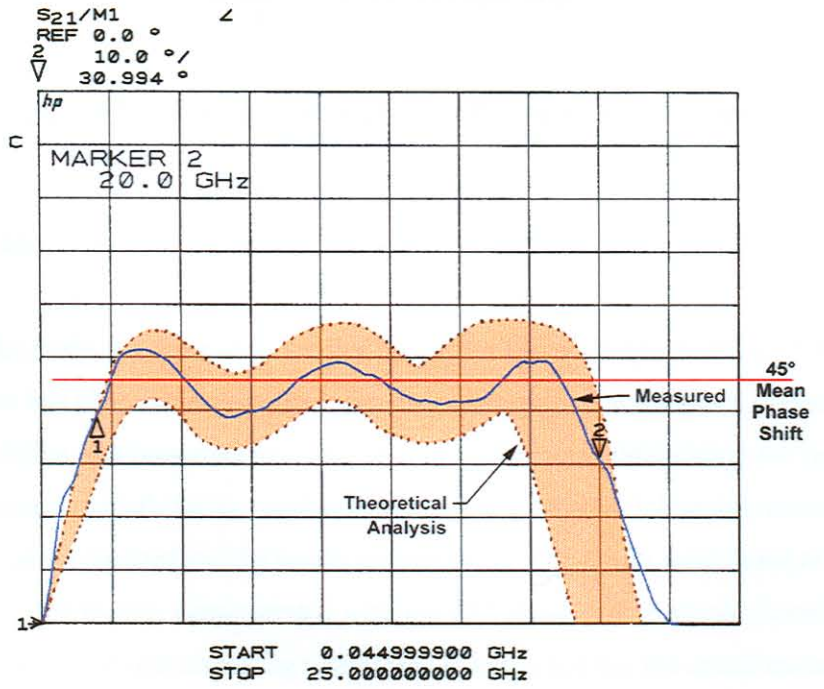

Figure 39 : Measurement and expected production tolerance of the phase shift response

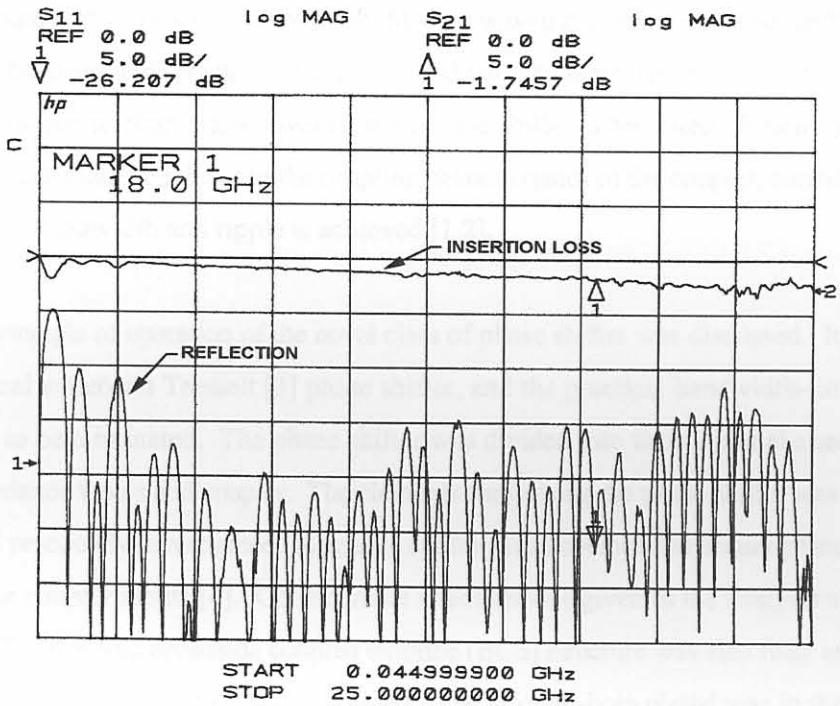

Figure 40 : Measured reflection and insertion loss response

5.6. Conclusion

To complete the study, the theory was verified by a phase shifter design example. A 45° phase shifter was chosen, as this phase shift provides a device most sensitive to tolerance variations. A general synthesis guideline was presented as an aid to future designers, highlighting the restrictions to the synthesis. Practical manufacturing requirements and typical process tolerances were discussed. The phase shifter was synthesized and the results are presented. The results were found to be in very close agreement with the theory, demonstrated with the 45° phase shifter which proved to be the most sensitive to material and manufacturing tolerances. It was found that the actual measured results fall within the analytical tolerance boundaries. Practically, the bandwidth was found to be slightly wider than predicted due to a combination of dielectric tolerance and scaling error. The in-band phase shift exceeded the 5° ripple at the first 2 ripple points by about one degree. Practically, the phase shift ripple value should therefore be chosen somewhat smaller than the specification. It can be expected that phase shift performance will be better at phase shift values further away from 45°.

CHAPTER 6. SUMMARY AND CONCLUSIONS

Realising the shortfalls of conventional microwave differential phase shifters, an in-depth study was launched into this area, focussing on the synthesis of ultra-wideband devices covering up to more than a decade of bandwidth. This excluded ferrite, MMIC, waveguide and some other technologies which are relatively band-limited. By noting the unique and very valuable frequency independent quadrature property of symmetric couplers, a novel class of phase shifter is proposed. Realising that the phase shift characteristics can be related to the coupling characteristics of the coupler, considerable freedom with respect to bandwidth and ripple is achieved [1,2].

Firstly, the principle of operation of the novel class of phase shifter was discussed. It was compared to the classical wideband Tresselt [3] phase shifter, and the practical bandwidth-limiting obstacles were shown to be eliminated. The phase shifter was divided into three main elements, namely the splitter, impedance tapers and coupler. The elements comprising the phase shifter was then separately analysed and practically investigated. A unique splitter was developed to ensure phase and amplitude tracking at the coupler inputs [4]. Considerable attention was given to the analysis and synthesis of the splitter. The periodic broadside coupled stripline (BCS) structure was also fully analysed and the resonance nature of the structure was predicted. The through-hole plated vias in the BCS structure were analysed by both a full-wave analysis and a finite element analysis to compare the results. Empirical element fit was conducted to provide a future designer with very accurate via models. The splitter performance was then mathematically predicted and compared to a physical practical example. A tolerance analysis was also conducted on each element comprising the phase shifter, and this was compared to the phase shifter sensitivity analysis demands.

The phase shifter was then analysed thoroughly to determine its sensitivity with respect to errors due to manufacturing tolerances. Error and performance parameters were defined and sensitivities to tolerance variations were calculated. These results clearly demonstrate the practicality of the idea and also pinpoint the areas of the phase shifter most sensitive to tolerances. It was demonstrated that the performance of the phase shifter is sensitive to phase imbalance errors, and that application of symmetry enhancement techniques is important to attain the desired performance of ultra-high bandwidth devices. It was also demonstrated that the phase shifter is relatively insensitive to amplitude errors. It was discovered that the phase performance of symmetrical couplers was not significantly influenced by normal material tolerances. Scaling errors and over- or under-etching also did not unduly influence phase performance, but rotational alignment was found to be critical to the

performance of the coupler. Restrictions to the theory were discussed and the manufacturing requirements were highlighted.

A general synthesis procedure was derived to aid in future designs. A computer program was written to fully design the tapered coupler from material and electrical specifications. The study ends with a design example, comparing analysis results with practical measured results. The results clearly indicates an excellent agreement between the analysis and measured performance, specifically demonstrated by the 45° phase shifter which proved to be the most sensitive to material and manufacturing tolerances. The practical measured results fall comfortably within expected production tolerance boundaries. At 45° nominal phase shift and a 5° Chebyshev ripple, a slightly larger bandwidth was achieved, and the phase shift attained the desired 5° ripple except for the first two ripple peaks which exceed the specification by approximately one degree.

It can therefore be concluded that a novel ultra-wideband class of phase shifter was found. It was demonstrated that this phase shifter can be practically implemented utilizing standard materials and processes. The design equations and practical implementation of this class of phase shifter were discussed and analysed in detail. It was also demonstrated that superior freedom with respect to bandwidth and ripple could be achieved, and the shortfalls of conventional wideband phase shifters can therefore be overcome.

References

[1] F.V.Minnaar, J.C.Coetzee, and J.Joubert, "The analysis and synthesis of a novel ultra - wideband microwave differential phase shifter," in IEEE AP MTT - Symp., Pretoria, S.A., pp. 138 - 433, Nov 1995.

[2] F.V.Minnaar, J.C.Coetzee, and J.Joubert, "A novel ultra - wideband microwave differential phase shifter, " IEEE Trans. Microwave Theory Tech., vol.45, pp. 1249 - 1252, Aug. 1997.

[3] C.P.Tresselt, "Broadband tapered - line phase shift networks, " IEEE Trans. Microwave Theory Tech., vol. MTT - 16, pp. 51 - 52, Jan 1968.

[4] F.V.Minnaar, J.C.Coetzee, and J.Joubert, "The development of an ultra - wideband via connected broadside coupled splitting structure, " in IEEE AP MTT - Symp., Cape Town, S.A., pp. 465 - 466, Sept. 1998.

APPENDIX A: S-PARAMETERS OF TANDEM CONNECTED COUPLERS

A.1 Introduction

For the realisation of phase shifters of nominal phase shift value higher than about 30°, the coupling requirements of a single coupler becomes too tight. By tandem connection of two or more couplers, any phase shift can be achieved. This appendix describes the properties of tandem connection of couplers, by using simple matrix manipulation.

A.2 *S*-Parameter Calculations

Standard theory of couplers may be expanded to derive the *S*-parameter nature of identical tandem-connected couplers. For a single coupler, the *S* parameter matrix equation can be defined as

$$\begin{bmatrix} b_1 \\ b_2 \\ b_3 \\ b_4 \end{bmatrix} = \begin{bmatrix} 0 & f_1 & 0 & f_2 \\ f_1 & 0 & f_2 & 0 \\ 0 & f_2 & 0 & f_1 \\ f_2 & 0 & f_1 & 0 \end{bmatrix} \begin{bmatrix} a_1 \\ a_2 \\ a_3 \\ a_4 \end{bmatrix} . \qquad \text{(A1)}$$

Where the coupling- and transmission coefficients are defined as

$$f_1 = j\ k(f) \qquad \text{The coupling coefficient ,} \qquad \text{(A2)}$$

$$f_2 = \sqrt{1 - k^2\ (f)} \qquad \text{The transmission coefficient .} \qquad \text{(A3)}$$

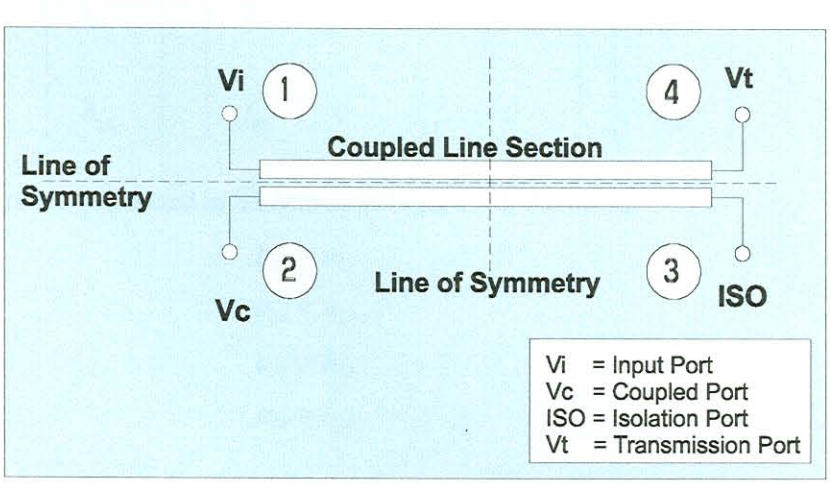

Figure A1 : Definition of a single symmetric coupler

The definition of such a symmetric coupler is shown in Figure A1. When excited from port (1) and with all other ports terminated, $a2 = a3 = a4 = 0$.

Then, from matrix A1, it is concluded that:

$$b_2 = f_c a_1 \quad b_1 = b_3 = 0\,, \qquad b_4 = f_t a_1 \quad . \tag{A4}$$

Then for the individual couplers, the two matrixes can be defined as

$$\begin{bmatrix} b_{11} \\ b_{12} \\ b_{13} \\ b_{14} \end{bmatrix} = \begin{bmatrix} 0 & f_{11} & 0 & f_{12} \\ f_{11} & 0 & f_{12} & 0 \\ 0 & f_{12} & 0 & f_{11} \\ f_{12} & 0 & f_{11} & 0 \end{bmatrix} \cdot \begin{bmatrix} a_{11} \\ a_{12} \\ a_{13} \\ a_{14} \end{bmatrix}, \tag{A5}$$

$$\begin{bmatrix} b_{12} \\ b_{22} \\ b_{23} \\ b_{24} \end{bmatrix} = \begin{bmatrix} 0 & f_{21} & 0 & f_{22} \\ f_{21} & 0 & f_{22} & 0 \\ 0 & f_{22} & 0 & f_{21} \\ f_{22} & 0 & f_{21} & 0 \end{bmatrix} \cdot \begin{bmatrix} a_{21} \\ a_{22} \\ a_{23} \\ a_{24} \end{bmatrix} . \tag{A6}$$

The two couplers are connected in tandem as in Figure A2, therefore

$$b_{21} = a_{12}\,, \tag{A7}$$

$$b_{14} = a_{23}\,, \tag{A8}$$

$$a_{21} = b_{12}\,, \tag{A9}$$

$$a_{14} = b_{23}\,. \tag{A10}$$

The matrixes can be written in equation form as

$$b_{11} = a_{12}f_{11} + a_{14}f_{12} \quad , \tag{A11}$$

$$b_{12} = a_{11}f_{11} + a_{13}f_{12} \quad , \tag{A12}$$

$$b_{13} = a_{12}f_{12} + a_{14}f_{11} \quad , \tag{A13}$$

$$b_{14} = a_{11}f_{12} + a_{13}f_{11} \quad , \tag{A14}$$

$$b_{21} = a_{22}f_{21} + a_{24}f_{22} \quad , \tag{A15}$$

$$b_{22} = a_{21}f_{21} + a_{23}f_{22} \quad , \tag{A16}$$

$$b_{23} = a_{22}f_{22} + a_{24}f_{21} \quad , \tag{A17}$$

$$b_{24} = a_{21}f_{22} + a_{23}f_{21} \quad . \tag{A18}$$

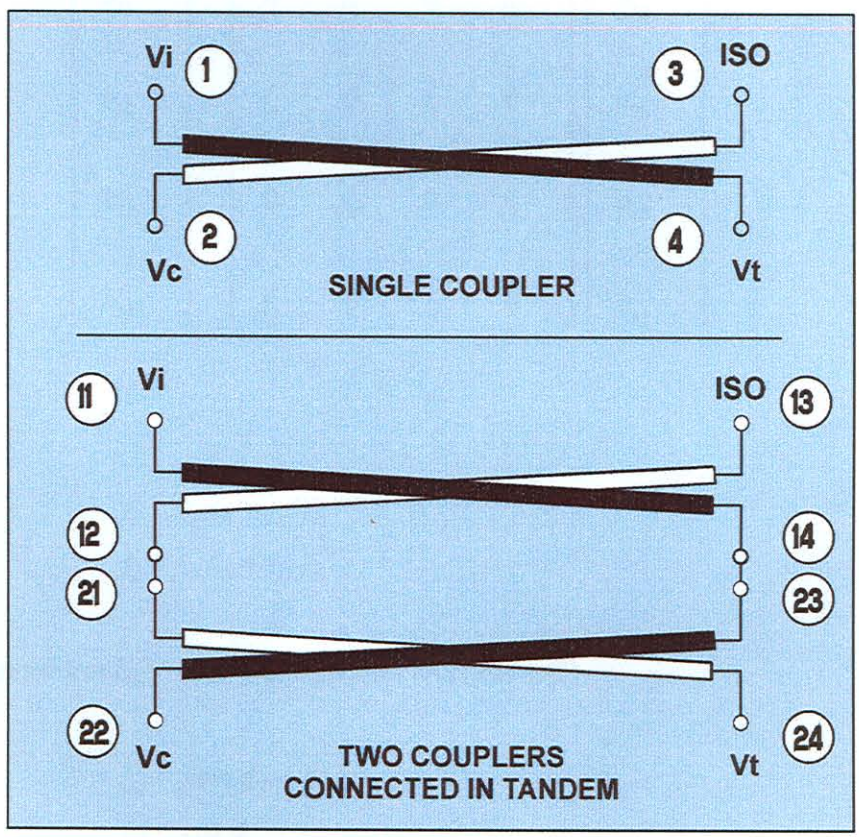

Figure A2 : Tandem connected couplers

Substituting

(A7) in (A15): $a_{12} = a_{22}f_{21} + a_{24}f_{22}$, (A19)

(A9) in (A12): $a_{21} = a_{11}f_{11} + a_{13}f_{12}$, (A20)

(A8) in (A14): $a_{23} = a_{11}f_{12} + a_{13}f_{11}$, (A21)

(A10) in (A17): $a_{14} = a_{22}f_{22} + a_{24}f_{21}$. (A22)

and

(A19) and (A22) in (A11): $b_{11} = [f_{11}f_{21} + f_{12}f_{22}]\, a_{22} + [f_{11}f_{22} + f_{12}f_{21}]\, a_{24}$, (A23)

(A19) and (A22) in (A13): $b_{13} = [f_{21}f_{12} + f_{11}f_{22}]\, a_{22} + [f_{11}f_{21} + f_{21}f_{22}]\, a_{24}$, (A24)

(A20) and (A21) in (A16): $b_{22} = [f_{11}f_{21} + f_{12}f_{22}]\, a_{11} + [f_{11}f_{22} + f_{12}f_{21}]\, a_{13}$, (A25)

(A20) and (A21) in (A18): $b_{24} = [f_{11}f_{22} + f_{12}f_{21}]\, a_{11} + [f_{11}f_{21} + f_{12}f_{22}]\, a_{13}$. (A26)

Equations (A23) to (a26) can be written in martrix form. Therefore, the tandem component matrix is as

$$\begin{bmatrix} b_{11} \\ b_{22} \\ b_{13} \\ b_{24} \end{bmatrix} = \begin{bmatrix} 0 & f_1 & 0 & f_2 \\ f_1 & 0 & f_2 & 0 \\ 0 & f_2 & 0 & f_1 \\ f_2 & 0 & f_1 & 0 \end{bmatrix} \begin{bmatrix} a_{11} \\ a_{22} \\ a_{13} \\ a_{24} \end{bmatrix} . \quad \text{(A27)}$$

where

$f_1 = f_{11}f_{21} + f_{12}f_{22}$, (A28)

$f_2 = f_{11}f_{22} + f_{12}f_{21}$. (A29)

Applying the transform $K(f) = \sin \phi$ to equations (A2) and (A3)

$f_{11} = j \sin \phi_1$, (A30)

$f_{12} = \cos \phi_1$, (A31)

$f_{21} = j \sin \phi_2$, (A32)

$f_{22} = \cos \phi_2$. (A33)

Substituting equations (A30) to (A33) in (A28) and (A29) yields

$f_1 = j \sin (\phi_1 + \phi_2)$, (A34)

$f_2 = \cos (\phi_1 + \phi_2)$. (A35)

A3. Conclusion

From the results it is clear that the coupling angles of tandem-connected couplers can be added directly. The ripple angles can be added too. The phase shifter design can therefore be simplified by equally dividing the phase shift between the couplers, and by having to design only a single coupler, since all stages are identical.

APPENDIX B: SYMMETRICAL PHASE SHIFTER PERFORMANCE ENHANCEMENT

B1. Introduction

Manufacturing tolerances usually degrade the performance of a component. It is assumed that the via interconnections in the splitter, or any other non-ideal effect, can be modelled as a small series parasitic inductance. This section demonstrates the valuable advantage to be gained by introducing symmetry to the phase shifter. It will be shown that particularly the via interconnection may severely degrade the phase shift performance of an asymmetric phase shifter. The symmetric phase shifter fully compensates for these effects.

B2. Asymmetric Phase Shifter Performance

To illustrate how symmetric construction decreases phase shift error, let us assume that the via can be represented by a small inductance L, of impedance E, in one line.

$$E = 2\pi fL \tag{B1}$$

The voltage transmission, V_0, over a series inductance jE can be derived:

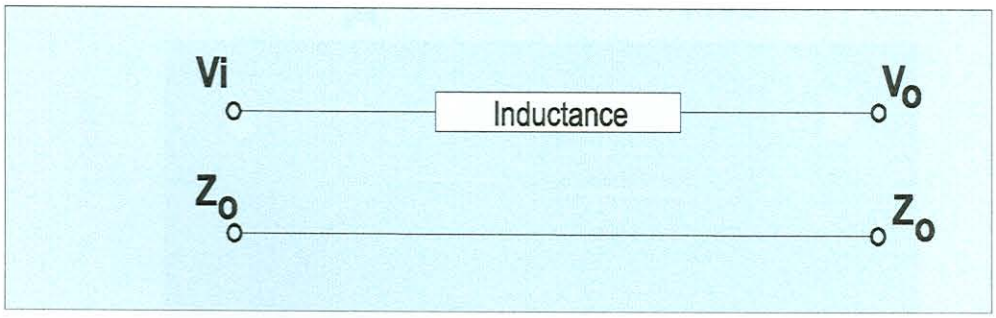

Figure B1 : Model of a single via through connection

$$V_0 = V_i - jE\left[\frac{V_i}{Z_0 + jE}\right], \tag{B2}$$

$$V_0 = V_i\left[\frac{1}{1 + je}\right] \quad \text{where} \quad e = E/Z_0 \ . \tag{B3}$$

Ignoring second-order effects ($e^2 << 1$), equation (B3) becomes

$$V_0 \approx V_i \ [1 - j\, e] \quad . \tag{B4}$$

For the asymmetric phase shifter, the transfer function can be derived as

$$B/A = (1 - j\, e)\, f_c + f_T \quad . \tag{B5}$$

Using definition (2.10) and (2.11)

$$f_c = j \sin \phi \quad , \tag{B6}$$

$$f_T = \cos \phi \quad . \tag{B7}$$

By neglecting second order effects, we simplify the equation (B5) and find

$$B/A \approx \sqrt{1 + e \sin 2\phi} \quad e^{\left(j \, atan \left[\frac{\tan \phi}{1 + e \tan \phi}\right]\right)} \quad . \tag{B8}$$

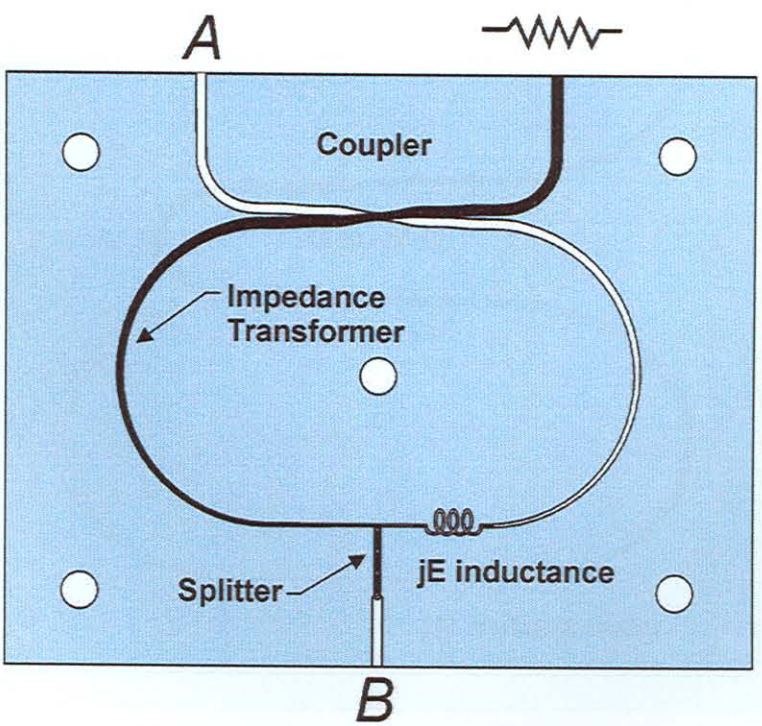

Figure B2 : The asymmetric phase shifter

Since the amplitude distortion is negligible (e is small) it can be seen that for large values of ϕ the phase therm has a large frequency-dependent error term. This can not be compensated for by simple means.

B3. Symmetric Phase Shifter Performance

Applying the same error symmetrically, the transfer function of the symmetric phase shifter becomes:

$$B/A \approx (1 - je)\left[f_c + f_T - \frac{e^2}{2\,(1 - j\,e)} \cdot f_c\right] . \qquad \text{(B9)}$$

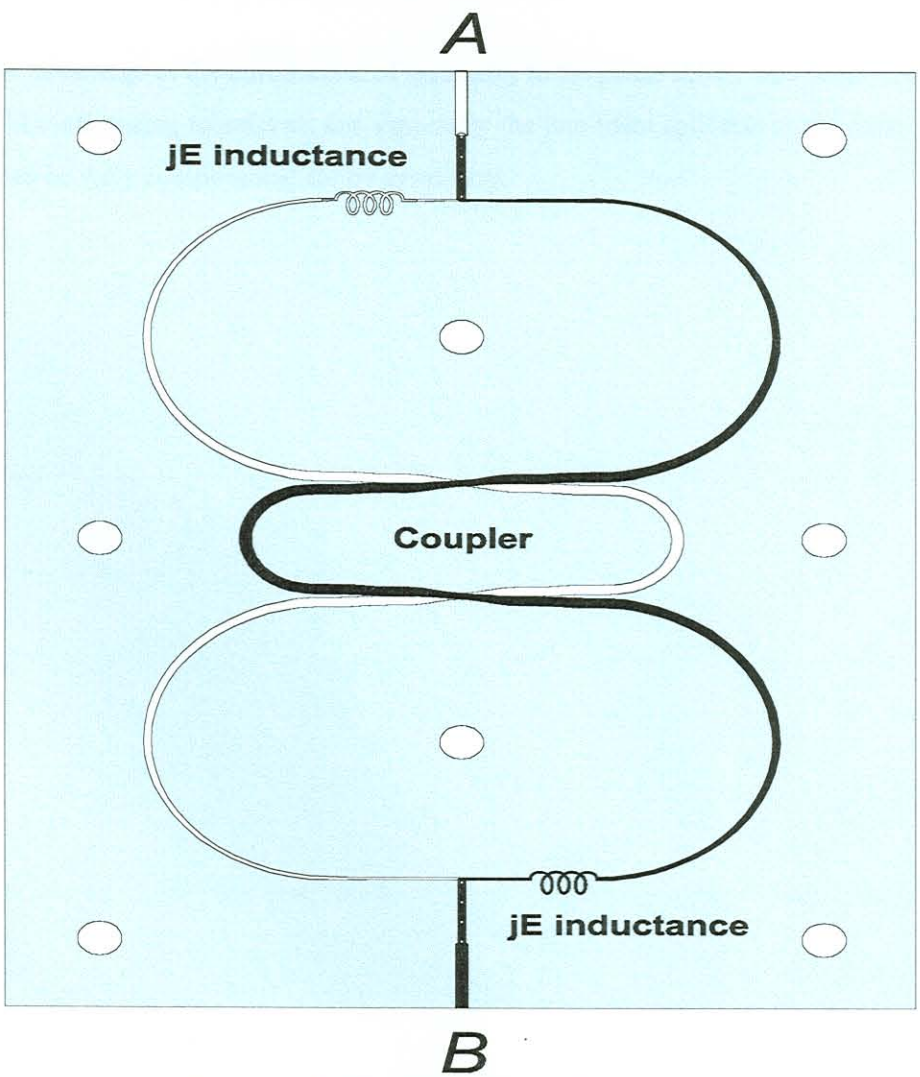

Figure B3 : The symmetric phase shifter

Ignoring second-order terms,

$$B/A \approx (1 - j\,e)\,(f_c + f_T) \quad , \tag{B10}$$

$$\approx 1.e^{-j \arctan(e)} \cdot e^{j\phi} \quad . \tag{B11}$$

The amplitude is virtually undistorted and a small additive phase delay of *arctan (e)* is introduced. This can be fully compensated for by a short line added to the reference line.

B4. Conclusion

The valuable advantage of the introduction of symmetry to the phase shifter was demonstrated in this appendix. Manufacturing tolerances, and especially the non-ideal split due to the finite number of vias used, can be fully compensated for by symmetry.

APPENDIX C: REFLECTION ANALYSIS OF A SYSTEM OF MULTIPLE IDENTICAL VIAS

C1. Introduction

To accurately determine the odd mode *S*-parameters of the splitter, it is necessary to determine the properties of a system of any number of equally spaced vias in a medium of odd-mode impedance. It is assumed that only the vias contribute to reflections in the structure. Standard S-parameter theory combined with the well-known reflectogram is used to add all transmission and reflection contributions in the structure. There terms form an arithmetic series which can be written in closed form.

C2. Reflectogram Analysis

Firstly, the reflection and transmission properties of a single via in odd mode medium is determined. The results will be used for multiple via analysis.

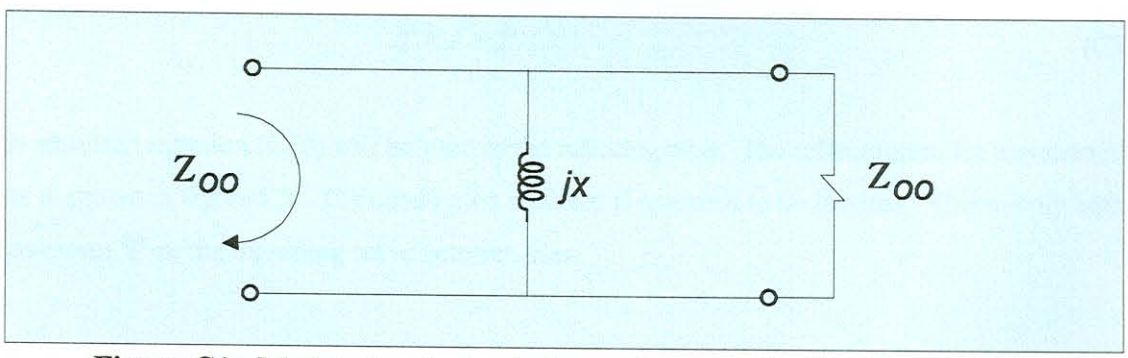

Figure C1 : Model of a single via through connection in the odd mode

The reflection coefficient is therefore

$$\Gamma = \frac{j\,X \,//\, Z_{00} - Z_{00}}{j\,X \,//\, Z_{00} + Z_{00}} \quad , \qquad = \frac{-1 + 2\,j\,x}{1 + 4\,x^2} \qquad \text{where} \qquad x = \frac{X}{Z_{00}} \quad . \tag{C1}$$

For lossless networks, energy conservation applied to *S*-parameters yield the following general equations

$$\sum_{j=1}^{2} |\, S_{ij} \,|^2 = 1 \quad , \tag{C2}$$

$$and \sum_{j=1}^{2} S_{jm} \,.\, S^{*}_{jn} = 0 \quad ; \qquad m \neq n \quad . \tag{C3}$$

For two-port networks, equations (C2) and (C3) can be written as

$$|\Gamma|^2 + |T|^2 = 1 \quad , \tag{C4}$$

and

$$\Gamma T^* + T \Gamma^* = 0 \quad . \tag{C5}$$

let

$$\Gamma = A + j B \quad , \tag{C6}$$

$$T = a + j b \quad . \tag{C7}$$

Substituting equations (C6) and (C7) into (C4) and (C5), and solving in terms of A and B, yields

$$T = \left[-\frac{B}{A} + j \right] \sqrt{\frac{1 - (A^2 + B^2)}{1 + (B/A)^2}} \quad , \tag{C8}$$

$$= \frac{4x^2 + j\,2x}{1 + 4x^2} \quad . \tag{C9}$$

Therefore:

$$T = 1 + \Gamma \quad . \tag{C10}$$

The resultant equation (C10) will be used in the reflectograms. The reflectogram for a system of 2 vias is shown in figure C2. The conduction medium is assumed to be lossless. This simply adds a phase term Ψ to the travelling wave between vias.

Let

$$\Psi = e^{-j\theta} \quad . \tag{C11}$$

Adding reflection and transmission terms, the following series can be written from Figure C2:

$$\Gamma_2 = \Gamma + T^2 \Psi^2 \Gamma + T^2 \Psi^4 \Gamma^3 + T^2 \Psi^6 \Gamma^5 + T^2 \Psi^8 \Gamma^7 + \ldots \tag{C12}$$

$$= \Gamma + \frac{T^2 \Psi^2 \Gamma}{(1 - \Psi^2 \Gamma^2)} \quad , \tag{C13}$$

$$T_2 = T^2 \Psi + T^2 \Psi^3 \Gamma^2 + T^2 \Psi^5 \Gamma^4 + T^2 \Psi^7 \Gamma^6 + \ldots \tag{C14}$$

$$= \frac{T^2 \Psi}{(1 - \Psi^2 \Gamma^2)} \quad . \tag{C15}$$

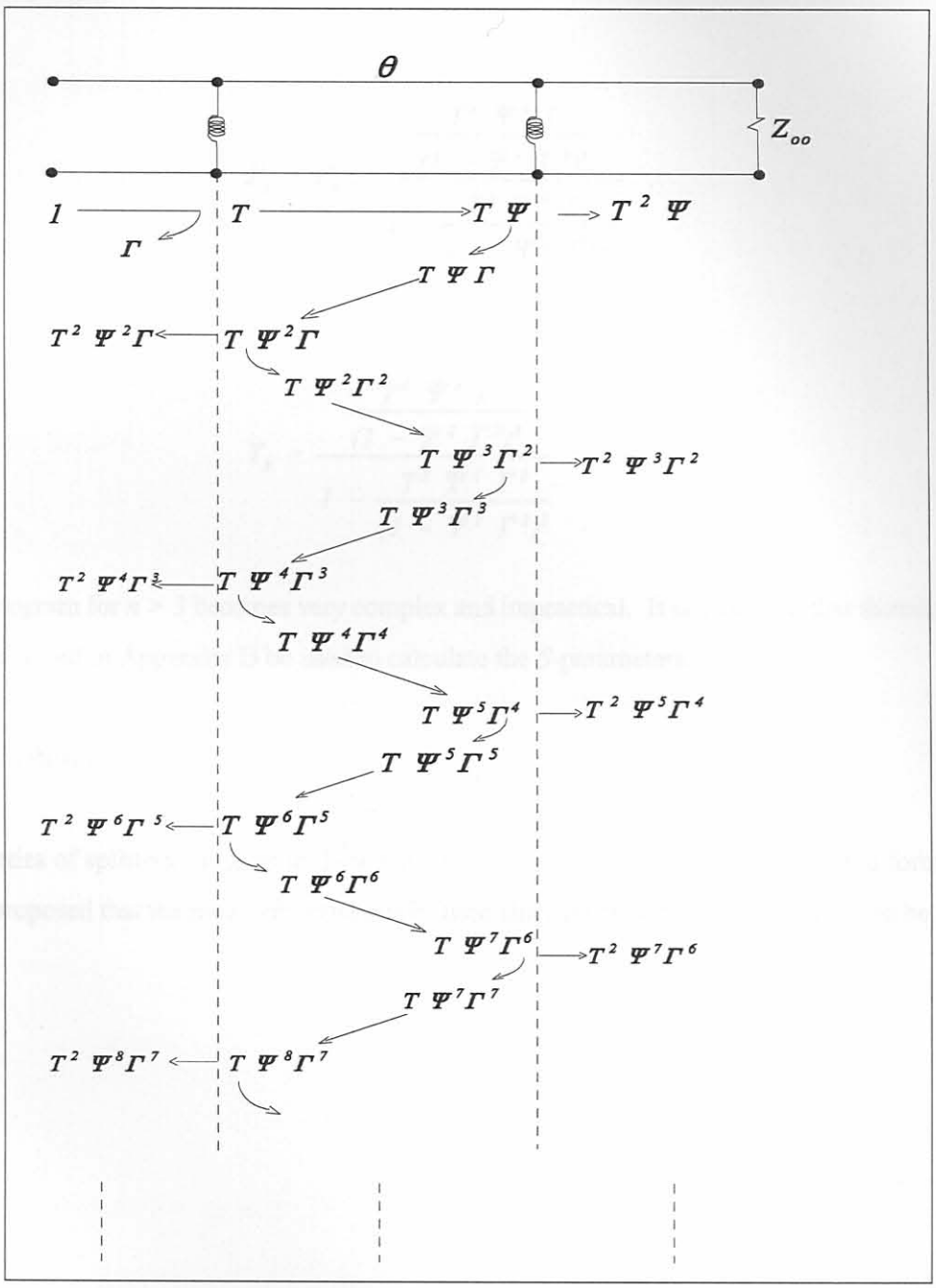

Figure C2 : Reflectogram of a system of two via interconnections

The reflectogram is not overly complicated, and identifying the series is fairly straight forward. Increasing the number of vias beyond three complicates matters.

It can be shown that

$$\Gamma_3 = \Gamma_2 + \frac{\dfrac{T^4 \Psi^4 \Gamma}{(1 - \Psi^2 \Gamma^2)^3}}{1 - \dfrac{T^2 \Psi^4 \Gamma^2}{(1 - \Psi^2 \Gamma^2)^2}}, \tag{C16}$$

$$T_3 = \frac{\dfrac{T^4 \Psi^4 \Gamma}{(1 - \Psi^2 \Gamma^2)^3}}{1 - \dfrac{T^2 \Psi^4 \Gamma^2}{(1 - \Psi^2 \Gamma^2)^2}}. \tag{C17}$$

This reflectogram for $n > 3$ becomes very complex and impractical. It is proposed that the recursion equations derived in Appendix D be used to calculate the *S*-parameters.

C3. Conclusion

The properties of splitters using up to three vias in the odd mode were derived in closed form. For $n > 3$ it is proposed that the recursion equations be used since no closed-form solution could be found.

APPENDIX D: RECURSION EQUATIONS OF A SYSTEM OF MULTIPLE IDENTICAL VIAS

D1. Introduction

To accurately determine the odd mode *S*-parameters of the splitter, it is necessary to determine the properties of a system of any number of equally spaced vias in a medium of odd-mode impedance. Standard *S*-parameter theory combined with the reflectogram is used to calculate recursion equations for a periodic structure of n identical vias spaced equally in BCS. The closed-form equations of up to three vias were calculated in Appendix C. For any number of vias $n = 1$ *to* ∞, the recursion equations can be used.

D2. Reflectogram Analysis

The assumptions used and results obtained in Appendix C will be built on. The reflectogram for determining the recursion equations is shown in figure D1. Summing the relevant terms, we find

$$\Gamma_{n+1} = \Gamma + T^2 \Gamma \Psi^2 \Gamma_n + T^2 \Psi^4 \Gamma \Gamma_n + T^2 \Psi^6 \Gamma^2 \Gamma^3_n + T^2 \Psi^8 \Gamma^3 \Gamma_n{}^4 + \ldots , \qquad \text{(D1)}$$

and

$$T_{n+1} = T \Psi T_n + T \Psi^3 \Gamma \Gamma_n T_n + T \Psi^5 \Gamma^2 \Gamma^2_n T_n + T \Psi^7 \Gamma^3 \Gamma_n{}^3 T_n + \ldots . \qquad \text{(D2)}$$

These terms can be written in closed form as

$$\Gamma_{n+1} = \frac{T^2 \Psi^2 \Gamma_n}{1 - \Psi^2 \Gamma \Gamma_n} + \Gamma , \qquad \text{(D3)}$$

$$T_{n+1} = \frac{T \Psi T_n}{1 - \Psi^2 \Gamma \Gamma_n} . \qquad \text{(D4)}$$

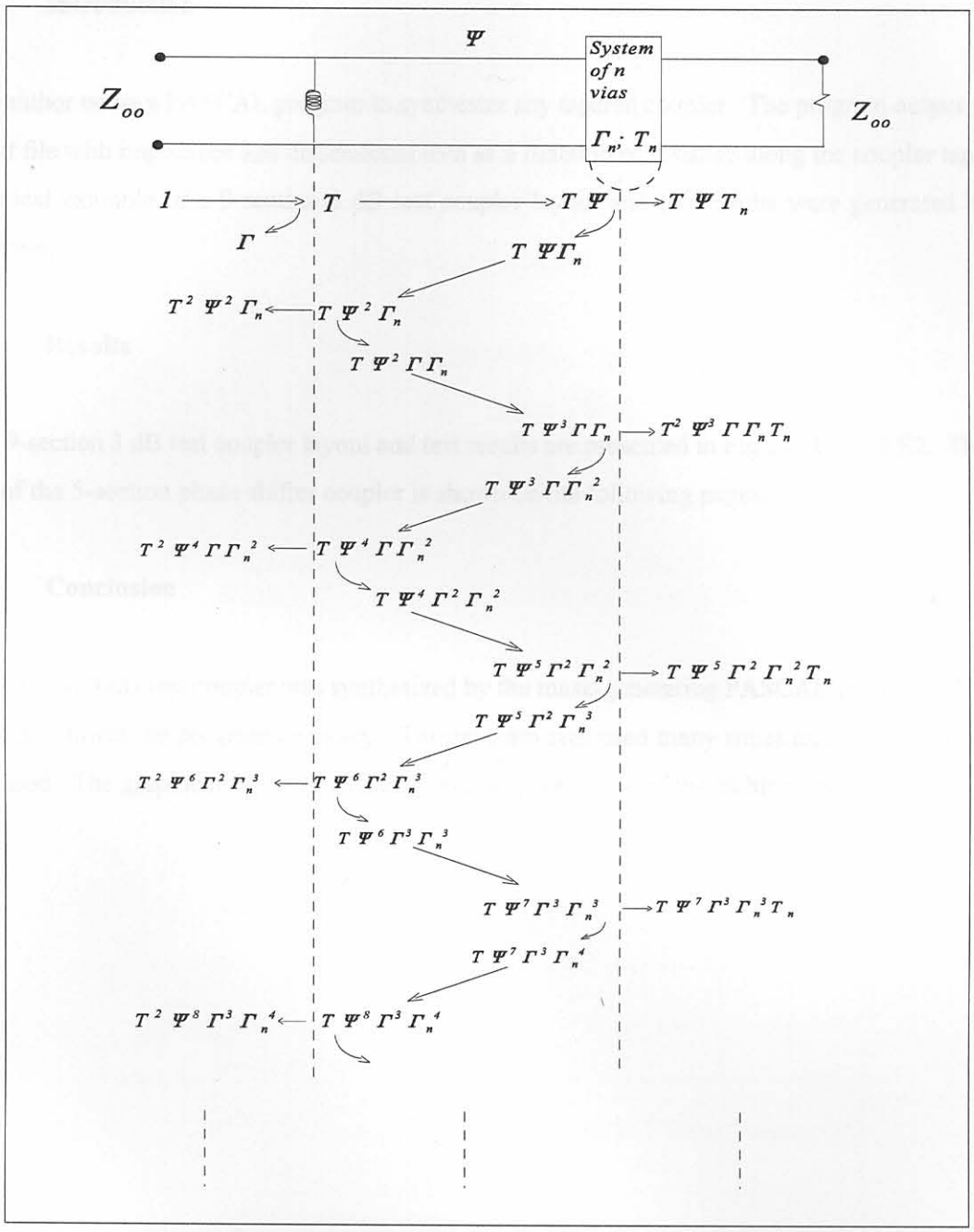

Figure D1 : Reflectogram for the derivation of the recursion equations

D3. Conclusion

The recursion equations of reflection and transmission properties of a system of any number of identical vias in odd-mode impedance have been derived. These equations yield the same results as the closed-form equations for $n = 1, 2, 3$ as derived in Appendix C.

APPENDIX E: COUPLER SYNTHESIS RESULTS

E1. Introduction

The author wrote a PASCAL program to synthesize any tapered coupler. The program output yields a text file with impedance and dimensional data as a function of distance along the coupler taper. A practical example of a 9-section 3 dB test coupler layout and test results were generated by the program.

E2. Results

The 9-section 3 dB test coupler layout and test results are presented in Figures E1 and E2. The text file of the 5-section phase shifter coupler is shown on the following pages.

E3. Conclusion

A 9-section 3 dB test coupler was synthesized by the mask-generating PASCAL program. The test results confirm the program accuracy. The program was used many times and good results were obtained. The graphical file was used to create the photomask of the etching process.

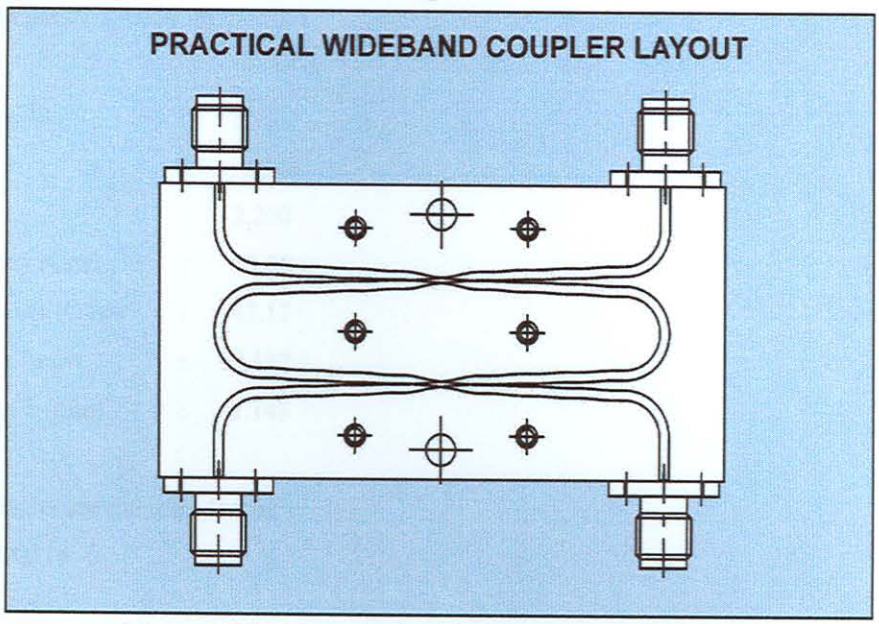

Figure E1 : Practical wideband coupler layout

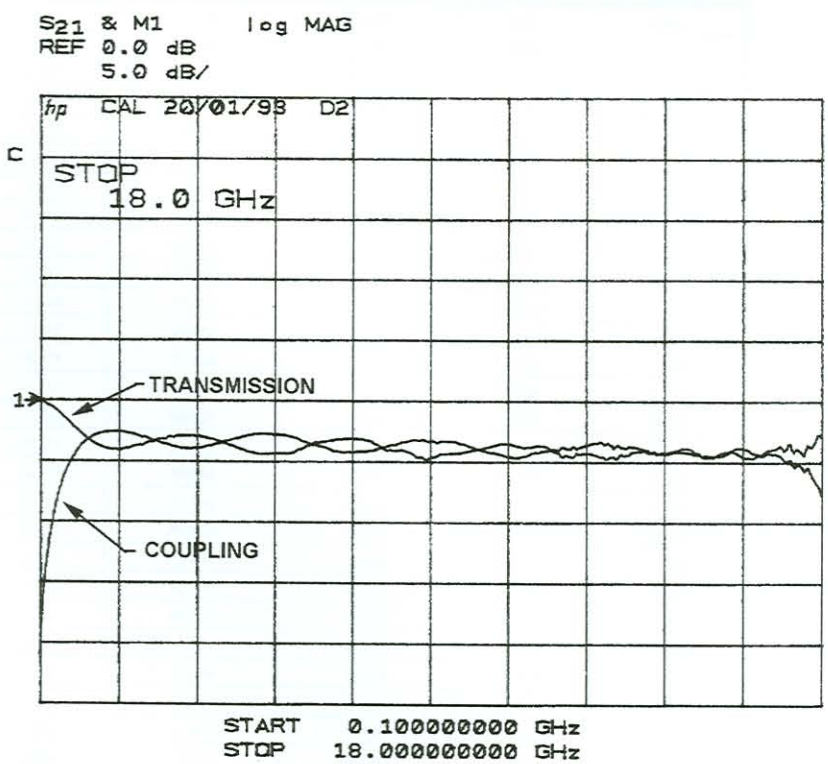

Figure E2 : Typical 9-Section test coupler measured frequency response

COUPLER DESIGN RESULTS

Number of sections : 5
Coupling (dB) : -8.343
Permittivity : 2.200
Centre frequency (Ghz) : 10.00
System impedance (Ohm) : 47.17
Track spacing s (mm) : 0.127
Ground spacing b (mm) : 1.143

Normalized coupler section impedances:

Z[1] : 1.09218
Z[2] : 1.26492
Z[3] : 2.09984

X(mm)	C(dB)	Zoe(Ohm)	Zoo(Ohm)	W(mm)	Wo(mm)
0.000	-3.175	110.948	20.053	0.589	0.001
0.101	-3.181	110.883	20.081	0.588	0.018
0.202	-3.201	110.598	20.150	0.589	0.036
0.303	-3.233	110.097	20.258	0.589	0.055
0.405	-3.279	109.387	20.407	0.591	0.075
0.506	-3.339	108.479	20.595	0.592	0.095
0.607	-3.412	107.383	20.822	0.595	0.117
0.708	-3.499	106.116	21.088	0.597	0.139
0.809	-3.600	104.693	21.393	0.601	0.162
0.910	-3.717	103.132	21.735	0.605	0.186
1.011	-3.848	101.452	22.113	0.610	0.211
1.112	-3.995	99.672	22.527	0.615	0.237
1.214	-4.158	97.812	22.974	0.621	0.264
1.315	-4.337	95.890	23.454	0.628	0.292
1.416	-4.532	93.926	23.964	0.636	0.320
1.517	-4.744	91.939	24.503	0.644	0.349
1.618	-4.973	89.944	25.067	0.653	0.379
1.719	-5.218	87.958	25.654	0.663	0.409
1.820	-5.480	85.996	26.261	0.673	0.440
1.921	-5.757	84.071	26.885	0.684	0.470
2.023	-6.050	82.194	27.521	0.695	0.501
2.124	-6.357	80.375	28.167	0.707	0.532
2.225	-6.678	78.625	28.818	0.719	0.564
2.326	-7.010	76.949	29.470	0.731	0.594
2.427	-7.353	75.353	30.119	0.744	0.623
2.528	-7.705	73.843	30.760	0.756	0.651
2.629	-8.062	72.422	31.390	0.769	0.679
2.731	-8.424	71.092	32.003	0.780	0.707
2.832	-8.786	69.855	32.597	0.792	0.733
2.933	-9.147	68.710	33.168	0.804	0.757
3.034	-9.502	67.658	33.711	0.814	0.781
3.135	-9.849	66.698	34.225	0.824	0.802
3.236	-10.185	65.827	34.706	0.834	0.823

X(mm)	C(dB)	Zoe(Ohm)	Zoo(Ohm)	W(mm)	Wo(mm)
3.337	-10.506	65.044	35.153	0.842	0.842
3.438	-10.810	64.345	35.563	0.850	0.860
3.540	-11.093	63.728	35.938	0.857	0.876
3.641	-11.354	63.188	36.274	0.863	0.890
3.742	-11.590	62.722	36.574	0.868	0.903
3.843	-11.801	62.324	36.838	0.873	0.914
3.944	-11.985	61.992	37.066	0.876	0.923
4.045	-12.142	61.718	37.260	0.879	0.931
4.146	-12.274	61.499	37.424	0.882	0.938
4.247	-12.382	61.329	37.558	0.884	0.943
4.349	-12.466	61.203	37.666	0.885	0.947
4.450	-12.530	61.115	37.752	0.886	0.950
4.551	-12.576	61.060	37.817	0.886	0.952
4.652	-12.607	61.031	37.866	0.886	0.953
4.753	-12.625	61.024	37.901	0.886	0.954
4.854	-12.635	61.032	37.927	0.886	0.954
4.955	-12.639	61.051	37.946	0.885	0.954
5.056	-12.639	61.074	37.963	0.885	0.953
5.158	-12.640	61.098	37.979	0.884	0.953
5.259	-12.643	61.118	37.998	0.884	0.953
5.360	-12.650	61.130	38.021	0.883	0.953
5.461	-12.664	61.131	38.052	0.883	0.953
5.562	-12.687	61.117	38.091	0.883	0.954
5.663	-12.719	61.086	38.142	0.883	0.955
5.764	-12.763	61.035	38.205	0.884	0.957
5.866	-12.820	60.964	38.281	0.884	0.959
5.967	-12.891	60.869	38.371	0.885	0.963
6.068	-12.976	60.752	38.477	0.886	0.967
6.169	-13.077	60.611	38.598	0.888	0.971
6.270	-13.195	60.446	38.734	0.889	0.977
6.371	-13.329	60.258	38.887	0.891	0.983
6.472	-13.480	60.047	39.055	0.893	0.990
6.573	-13.649	59.816	39.238	0.896	0.998
6.675	-13.835	59.566	39.434	0.898	1.007
6.776	-14.038	59.299	39.644	0.901	1.017
6.877	-14.259	59.017	39.866	0.904	1.027
6.978	-14.496	58.722	40.099	0.907	1.038
7.079	-14.749	58.417	40.340	0.910	1.050
7.180	-15.017	58.106	40.590	0.913	1.062
7.281	-15.300	57.789	40.845	0.916	1.075
7.382	-15.596	57.472	41.104	0.919	1.088
7.484	-15.903	57.155	41.365	0.922	1.102
7.585	-16.221	56.841	41.627	0.925	1.116
7.686	-16.547	56.534	41.887	0.928	1.131
7.787	-16.879	56.235	42.144	0.931	1.145
7.888	-17.215	55.947	42.395	0.933	1.160
7.989	-17.551	55.672	42.639	0.935	1.175
8.090	-17.887	55.411	42.875	0.937	1.190
8.192	-18.217	55.165	43.100	0.939	1.204
8.293	-18.541	54.937	43.314	0.941	1.218
8.394	-18.853	54.727	43.516	0.942	1.231
8.495	-19.152	54.535	43.704	0.943	1.244
8.596	-19.434	54.363	43.877	0.944	1.256
8.697	-19.697	54.210	44.036	0.945	1.267
8.798	-19.938	54.077	44.181	0.946	1.277
8.899	-20.155	53.963	44.310	0.946	1.286
9.001	-20.348	53.867	44.424	0.947	1.294

X(mm)	C(dB)	Zoe(Ohm)	Zoo(Ohm)	W(mm)	Wo(mm)
9.102	-20.516	53.789	44.524	0.947	1.301
9.203	-20.658	53.728	44.611	0.947	1.307
9.304	-20.775	53.682	44.685	0.947	1.311
9.405	-20.868	53.651	44.747	0.947	1.315
9.506	-20.939	53.632	44.798	0.946	1.317
9.607	-20.991	53.625	44.840	0.946	1.319
9.708	-21.026	53.627	44.875	0.945	1.320
9.810	-21.048	53.637	44.903	0.945	1.321
9.911	-21.059	53.652	44.926	0.944	1.321
10.012	-21.063	53.671	44.946	0.944	1.321
10.113	-21.064	53.692	44.964	0.943	1.320
10.214	-21.065	53.713	44.982	0.943	1.320
10.315	-21.069	53.732	45.002	0.942	1.320
10.416	-21.080	53.748	45.025	0.942	1.320
10.518	-21.100	53.758	45.053	0.941	1.320
10.619	-21.133	53.762	45.086	0.941	1.321
10.720	-21.180	53.758	45.125	0.940	1.323
10.821	-21.245	53.744	45.173	0.940	1.325
10.922	-21.330	53.720	45.229	0.940	1.328
11.023	-21.436	53.684	45.295	0.940	1.332
11.124	-21.567	53.638	45.371	0.939	1.338
11.225	-21.723	53.579	45.457	0.939	1.344
11.327	-21.907	53.507	45.554	0.939	1.351
11.428	-22.120	53.424	45.661	0.939	1.360
11.529	-22.364	53.328	45.779	0.940	1.370
11.630	-22.641	53.222	45.908	0.940	1.382
11.731	-22.952	53.104	46.046	0.940	1.395
11.832	-23.299	52.977	46.194	0.940	1.409
11.933	-23.684	52.840	46.350	0.940	1.425
12.034	-24.108	52.696	46.514	0.941	1.443
12.136	-24.573	52.545	46.684	0.941	1.462
12.237	-25.082	52.389	46.860	0.941	1.483
12.338	-25.636	52.229	47.041	0.941	1.506
12.439	-26.238	52.067	47.225	0.942	1.532
12.540	-26.890	51.904	47.411	0.942	1.559
12.641	-27.595	51.741	47.598	0.942	1.588
12.742	-28.356	51.581	47.784	0.942	1.620
12.844	-29.178	51.423	47.968	0.942	1.654
12.945	-30.062	51.271	48.149	0.942	1.691
13.046	-31.015	51.124	48.326	0.942	1.731
13.147	-32.041	50.984	48.497	0.941	1.773
13.248	-33.146	50.852	48.661	0.941	1.819
13.349	-34.337	50.728	48.818	0.941	1.869
13.450	-35.622	50.615	48.966	0.940	1.923
13.551	-37.010	50.511	49.106	0.940	1.980
13.653	-38.513	50.418	49.235	0.940	2.043
13.754	-40.143	50.335	49.355	0.939	2.111
13.855	-41.917	50.264	49.464	0.939	2.185
13.956	-43.855	50.203	49.563	0.938	2.266
14.057	-45.981	50.153	49.652	0.938	2.354
14.158	-48.325	50.113	49.730	0.937	2.452
14.259	-50.928	50.083	49.799	0.936	2.561
14.360	-53.838	50.062	49.859	0.936	2.682
14.462	-57.121	50.050	49.911	0.935	2.820
14.563	-60.857	50.045	49.955	0.935	2.976